Alma Mater Studiorum – Università di Bologna

DOTTORATO DI RICERCA IN

Scienze Biomediche e Neuromotorie

Ciclo **XXXIV**

Settore Concorsuale: 05/D1

Settore Scientifico Disciplinare: BIO/09

DEVELOPMENT OF AN INNOVATIVE STRATEGY TO ENHANCE THE EFFICACY OF GENE THERAPY FOR CDKL5 DEFICIENCY DISORDER

Presentata da: Marianna Tassinari

Coordinatore Dottorato

Prof.ssa Matilde Y. Follo

Supervisore

Prof.ssa Elisabetta Ciani

Esame finale anno 2021

SUMMARY

ABSTRACT

CDKL5 (cyclin-dependent kinase-like 5) deficiency disorder (CDD) is a severe X-linked neurodevelopmental disease caused by mutations in the *CDKL5* gene. CDD is characterized by early-onset epileptic seizures, hypotonia, intellectual disability, motor and visual impairment and respiratory dysregulation. Although pharmacological treatments are used to control seizures, there is currently no cure or effective treatment to ameliorate cognitive and behavioral symptoms for CDD.

Albeit delivery of a wild-type copy of the mutated gene to cells represents the most curative approach for a monogenic disease, proof-of-concept studies highlight significant efficacy caveats for brain gene therapy. The major one regards the low efficiency of gene delivery to the CNS by viral vectors that requires large vector doses and, consequently, brings the risk of immune reaction.

In this study, we used a secretable Igk-TATk-CDKL5 protein to enhance the efficiency of a gene therapy for CDD. In view of the properties of the Igk-chain leader sequence, the TATk-CDKL5 protein produced by infected cells is secreted via constitutive secretory pathways. Importantly, due to the transduction property of the TATk peptide, the secreted CDKL5 protein is internalized by cells.

We compared the effects of a CDKL5 gene therapy with an IgK-TATk-CDKL5 gene therapy in a *Cdkl5* KO mouse model to validate whether the Igk-TATk-CDKL5 approach, that enhances the biodistribution of the therapeutic CDKL5 kinase from genetically-corrected cells to non-corrected cells via a cross-correction mechanism, significantly enhances the therapeutic efficacy. We found that, although AAVPHP.B_Igk-TATk-CDKL5 and AAVPHP.B_CDKL5 vectors had similar brain infection efficiency, the AAVPHP.B_Igk-TATk-CDKL5 vector led to a higher CDKL5 protein replacement due to secretion and transduction of the TATk-CDKL5 protein into the neighboring cells. Importantly, *Cdkl5* KO mice treated with the AAVPHP.B_Igk-TATk-CDKL5 vector showed a behavioral and neuroanatomical improvement in comparison with vehicle-treated *Cdkl5* KO mice or *Cdkl5* KO mice treated with the AAVPHP.B_CDKL5 vector, indicating that a gene therapy based on a secretable recombinant TATk-CDKL5 protein is more effective at compensating *Cdkl5*-null brain defects than gene therapy based on the expression of the native CDKL5.

Based on these results, we are confident that this study has provided a first proof-of-principle that an innovative gene therapy approach based on the unique advantages of the IgK-TATk-CDKL5 transgene is highly efficient in improving neurodevelopmental and behavioral impairments in a mouse model of CDD and could open avenues to the development of gene therapy for other monogenic diseases based on the unique and compelling properties of the Igk-TATk-fusion protein approach.

1. AIM OF THE STUDY

CDKL5 (cyclin-dependent kinase-like 5) deficiency disorder (CDD) is a severe X-linked neurodevelopmental disease caused by mutations in the *CDKL5* gene, which lead to a lack of CDKL5 protein expression or function. CDD mostly affects girls and is characterized by early-onset epileptic seizures, hypotonia, intellectual disability, motor and visual impairment, and, in some cases, respiratory dysregulation. Although pharmacological treatments are used to control seizures, there is currently no cure or effective treatment to ameliorate cognitive and behavioral symptoms for CDD.

Animal models of CDKL5 disorder, *Cdkl5 knockout* (KO) mice, recapitulate different features of CDD, exhibiting severe impairment in learning and memory, visual and respiratory deficits, and motor stereotypies and, therefore, they are a good model with which to study the positive effects of therapeutic strategies.

In theory, for a monogenic disease such as CDD, the delivery of a wild-type copy of the mutated gene to cells which lack functional protein represents the most curative approach. However, gene therapy is not without risks for humans. The major caveat regards the low efficiency of gene delivery to the CNS by viral vectors that requires large vector doses and, consequently, brings the risk of immune reaction. Moreover, the new gene might be inserted into the DNA in the wrong location, possibly causing harmful mutations to the DNA or even cancer. If the protein produced by the infected cells can be secreted and enter into neighboring cells, this will amplify the effect of the gene therapy because, even if the transduced cells are low in number, they will become a “factory” for the production of the therapeutic protein in neighboring cells. In this scenario, the efficiency of gene delivery does not necessarily need to be high. This decreases the risk of insertional mutagenesis and toxic side effects connected with large vector doses.

The idea of this project was to enhance the efficiency and safety of the gene therapy for CDKL5 disorder by exploiting the unique properties of the Igk-TATk-CDKL5 gene approach. The Igk-TATk-fusion gene approach has the potential to significantly improve the biodistribution of the therapeutic protein from genetically corrected cells to non-corrected cells via a cross-correction mechanism. Therefore, this new gene therapy approach is expected to improve the efficiency of therapeutic protein replacement into the brain and reduce the risks of toxicity associated with the therapy.

The aim of the proposed study was to compare the effects of a CDKL5 gene therapy with an IgK-TATk-CDKL5 gene therapy in a *Cdkl5* KO mouse model to validate whether the Igk-TATk-CDKL5 approach, that enhances the biodistribution of the therapeutic CDKL5 kinase from genetically-corrected cells to non-corrected cells via a cross-correction mechanism, significantly enhances the therapeutic efficacy.

As a viral vector, we used the latest adeno-associated virus (AAV) vector, that delivers therapeutic payloads to the brain neurons at high efficiency with minimal off-target effects.

The results of this study represent a first proof-of-principle that this innovative gene therapy approach may be a powerful tool for the cure of CDD, and could open avenues to the development of gene therapy for other monogenic diseases based on the unique and compelling properties of the Igk-TATk-fusion protein approach.

2. INTRODUCTION

2.1 CDKL5 deficiency disorder (CDD): identification of the disorder

CDKL5 deficiency disorder (CDD, OMIM * 300672) is a rare early infantile epileptic encephalopathy caused by mutations in the cyclin-dependent kinase-like 5 (CDKL5) gene, which is located on the X chromosome (Weaving *et al.,* 2004). Cyclin-dependent kinase-like 5 (CDKL5) is a serine/threonine protein kinase and its gene, *CDKL5*, was originally identified in 1998 during a transcriptional mapping project of the human X chromosome (Montini *et al.,* 1998). In 2003, the relationship between *CDKL5* mutations and X-linked neurodevelopmental disorders was reported (Kalscheuer *et al.,* 2003). The disease associated with CDKL5 deficiency was initially diagnosed as an early-onset seizure variant of Rett syndrome. Rett syndrome (RTT) is a neurodevelopmental disorder caused by mutations in the gene coding for the MeCP2 protein (methyl-CpG-binding2) that is located on the X chromosome (Amir *et al.,* 1999; Cheadle *et al.,* 2000). RTT is a progressive neurodevelopmental disorder that affects the patient's ability to communicate and perform simple motor tasks. RTT mainly affects females, and occurs with an incidence of up to 1:10,000 (Hagberg *et al.,* 1983). Although the RTT phenotype is variable, most RTT patients show a distinctive disease course. They develop normally up to 6–18 months; subsequently, in the classic form, patients show growth retardation, regression of speech, and the appearance of stereotyped hand movements. RTT variants have been described, including the preserved speech variant (PSV), characterized by the recovery of speech to some degree; the congenital variant (recognized from birth); the ''early seizure variant'' (seizure onset before regression); and the ''forme fruste'', with a milder, incomplete clinical course (with regression occurring at between 1 and 3 years of age) (Weaving *et al.,* 2004). These variants present some symptoms of RTT, but show considerable variation in type and age of onset, severity of impairment, and clinical course. Among these variants, the ''early seizure variant'' was initially described by Hanefeld in 1985, who reported a girl with infantile spasms with hypsarrhythmia in her early development (Hanefeld, 1985). Even if initially *diagnosed as early-onset seizure variant of Rett syndrome (*Hanefeld's variant), it has now become clear that CDKL5 disorder is an independent clinical entity associated with early-onset encephalopathy (Fehr *et al.,* 2013, Katayama *et al.,* 2020).

2.1.1 Clinical features

CDD has an estimated incidence of 1: 41,000 live births (Symonds *et al.,* 2019) and it affects four females to every male (Demarest *et al.,* 2019). The difference between males and females suggests that *CDKL5* mutations are quite often lethal during fetal life in hemizygous males, because of the single mutated copy of the gene. Hemizygous males and heterozygous females are equally and severely affected (Demarest *et al.*, 2019). In heterozygous females, however, the severity of the disease is influenced by the Lyonization mechanism (inactivation of X). This physiological process of compensating the gene dosage of the X chromosome seems to be a determining factor in the heterogeneity of symptoms. As a consequence of the inactivation of one of the two X chromosomes, each female cell can express either the mutated copy or the normal copy of the CDKL5 gene, causing so-called somatic mosaicism (Zhu & Xiong, 2019). However, to date, it is not deeply understood to what extent somatic mosaicism affects the clinical phenotype in CDD (Olson *et al.,* 2019).

Given these premises, there is a great heterogeneity in the symptoms. In fact, the clinical picture of patients extends from mild forms, with independent walking and controlled epilepsy, to severe forms with untreatable and refractory seizures that are resistant to drugs, in addition to microcephaly and the inability to achieve a complete motor development. Notwithstanding this heterogeneity, the major feature of CDD is the appearance of drug-resistant epileptic seizures in the first few months of life. Epilepsy is typically manifested as an epileptic encephalopathy with infantile spasms starting between the first few days and fourth month of life; patients show a peculiar seizure pattern with generalized tonic–clonic events, gradually translating into repetitive distal myoclonic jerks (Guerrini & Parrini, 2012). Patients may also present generalized hypotonia, intellectual disability, visual and motor deficits, and stereotypy of the hands (Bahi-Buisson *et al.,* 2008; Fehr *et al.,* 2013). Cortical visual impairment is common in patients with CDD, and other features include autistic features, language impairment, feeding intolerance, constipation, dysautonomia, breathing abnormalities, sleep disorders, and scoliosis (Fig. 1) (Rosas-Vargas *et al.,* 2008; Bahi-Buisson & Bienvenu, 2012; Kadam *et al.,* 2019; Demarest *et al.,* 2019).

Clinical features	Female patients/total (n = 88)	Male patients/total (n = 7)
Mean age in years at last evaluation (range)	15 (0.6–41)	6 (3.5–16)
Deceleration of head growth	61/72 (84.7)	3/4 (75)
Regression	16/69 (23.2)	3/7 (42.8)
Severe intellectual disability	83/85 (96.6)	7/7 (100)
Poor eye fixation and pursuit	61/72 (84.7)	7/7 (100)
Language	9/73 (12.3)	0/7 (0)
Walk with aid or unaided	24/74 (32.4)	0/7 (0)
Limited hand skills	47/62 (75.8)	7/7 (100)
Hand stereotypies	63/69 (91.3)	1/7 (14.2)
Autonomic features	21/50 (42)	1/7 (14.2)
Early seizures	86/87 (98.8)	7/7 (100)
Average seizure onset, weeks	12.5 ± 9.3	10.9 ± 9.8
Infantile spasms/epileptic encephalopathy	56/71 (78.8)	7/7 (100)
Persistent epilepsy	47/66 (71.2)	6/7 (85.7)

Patients who presented with a disrupted *CDKL5* gene due to unbalanced translocations were excluded. Figures in parentheses are percentages, except where otherwise indicated.

Fig. 1: Clinical features of female patients with *CDKL5* mutations compared to males (Bahi-Buisson & Bienvenu, 2012).

Brain MRI demonstrates nonspecific abnormalities in *CDKL5* mutation patients. Most of them exhibit cortical atrophy combined with hyperintensities in the white matter of the temporal lobe (Fig. 2) (Bahi-Buisson *et al.,* 2008).

The EEG typically shows hypsarrhythmia or epileptiform discharges in the temporal or tempo-occipital head regions. Neuroimaging may show delayed myelination in the temporal lobes, cerebral atrophy, hyperintensities in the posterior white matter, and dentate nuclei (Morrison-Levy *et al.,* 2021).

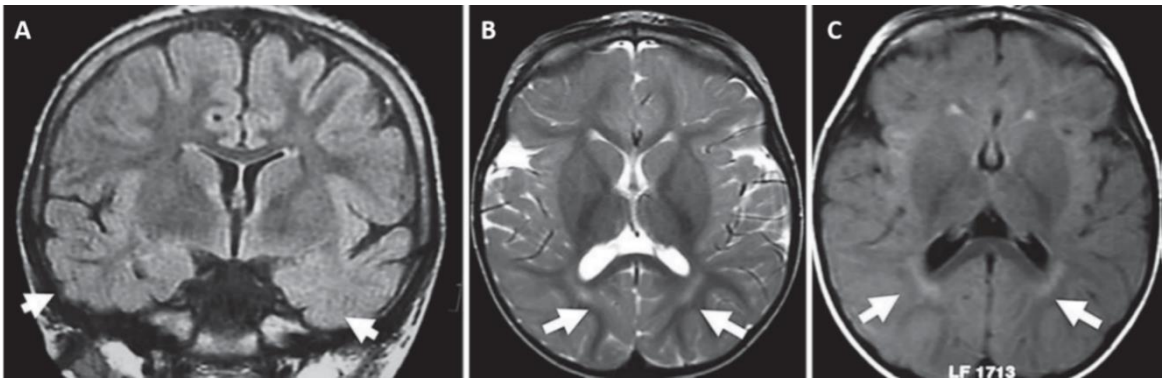

Fig. 2: Brain MRI findings for patients with *CDKL5* point mutations. **A**- Nonspecific hyperintensities in both temporal lobes (T2 FLAIR coronal section) in a 12-year-old *CDKL5* mutation patient. **B-** Nonspecific periventricular hyperintensities (T2 axial section) in a 3-year-old *CDKL5* mutation patient. **C-** Nonspecific periventricular hyperintensities (T2 FLAIR axial section) in a 9-month-old *CDKL5* mutation patient. Arrows show the location of the main abnormalities in each figure (Bahi-Buisson & Bienvenu, 2012).

2.1.2 *CDKL5* gene: mutations and genotype-phenotype correlation

The majority of CDD cases are the result of *de novo* mutations. Nevertheless, cases of a family history of CDKL5 mutations have also been reported, which probably result from germline mosaicism in one of the parents; in these situations the offspring may inherit the mutated gene (Jakimiec *et al.,* 2020). A wide range of pathogenic mutations including missense and nonsense mutations, small and large deletions, frameshifts, and aberrant splicing have been described (Kilstrup-Nielsen *et al.,* 2012, Hector *et al.,* 2017). This mutational heterogeneity may play a part in the clinical variability of CDD. To underline the heterogeneity of the disease, it is worth noting the phenotypic differences among siblings in whom the same mutation was confirmed, suggesting the involvement of epigenetic and environmental factors, as well as the relationship with the inactivation of the X chromosome, in determining the final phenotypic picture of particular patients (Bahi-Buisson *et al.,* 2008, Hagebeuk *et al.,* 2015). Early studies into the disorder were often limited to case descriptions of individual patients with CDKL5 variants (Weaving *et al.,* 2004, Bahi-Buisson *et al.,* 2008, Melani *et al.,* 2011) and subsequent efforts to elucidate genotype–phenotype relationships have proven challenging due to small sample sizes and a paucity of recurrent variants (Fehr *et al.,* 2015). Genotype-phenotype characterization

is, in any case, useful both for the understanding of CDKL5 function and for prognostic family counseling.

After almost a decade of data collection, in 2021 Mackay and colleagues published a study in which information regarding individuals with CDD was reported and submitted to the International CDKL5 Disorder database (https://www.cdkl5.com/cdkl5-international-registry-database). This data derived from online or paper-based questionnaires completed by the families (MacKay *et al.,* 2021). During the data analysis, in order to characterize the genotype-phenotype relationships the CDKL5 variants were grouped into four categories, based on their predicted functional consequences: (1) no functional protein, (2) missense/inframe within the catalytic domain, (3) truncations between amino acid (aa) 172 and aa 781, (4) truncations after aa 781 (Bertani *et al.,* 2006; Fehr *et al.,* 2015). However, to date, it is unclear whether these groups are optimal. To optimize data collection, a questionnaire was then devised with responses pertaining to developmental milestones, gross motor and fine motor skills, seizures, feeding and GI health, respiratory illness, behavior, communication, sleep, vision, and scoliosis. In order to group individuals of similar expected developmental abilities together, individuals were assigned to an age category.

Using a large international dataset, Mackay and colleagues showed that there are appreciable differences in phenotypic severity between some recurrent variants in CDKL5. For example, individuals with missense variants, p. Arg178Trp and p.Arg178Gln, and nonsense variant p.Arg559*, had the most severe phenotypes with high severity scores that indicated the poorest achievement of developmental milestones. In contrast, those with p.Arg134* and p.Arg550* variants displayed milder phenotypes with lower severity scores, indicating better achievement of milestones.

The data collected through the International CDKL5 Disorder Database are extensive and robust and they may provide an idea as to prognostic information at the time of genetic counseling. Despite the first research findings showing that this is feasible, just a small number of variants are sufficiently recurrent, approximately 22% (62/285) of the individuals in the database (MacKay *et al.,* 2021). To date, although a relative homogeneity of some clinical phenotypes in patients bearing the same mutation has been observed, we are still far from having a clear and definitive picture of the genotype-phenotype

correlation: this, once again, brings to light the complexity and heterogeneity of this disorder.

2.2 CDKL5 protein

2.2.1 Protein structure

CDKL5 protein is a member of the CMGC family of serine/threonine kinases (which includes cyclin-dependent kinases (CDK), mitogen-activated protein kinases (MAP kinases), glycogen synthase kinases (GSK), and CDK-like kinases) and is defined by an N-terminal catalytic domain (amino acids 13–297), that is homologous to that of the other members of the CDKL family. CDKL5 is peculiar in this family of kinases as it exhibits an unusually long tail of over 600 amino acids with no obvious similarities to other protein domains but with a high degree of conservation between the different CDKL5 orthologs which differ only in the most extreme C-terminal (Fig. 3) (Kilstrup- Nielsen *et al.,* 2012).

The catalytic domain of the CDKL5 enzyme has a 12-subdomain structure of Ser/Thr kinases, the sequence of which is highly conserved among different species, from mammals to fish (Katayama *et al.,* 2016).

Considering the 12 subdomains of CDKL5, most of the mutations occur in subdomains I–IV, or between the C-terminal portion of subdomain VIA and subdomain X. Hardly any mutations have been detected between subdomain V and the first half of subdomain VIA. This suggests that subdomains I to IV and the C-terminal portion of subdomains VIA and X are particularly important for the activity of CDKL5 (Katayama *et al.,* 2020). An activation cycle, which includes the TEY sequence observed in MAPK family kinases, is present between subdomains VII and VIII of the catalytic domain. Autophosphorylation of this activation cycle is known to activate CDKL5 catalytic functions. The regulatory domain at the C-terminus of CDKL5 contains two nuclear localization signal sequences (NLS) and a nuclear export signal (NES); it has been documented that these signal sequences regulate the intracellular localization of CDKL5 in vitro (Rusconi *et al.,* 2008).

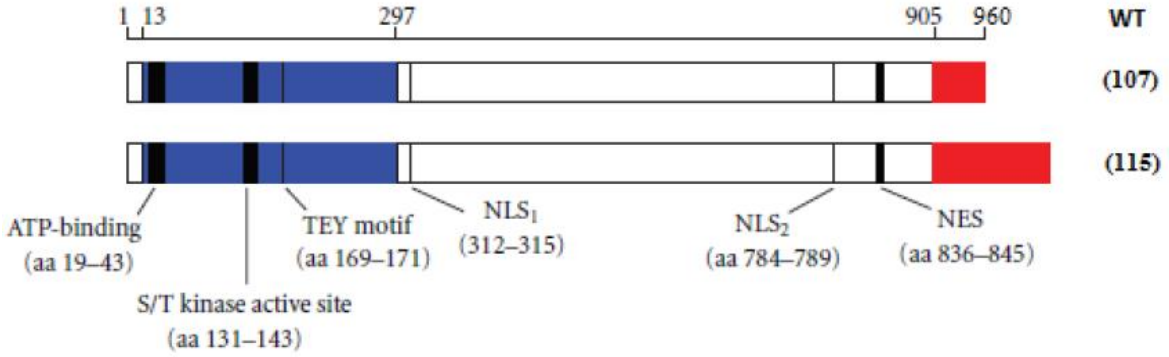

Fig. 3: Schematic image of the structure of the protein isoforms hCDKL5_1 (CDKL5107) and hCDKL5_5 (CDKL5115) (Kilstrup-Nielsen *et al.,* 2012).

2.2.2 Protein isoforms

The human *CDKL5* gene is located on the short arm of the X chromosome (Xp22), extends for a region of 228 kb and comprises 27 exons, arranged to form the 5'-UTR region (exons 1-6), the coding region (exons 2-19) and the 3'-UTR region (exons 19-22). The exons are combined into different *CDKL5* transcripts (Fig.4) by alternative splicing giving rise to five known transcription isoforms (hCDKL5_1 - hCDKL5_5) (Hector *et al.,* 2016).

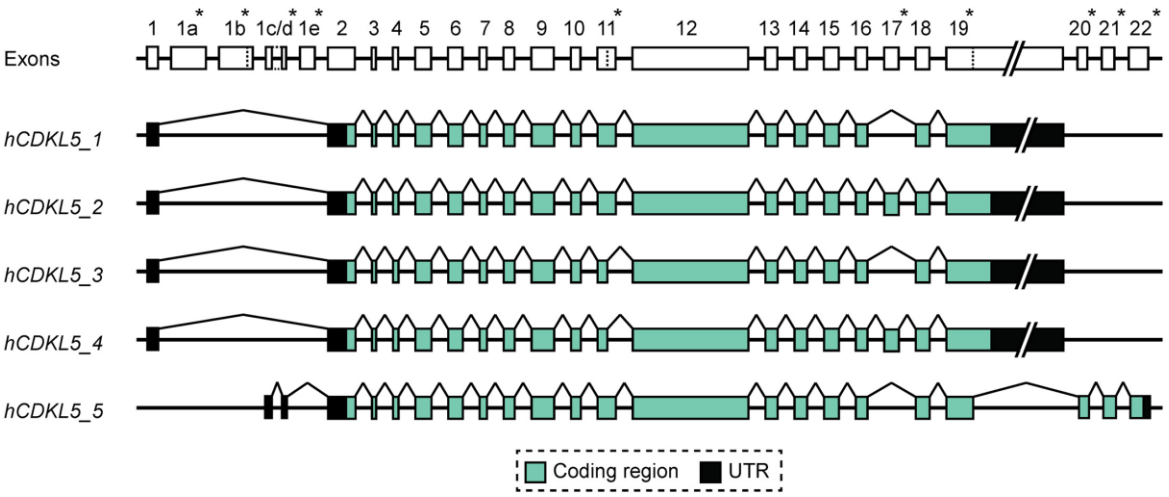

Fig.4: Human *CDKL5* gene and transcription isoforms. The splicing events are marked by lines connecting the exons while the dotted lines within the exons indicate the alternative splicing sites. The asterisks indicate the exons where differences were found between the different isoforms (Hector *et al.,* 2016).

Although the presence of the hCDKL5_1 isoform in all tissues analyzed suggests its ubiquitous character, this is also the most expressed isoform in the central nervous system. This isoform encodes the same protein as the CDKL5107 transcript reported previously (Williamson *et al.,* 2012). The hCDKL5_2 isoform is identical to hCDKL5_1 and also includes exon 17, formerly called 16a or 16b (Fichou *et al.,* 2011, Rademacher *et al.,* 2011), which forms a coding sequence of 123 bases (41 aa) that is larger than that of hCDKL5_1. The hCDKL5_3 and hCDKL5_4 isoforms are identical to hCDKL5_1 and hCDKL5_2, respectively, but lack 51 coding sequence bases at the 3' end of exon 11. The predicted protein produced by these transcripts is 17 aa shorter than hCDKL5_1 and hCDKL5_2. The three isoforms hCDKL5_2, hCDKL5_3, and hCDKL5_4 are also widely expressed but appear to be slightly less abundant than hCDKL5_1 (Hector *et al.,* 2016). In contrast to the first four isoforms, hCDKL5_5, formerly known as CDKL5115, was detected only in the testes.

For the purposes of this study, to complete the overview of CDKL5 isoforms, it is also important to mention murine isoforms. Recent data also document the existence of five major transcription isoforms containing distinct coding regions in mice. The first two isoforms have been named mCdkl5_1 and mCdkl5_2 and are orthologous to human isoforms _1 and _2, respectively. In contrast, the coding regions of the other three transcripts do not show complete orthology to human isoforms and are therefore called mCdkl5_6, mCdkl5_7 and mCdkl5_8 (Hector *et al.,* 2016).

2.2.3 Tissue expression and subcellular localization

Expression studies in human and mouse tissues have shown that *CDKL5/Cdkl5* mRNA is present in a wide range of tissues besides the brain, where transcription levels are at their highest (Kalscheuer *et al.,* 2003). Indeed, *CDKL5* mRNAs can easily be detected in tissues such as the testis, lung, spleen, prostate, uterus, and placenta, and to a lesser extent in the heart, kidneys, liver, and skeletal muscles (Kilstrup-Nielsen *et al.,* 2012). In the brain, CDKL5 expression levels have been shown to reach their peak in conjunction with the development and differentiation of this organ. In fact, CDKL5 is only weakly present during embryogenesis and is then strongly induced in the early postnatal phases up to P14 (post-natal day 14) (Rusconi *et al.,* 2008).

A detailed analysis of Cdkl5 expression in the mouse brain showed different levels of *CDKL5* mRNA in various brain regions. Specifically, its levels are particularly high in the adult

forebrain. It is interesting to note that higher levels of expression were found in the more superficial cortical layers, involved in the connection of the two hemispheres through the corpus callosum, and in the frontal cortical areas, suggesting that CDKL5 plays a role in the physiology of these brain districts. In particular, a large amount of CDKL5 has been detected in the motor cortex and cingulate cortex, an area of great interest due to it being the origin of a plethora of mental illnesses. The hippocampus, an area of the brain that partly shares the same evolutionary origin as the cortex, shows very high levels of *Cdkl5* mRNA in all CA fields. In the cerebellum, *Cdkl5* mRNA is transcribed in all lobules in Purkinje cells; its levels, however, appear to be significantly lower than in other areas of the brain (Kilstrup-Nielsen *et al.,* 2012).

At the cellular level, Cdkl5 is readily detectable in neurons while it is expressed at very low levels in the glia (Chen *et al.,* 2010). The presence of different Cdkl5 splice variants with different relative abundance depending on localization indicates that alternative splicing is part of the functional regulation of Cdkl5 (Kilstrup-Nielsen *et al.* 2012). The localization of Cdkl5 varies not only regionally in the brain, but also at subcellular levels. In fact, in the brain, it is initially predominantly cytoplasmic and then progressively accumulates in the nucleus, starting from P14 (post-natal day fourteen), when about 40% of the total Cdkl5 can be detected in this compartment. However, this localization turns out to be region-specific. In fact, Cdkl5 is significantly translocated into the nucleus only in certain areas of the brain: in the cerebellum, for example, more than 80% of Cdkl5 remains cytoplasmic while in the cortex it is almost equally distributed between cytoplasm and nucleus (Rusconi *et al.,* 2008).

Cdkl5 was also found to be present in excitatory postsynaptic structures, where it regulates dendritic spine maturation and growth, and controls excitatory synaptic function (Ricciardi *et al.,* 2012; Pizzo *et al.,* 2020). Synaptic localization of CDKL5 is mediated by its interaction with the palmitoylated form of postsynaptic density protein 95 (PSD-95) (Zhu *et al.,* 2013; Zhang *et al.,* 2014).

2.2.4 CDKL5 interactors and phosphorylation targets

To date, several different mutations have been described in the *CDKL5* gene, mainly located within the CDKL5 catalytic domain (Kilstrup-Nielsen *et al.* 2012). This strongly suggests that impaired CDKL5 kinase activity plays an important role in the pathogenesis

of this encephalopathy. Therefore, the identification of CDKL5 substrates is an important prerequisite in order to elucidate the role of CDKL5 in the brain and to identify relevant targets for therapeutic approaches.

In 2020, Katayama and colleagues listed all CDKL5 substrates identified so far (Fig. 5), however, the list is incomplete, as most kinases have many different phosphorylation targets (Katayama et al., 2020). Moreover, according to recent studies, the localization of CDKL5 depends on the cell cycle. Therefore, CDKL5 localization is believed to be constantly evolving. These changes allow CDKL5 to phosphorylate a variety of proteins located in the various cell compartments (Barbiero *et al.,* 2017).

Substrate	Localisation	Phosphorylation site(s)	Detection of phosphorylated protein	CDKL5 form
MeCP2	Nucleus	Not determined	*In vitro*	Full length and catalytic
Dnmt1	Nucleus	Not determined	*In vitro*	Catalytic
NGL-1	Plasma membrane	RMNS^{631}KDN	*In vitro*	Full length
Amph1	Cytoplasm	*Mus musculus*: RPRS^{293}PSQ *Danio rerio*: RPTS^{285}PGP and RPKS^{293}PSQ	*In vitro*	Full length and catalytic
HDAC4	Cytoplasm and nucleus	RAQS^{632}SPA	*In vitro*	Full length
MAP1S	Cytoplasm	*Mus musculus*: RPSS^{786}ASA and RPLS^{812}ARS *Homo sapiens*: RPLS^{900}ARS	*In vitro* and *in vivo*	Full length
CEP131	Cytoplasm (centrosome)	RPGS^{35}AAT	*In vitro*	Full length
DLG5	Cytoplasm	RPKS^{1115}APS	*In vitro*	Full length
ARHGEF2	Cytoplasm	RPTS^{122}AIY	*In vitro*	Full length
EB2	Cytoplasm	RPSS^{222}AKR	*In vitro* and *in vivo*	Full length
SMAD3	Cytoplasm and nucleus	Not determined	*In vitro*	Full length

Fig. 5: Substrates of CDKL5 (Katayama *et al.,* 2020)

The main substrates known to date are briefly analyzed below (Fig. 5). One of the most studied substrates/interactors of CDKL5 is MeCP2, due to the common history of the two proteins. In 2005, it was first reported that, in vitro, CDKL5 phosphorylates MeCP2 (Mari *et al.,* 2005). Since *MeCP2* is the primary etiological gene of Rett syndrome, assessing the biological significance of CDKL5-mediated phosphorylation of MeCP2 is important in order to identify the common physio-pathology between Rett syndrome and CDD at the molecular level. Despite this early evidence, it was then found that CDKL5 phosphorylates MeCP2 only weakly (Sekiguchi *et al.,* 2013). Based on these currently discordant results, further analysis of the association between these two proteins is required.

In 2008, Kameshita and colleagues discovered that the catalytic fragment of CDKL5 phosphorylates DNA methyltransferase 1 (Dnmt1) *in vitro*. Since Dnmt1 preferentially methylates hemimethylated DNA, it might act to maintain genome methylation patterns

across the replication cycle (Yoder *et al.,* 1997). CDKL5 phosphorylation sites are located at the N-terminus of Dnmt1 (residues 1–290), but the specific location of these sites remains unknown (Kameshita *et al.,* 2008). The significance of phosphorylation of Dnmt1 by CDKL5 remains to be identified; it is possible that phosphorylation of Dnmt1 by CDKL5 may also regulate its DNA-methylation ability, thereby epigenetically controlling the expression of various genes (Katayama *et al.,* 2020).

Further research has shown that Ser-631 of the netrin-G1 ligand protein (NGL-1, also known as LRRC4C) is phosphorylated by CDKL5 in vitro (Ricciardi *et al.,* 2012). NGL-1 is a membrane protein localized at the postsynaptic level, binding the presynaptic protein netrin-G1 (NTNG1), and it plays an important role in the formation of neural circuits (Lin *et al.,* 2003). Since mutations of *CDKL5* and *NTNG1* genes cause a severe neurodevelopmental disorder with clinical features that are closely related to Rett syndrome (RTT), it is highly plausible that CDKL5 and NGL-1 might work, at least in part, in a common pathway, thus providing a molecular framework that explains the similar neuropathological outcome of *NTNG1* and *CDKL5* mutations (Ricciardi *et al.,* 2012).

In 2015, by using a unique substrate search method involving isoelectric focusing electrophoresis, Sekiguchi *et al.* discovered that Ser-293 of amphiphysin 1 (Amph1), a protein involved in clathrin-mediated endocytosis, is phosphorylated by CDKL5 *in vitro*. Because phosphorylation of Ser-293 of Amph1 inhibits its ability to bind the endocytosis-related factor endophilin, CDKL5 phosphorylation of Amph1 is thought to suppress endocytosis. The CDKL5 interactor Amph1, and its non-phosphorylated homologue Amph2, were used *in vitro* to investigate the molecular mechanisms of substrate recognition. In the study in question, RPXSX emerged as a putative consensus sequence (Katayama *et al.,* 2015).

In 2016, histone deacetylase 4 (HDAC4) was identified as an *in vitro* CDKL5 substrate (Trazzi *et al.,* 2016). By catalyzing histone deacetylation, HDAC4 regulates the expression of many different genes. In addition, by responding to stimulation via the N-methyl-D-aspartate (NMDA) receptor, a typical glutamate receptor, HDAC4 ensures the survival of nerve cells and is involved in various aspects of their functions. Interestingly, HDAC4 contains the RPXSX consensus site.

Very recently, two different research groups independently performed comprehensive screening for CDKL5 substrates and identified several candidate protein substrates. Among

these, both groups identified microtubule associated protein 1S (MAP1S) as a possible substrate. In addition to MAP1S, both groups also identified centrosomal protein of 131kDa (CEP131), disc large membrane-associated guanylate kinases scaffold protein 5 (DLG5), and Rho/Rac guanine nucleotide exchange factor 2 (ARHGEF) as *in vitro* CDKL5 substrates. Moreover, a microtubule-associated protein RP/EB family member 2 (EB2) was identified as an *in vivo* CDKL5 substrate. EB2 is one of the microtubules plus-end tracking proteins that may be involved in microtubule reorganization (Muñoz *et al.,* 2018; Baltussen *et al.,* 2018). A minimal CDKL5 phosphorylation consensus for the amino acid sequence RPX[S/T][A/P] emerged in both papers, confirmed biochemically with model peptide substrates. Interestingly, this is the first *in vitro* evidence that CDKL5 is also able to phosphorylate Thr residue, albeit to a much lesser extent.

Last, in 2019, Fuchs and colleagues found that CDKL5 phosphorylates SMAD3 *in vitro*. SMAD3 is a transcription factor that plays a central role in neuronal function mediated by transforming growth factor-*β* signaling. The authors showed that protein levels of SMAD3 are reduced in the cortex and hippocampus of the *Cdkl5* KO mouse (Fuchs *et al.,* 2019).

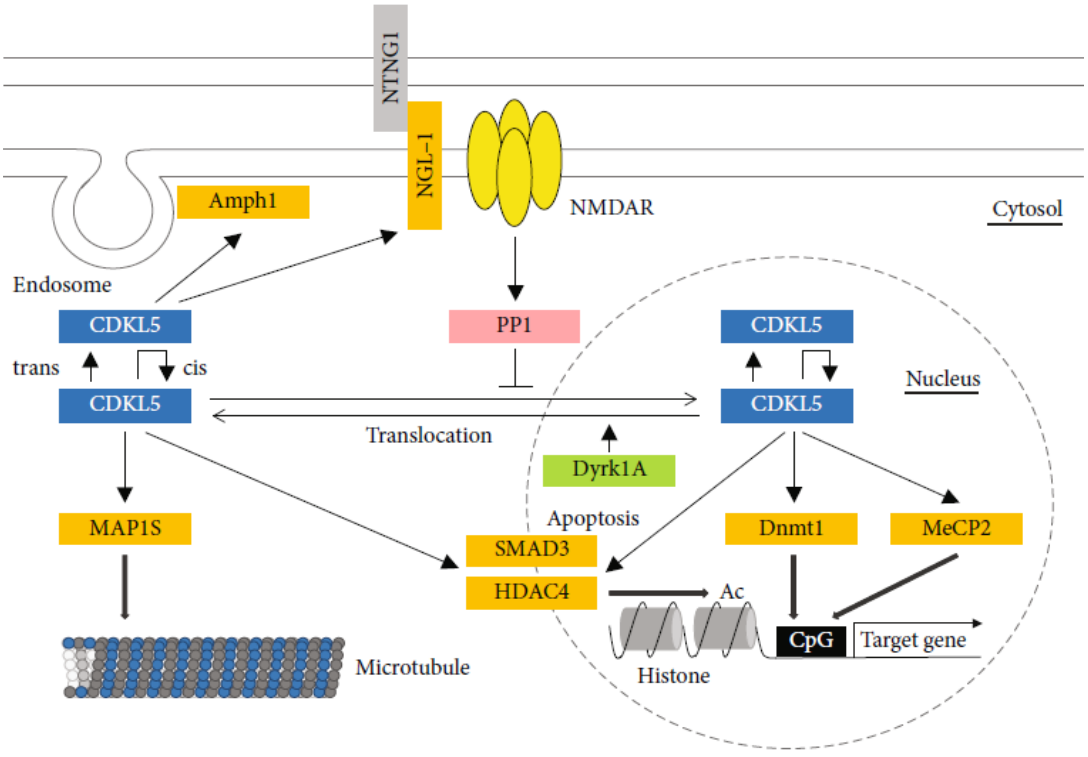

Fig. 6: CDKL5 and phosphorylation pathways (Katayama *et al.,* 2020).

2.2.5 Signaling modulated by CDKL5

Similar to the protein interaction network of CDKL5, much remains to be understood as to its functions in downstream signaling pathways. The development of *Cdkl5* KO mice has enabled an initial discovery of several intriguing signaling changes. Through kinome profiling study, Wang and colleagues demonstrated that several signaling transduction pathways involved in neuronal and synaptic plasticity are disrupted in the forebrain of *Cdkl5* KO male mice (Wang *et al.,* 2012), with changes in the phosphorylation profiles of AMPK, AKT, PKC, and MAPK substrates. These pathways represent a convergent network downstream of PTEN signaling, which has previously been implicated in the etiology of several neurodevelopmental disorders such as autism, RTT, FXS, and Tuberous Sclerosis (Crino, 2011; Chen *et al.,* 2014). Similarly, Amendola *et al*. found a decrease in the phosphorylation of AKT Ser473 and rpS6 Ser240/244 in several brain structures (cortex and hippocampus) of hemizygous male and heterozygous and homozygous female *Cdkl5* KO mice (Amendola *et al.,* 2014). A further characterization of AKT-dependent pathways showed a disruption of AKT-GSK3β signaling in *Cdkl5* KO mice (Fuchs *et al.,* 2014; Fuchs *et al.,* 2015).

Given its putative synaptic localization and functions, it is likely that CDKL5 also regulates one or more aspects of synaptic transmission. Recent work by Okuda *et al.* (Okuda *et al.,* 2017) demonstrated an alteration in N-methyl-D-aspartate (NMDA) receptor subunit composition at the CA1 hippocampal glutamatergic synapses of *Cdkl5* KO mice. Specifically, KO mice had increased GluN2B levels at the post-synaptic density fractions, with unaltered GluN1 and GluN2A levels, resulting in an overall enhancement of NMDA-dependent signaling. This finding was also associated with increased levels of SAP-102, a scaffolding protein that regulates the membrane localization of GluN2B. However, the direct role of CDKL5 within the SAP-102-GluN2B pathway and the mechanism of dysregulation in *Cdkl5* KO mice require further investigation.

2.2.6 Modulation of CDKL5 activity

The activity of many protein kinases is regulated through autophosphorylation and phosphorylation by upstream kinases. CDKL5 contains an activation loop characteristic for MAPK and CDK, which contains the sequence ANYTEYVAT. While it is believed that these residues are auto phosphorylated, the question as to whether this process is truly

important for kinase activation has long remained open (Lin *et al.,* 2005). Recently, Muñoz *et al.* analyzed the TEY motif of CDKL5 and found that substitution of the Tyr-171 residue with Ala substantially lowers CDKL5 activity in vitro. Nevertheless, the importance of the Thr residue phosphorylation of the TEY motif remains unknown (Muñoz *et al.,* 2017).

Recently, Oi *et al*. found that Dyrk1a phosphorylates CDKL5 *in vitro* (Oi *et al.,* 2017). Because DYRK1a is located in a region of chromosome 21 that is critical for Down syndrome, it is believed to be closely involved in the abnormal neurodevelopment observed in the condition (Nakano-Kobayashi *et al.,* 2017). Dyrk1a phosphorylates the Ser-308 residue of CDKL5, located near the NLS1 sequence, inhibiting CDKL5 nuclear localization. CDKL5 accumulates in the nucleus (by translocating from the cytoplasm) as part of the developmental process, and it has been revealed that *in vitro* NMDA stimulation causes CDKL5 translocation from the nucleus to the cytoplasm (Rusconi *et al.,* 2008; Rusconi *et al.,* 2011).

In 2015, La Montanara *et al*. showed that CDKL5 is dephosphorylated upon in vitro NMDA stimulation and that this process is catalyzed by protein phosphatase 1 (PP1) (La Montanara *et al.,* 2015). Since NMDA receptor-mediated signaling increases cytoplasmic localization of CDKL5 in hippocampal neurons (Rusconi *et al.,* 2011), it is believed that PP1-mediated dephosphorylation confines CDKL5 to the cytoplasm. It is also apparent that long-term neural activity induces CDKL5 expression and degradation, and that the responsiveness of KCl stimulation is dependent on neuronal maturity in vitro, suggesting a relationship between these mechanisms of CDKL5 regulation. Detailed knowledge of CDKL5 activity will promote the development of new therapeutic approaches to CDD and further elucidate the mechanisms underlying neuronal development and function (Katayama *et al.,* 2020) (Fig. 6).

2.3 CDD models

Given the complexity and lack of knowledge of this condition, CDD models are fundamental allies in increasing the chances of finding effective therapeutic approaches. Below are described the cellular and *in vivo* models developed so far.

2.3.1 Cellular models: hippocampal neurons and neuroblastoma cell lines

Neuronal synapses are densely packed in the brain, making them difficult to analyze and visualize individually *in vivo*. The most obvious advantage of dissociated neuronal culture is that it makes individual living cells and their synapses more accessible. Dissociated neurons will grow as a monolayer and the surface-expressed neurotransmitter receptors and other membrane proteins are therefore accessible for both immunocytochemical and biochemical analysis. Hippocampal neurons in dissociated cultures retain their characteristics, from the properties of the transmitter receptors and ion channels they express, to the organization of their cytoskeletal constituents and the characteristics of specific synapses. This is due to the fact that they are postmitotic and are therefore committed in their differentiation at the time they are introduced into culture. Primary hippocampal neuronal cultures have been extensively used to understand the formation and development of synapses (Morales-Garcia *et al.,* 2012).

RNA interference in cultured primary neurons has shown that CDKL5 regulates neuronal outgrowth and migration by forming a complex with the RhoGTPase Rac1, a known regulator of actin dynamics and neuronal morphology, and is required for brain-derived neurotrophic factor (BDNF)-induced activation of Rac1 (Chen *et al.,* 2010). Through an analogous knockdown approach, Ricciardi and colleagues demonstrated that CDKL5 is required for correct spine maturation and stability; it directly phosphorylates the cell adhesion molecule NGL-1, therefore promoting a stable association between NGL-1 and postsynaptic density protein-95 (PSD-95) (Ricciardi *et al.,* 2012). Interestingly, defects in neuronal maturation, spine density, and synaptic connectivity are present in primary hippocampal cultures from *Cdkl5* KO mice (Trazzi *et al.,* 2016). Importantly, defects in dendritic spine formation and synaptic connectivity are consistent with cellular phenotypes described in neurons derived from induced pluripotent stem cells reprogrammed from patients' fibroblasts (see below), suggesting that spine and synaptic abnormalities are likely to be present in CDKL5 patients (Ricciardi *et al.,* 2012).

An elegant study carried out by Valli and colleagues in 2012, before the creation of *Cdkl5* KO mouse models, took advantage of neuroblastoma cell cultures (SH-SY5Y and SKNBE cell lines) to study CDKL5 functions *in vitro*. Neuroblastoma cells share several features with normal neurons and thus are considered a good *in vitro* model with which to study the

biochemical and functional properties of neuronal cells, particularly when they are induced to differentiate following treatment with agents such as retinoic acid. The authors described a correlation between CDKL5 expression and SH-SY5Y differentiation: differentiating SH-SY5Y neuroblastoma cells exhibited strong up-regulation of CDKL5 expression. Conversely, over-expression of CDKL5 protein in SH-SY5Y cells was shown to promote neuronal differentiation (Valli *et al.,* 2012). Consistently with these data, it was observed that CDKL5 negatively regulates cell proliferation in the SH-SY5Y neuroblastoma cell line by arresting the cell cycle in the G0/G1 phases. Neuronal proliferation and differentiation represent two closely related processes which are of primary importance during brain development. Interestingly, CDKL5 expression was shown to be inhibited by MYCN, a transcription factor that promotes cell proliferation during brain development and plays a relevant role in neuroblastoma biology (Valli *et al.,* 2012).

In 2020, Loi and colleagues generated a human cellular model of CDD, CRISPR-induced *CDKL5* KO SH-SY5Y cells, starting from the human neuroblastoma cell line SH-SY5Y (Loi *et al.,* 2020). Loi and colleagues demonstrated that CDKL5 deletion in human neuroblastoma SH-SY5Y cells not only impairs neuronal maturation but also reduces cell proliferation and survival. Furthermore, CDKL5-deficient cells were hypersensitive to DNA damage-associated stress, accumulated more DNA damage foci (γH2AX positive), and were more prone to cell death than controls (Loi *et al.,* 2020). This study suggests that CDKL5 plays a role in DNA damage response that was previously unknown, and that could underlie the pro-survival function of CDKL5.

2.3.2 iPSC and cortical organoids

The development of induced pluripotent stem cells (iPSCs) offered an unprecedented opportunity for the creation of patient and disease-specific human cellular models. iPSCs are similar to human embryonic stem cells (hESCs) in morphology, proliferation, gene expression, and in vitro differentiation potential (Amenduni *et al.,* 2011). Like hESCs, they can be expanded indefinitely and differentiated in vitro into many different cell types (Takahashi *et al.,* 2007). These features make them the ideal tool with which to study disease mechanisms directly on the primary affected cells. Up to now, iPSCs have been successfully derived from patients with both neurodegenerative (ALS, SMA, Parkinson, HD,

FD) and neurodevelopmental (FRAXA, PW-AS) disorders, and neuronal differentiation has been performed.

In 2012, Ricciardi and colleagues, using IPS-derived cells from two different patients, discovered that CDKL5 mainly localizes to dendritic spines where it is juxtaposed to the PSD. The results revealed that CDKL5 is a key limiting factor in regulating glutamatergic synapse formation and suggest that changes in excitatory synaptic strength might be responsible, at least in part, for the neurodevelopmental symptoms associated with its deficiency (Ricciardi *et al.,* 2012).

Another recent study carried out by the University of Siena (Livide *et al.,* 2015), correlates CDKL5 to neuronal differentiation. Using induced pluripotent stem (iPS) cells derived from fibroblasts CDKL5-mutated patients, the authors showed that neurons with CDKL5 mutation have an altered *GRID1* gene expression. *GRID1* encodes for glutamate D1 receptor and it is a member of the delta family of ionotropic glutamate receptors which is involved in neuronal maturation. It does not form AMPA or NMDA glutamate receptors, yet it acts like an adhesion molecule by linking the postsynaptic and presynaptic compartments, preferentially inducing the inhibitory presynaptic differentiation of cortical neurons. The results demonstrated that GRID1 expression is down-regulated in CDKL5-mutated iPS cells and up-regulated in neuronal precursors and mature neurons (Livide *et al.,* 2015). The available data point to GRID1 playing a role in neuronal maturation, since both Glutamate and GABA ionotropic receptor subunits and functional receptor channels are expressed very early on during brain development in proliferating neuroepitelial cells and are considered important for events such as precursor proliferation, migration, differentiation, and survival. It is thus possible that an alteration of GluD1 levels in precursor cells might influence one of these processes and result in the alteration of subsequent brain development. In conclusion, there is strong evidence that demonstrates that loss of CDKL5 in IPS severely affects spine morphology and reduces functional synaptic contacts, thus impairing neuronal activity (Livide *et al.,* 2015).

In 2021, Negraes and colleagues performed a proteomic and phosphoproteomic characterization of induced pluripotent stem cell (iPSC)-derived neural cells and cortical organoids, and found a dysregulation of the pathways involved in neural development, of cytoskeleton-related proteins and of connectivity (Negraes *et al.,* 2021). In line with the molecular alterations, they observed consistent proliferation and viability phenotypes in

neural progenitor cells (NPCs), and alterations in the morphology and synaptogenesis of cortical excitatory neurons. The dynamic recording of CDD neural networks in cortical organoids revealed early hyperexcitation caused by the intrinsic electrophysiological properties of glutamatergic neurons, and an overly synchronized network (Negraes *et al.,* 2021). This hyperexcitability of CDD cortical neurons could explain the occurrence of seizures early on in the life of CDD patients (Wang *et al.,* 2021).

2.3.3 Animal models

Animal models allow the study of the pathological and physiological mechanisms underlying diseases. In particular, the mouse has become the most commonly used model organism in human disease research. Compared to other mammals, a mice colony has a low maintenance cost and is simple to breed in captivity. Among the many reasons for the privileged position of mice are, of course, the genetic proximity to humans with whom they share 99% of their genes, and the possibility of manipulating their genomes to generate models of human pathologies. The mouse, therefore, can be subjected to biomedical experimentation, preliminary to testing in humans. Human diseases that mice usually do not contract can be studied thanks to experimental approaches used to "humanize" the physiology of the mouse thus mimicking the clinical manifestations of the disease to be studied (Rosenthal *et al.,* 2007). In the specific case of CDD, the use of mouse models as a starting point for the study of the human disease is supported by the fact that the CDKL5 coding sequence is well preserved across the two species. In fact, the murine Cdkl5 gene is orthologous to the human one (Hector *et al.,* 2016).

Several KO mouse models for Cdkl5 have been created and extensively characterized over the years using site-specific Cre-Lox recombinase technology (Amendola *et al.,* 2014, Wang *et al.,* 2012, Okuda *et al.,* 2017). In particular, a premature stop codon was inserted in these models: in exon 6 (Wang *et al.,* 2012; Jhang *et al.,* 2017), in exon 4 (Amendola *et al.,* 2014), or in exon 2 (Okuda *et al.,* 2017) of the Cdkl5 gene, thus causing a mutation within the N-terminal catalytic domain of the kinase with loss of function.

In addition to constitutive models, three *Cdkl5* conditional KO mouse models provide further insight into the cellular origins of CDKL5 deficiency-related symptoms (Amendola *et al.,* 2014; Tang *et al.,* 2017). Amendola *et al*. crossed mice carrying a Cre-conditional *knockout* (*c*KO) allele of *Cdkl5* either with the Dlx5/6::Cre transgene (to ablate Cdkl5

expression specifically from cortical GABAergic neurons; e.g., cortical interneurons, striatal medium spiny neurons) or the Emx1::Cre transgene (to ablate Cdkl5 expression specifically from cortical glutamatergic neurons; e.g., cortical and hippocampal pyramidal neurons) (Amendola *et al.,* 2014). Similarly, Tang and colleagues created an additional conditional KO mouse line in which CDKL5 loss is restricted to forebrain glutamatergic neurons or to GABAergic neurons (Tang *et al.,* 2017).

Behavioral features

To date, two constitutive KO mouse models of CDKL5 deficiency have undergone detailed behavioral phenotyping (Wang *et al.,* 2012; Amendola *et al.,* 2014; Jhang *et al.,* 2017). The *Cdkl5* KO mouse exhibits numerous behavioral deficits that are reminiscent of human symptomatology across motor, sensory, cognitive, and socio-emotional domains.

Motor dysfunction is a prominent feature of CDKL5 deficiency, with the majority of patients having some degree of impairment in gross and fine motor skills, including sitting, standing, walking, and grasping (Fehr *et al.,* 2015). Similarly, motor function has been consistently found to be altered in Cdkl5 constitutive KO mice (Wang *et al.,* 2012; Amendola *et al.,* 201; Jhang *et al.,* 2017 PsychoGenics). Hind-limb clasping, a phenotype that is reminiscent of hand-wringing in CDD patients and related neurodevelopmental disorders, is found in a significant fraction of *Cdkl5* KO mice and appears to increase in prevalence during development (Wang *et al.,* 2012; Amendola *et al.,* 201; Jhang *et al.,* 2017 PsychoGenics). Impaired motor coordination, as evaluated using the accelerating Rotarod assay, has also been a reproducible finding, although KO mice appear to retain some capability to improve over multiple trials (Wang *et al.,* 2012; Amendola *et al.,* 201; Jhang *et al.,* 2017). With regard to locomotor activity, KO mice appear to be hyperactive in novel environments in the context of various behavioral assays (Wang *et al.,* 2012; Jhang *et al.,* 2017), but hypoactive in a familiar home-cage setting with extended monitoring (Amendola *et al.,* 2014).

Severe intellectual disability is a central feature of human CDKL5 deficiency (Bahi-Buisson *et al.,* 2008). Similarly, mouse models of CDKL5 deficiency have reproducibly demonstrated an impairment in various learning and memory tasks (Wang *et al.,* 2012; Fuchs *et al.,* 2014; Fuchs *et al.,* 2015; Trazzi *et al.,* 2016; Tang *et al.,* 2017; Jhang *et al.,* 2017). These include tasks that are highly hippocampal-dependent, including the Barnes maze, Morris water maze, and contextual fear conditioning, as well as working memory tasks that are also

likely to involve additional brain regions. Interestingly, these deficits are recapitulated in a conditional KO mouse line in which CDKL5 loss is restricted to forebrain glutamatergic neurons, suggesting that CDKL5 exerts a key function in this neuronal population (Tang *et al.,* 2017).

Many CDKL5 deficiency patients also exhibit features that are characteristic of autism spectrum disorders and attention-deficit/hyperactivity disorder (Fehr *et al.,* 2015). These include impaired social and communication deficits, stereotypic behaviors, and hyperactivity. Cdkl5 constitutive KO mice consistently demonstrate socio-emotional deficits that are reminiscent of these aspects of human symptomatology (Wang *et al.,* 2012; Jhang *et al.,* 2017; PsychoGenics). These include reduced preference for social interaction in the classic three-chamber assay, increased stereotypic digging and grooming behaviors, alterations in ultrasonic vocalizations, reduced anxiety, and aggressive behaviors (Jhang *et al.,* 2017).

In the past few years Tang and colleagues have developed different conditional mouse models. In 2017 they uncovered the cellular origins of learning and memory impairment in a mouse model of CDD through the generation of a forebrain excitatory neuron-specific *Cdkl5* knock-out line (Nex-*c*KO). Nex-*c*KO mice demonstrate impaired hippocampal-dependent memory, along with context-dependent hyperactivity and hindlimb clasping. At the cellular level, altered neuronal morphology in Nex-*c*KO mice was observed to be accompanied by increased spontaneous excitatory and inhibitory synaptic activity, leading to altered spatiotemporal dynamics in the CA1 microcircuit that is relevant to learning and memory. Together, these findings reveal the glutamatergic origins of learning and memory impairment in CDKL5 deficiency and support the novel premise that CDKL5 plays a role in regulating synaptic and circuit function in glutamatergic neurons (Tang *et al.,* 2017).

In 2019, the authors selectively ablated CDKL5 expression in murine forebrain GABAergic neurons (Dlx-*c*KO), finding that these mice exhibit an autistic-like phenotype, but, in contrast to Nex-*c*KO mice, show preserved learning and memory. In addition, Dlx-*c*KO mice show an enhancement of excitatory synaptic transmission and circuit-level hyperexcitability, coupled with elevated levels of NMDA receptors. Reducing NMDAR activity using an uncompetitive antagonist, memantine, significantly mitigated the behavioral deficits found in Dlx-*c*KO mice. To examine the translational potential of these findings, Tang et al. generated a novel CDD model bearing a patient mutation, CDKL5 R59X,

and found that these mice, similarly to Dlx-*c*KO mice, show an elevation of NMDA receptors. Taken together, our findings support a novel mechanism through which CDKL5 loss in GABAergic neurons leads to excessive NMDAR signaling and contributes to the etiology of autistic-like behaviors in mouse models of CDD (Tang *et al.,* 2019).

Neurophysiological features

Sleep and respiratory abnormalities are also commonly reported features of CDKL5 deficiency (Hagebeuk *et al.,* 2013; Mangatt *et al.,* 2016). These features have also been found in *Cdkl5* KO mice, which exhibit increased numbers of sleep apneas in both NREM and REM sleep (Lo Martire *et al.,* 2017).

Although female CDKL5 deficiency patients far outnumber their male counterparts, recent studies have begun to reveal similarities and differences between the sexes (Fehr, *et al.,* 2015). Although epilepsy appears to be a nearly universal feature, male patients appear to have more severe developmental delay, particularly with regards to motor function, with a smaller proportion of male patients attaining the ability to sit, stand, walk, grasp, and babble. Mouse studies have largely reflected this trend, with heterozygous female KO mice showing somewhat milder deficits in comparison to homozygous female and hemizygous male KO mice (Amendola *et al.,* 2014; Fuchs *et al.,* 2014; Fuchs *et al.,* 2018).

Studies in two independent CDKL5 deficient mouse lines indicate significant abnormalities in both auditory and visual evoked potentials (AER and VEP respectively) (Wang *et al.,* 2012; Amendola, *et al.,* 2014; Mazziotti *et al.,* 2017). Cortical visual response is severely impaired both in hemizygous males and heterozygous females (Mazziotti *et al.,* 2017), supporting the idea that CDKL5 is needed for the proper functioning of cortical circuits.

Recently, using a conditional *Cdkl5* KO model, Lupori and colleagues demonstrated that selective cortical deletion of CDKL5 from excitatory cells is sufficient to produce abnormalities in visual cortical responses, demonstrating that the normal functioning of cortical circuits is dependent on CDKL5 (Lupori *et al.,* 2019).

Interestingly, in 2020 La Montanara and colleagues found that CDKL5 is required for CaMKII-dependent TRPV1 signaling and outgrowth of sensory neurons in both murine and human CDD neurons. In vivo, in a CDD animal model, this translates into impaired capsaicin-dependent nociceptive signaling and behavioral responses as well as in reduced epidermal innervation (La Montanara *et al.,* 2020).

Epileptic features

Although early onset epileptic seizures and infantile spasms are a hallmark clinical feature of CDKL5, spontaneous seizures have not been reported in three independently generated lines of constitutive *Cdkl5* KO mice (Wang *et al.,* 2012; Amendola *et al.,* 2014; Okuda *et al.,* 2017) or in conditional *Cdkl5* KO lines restricting deletion to forebrain glutamatergic neurons (Tang *et al.,* 2017) or forebrain GABAergic neurons (Amendola *et al.,* 2014). However, abnormal EEG responses and altered seizure susceptibility to convulsant treatments were observed in different *Cdkl5* KO models. Amendola *et al*. observed that high-dose kainic acid induced tonic-clonic seizures and epileptiform EEG activity in both hemizygous *Cdkl5* KO and wild-type mice (Amendola *et al.,* 2014). Although latency to seizures was similar between genotypes, *Cdkl5* KO mice showed a greater mean duration of high amplitude bursts, although the frequency was significantly lower compared to their wild-type littermates. In addition, *Cdkl5* KO mice appeared to exhibit increased low frequency-band EEG power in response to kainic acid.

Another study showed increased seizure susceptibility in *Cdkl5* KO mice in response to NMDA (52.5 mg/kg at 4 weeks of age; 60 mg/kg at 13-15 weeks of age) (Okuda *et al.,* 2017). Interestingly, the NMDA-induced seizure enhancement in *Cdkl5* mutant mice was rescued by ifenprodil, a GluN2B-selective NMDAR antagonist, suggesting that upregulation of GluN2B in *Cdkl5* mutants might be responsible for the enhanced seizure susceptibility. It is relevant to note that this group did not find a significant difference in seizure susceptibility to kainic acid. In the wake of this study, it was recently shown that NMDA-treated heterozygous Cdkl5 female mice showed increased seizure persistence compared to their wild-type counterparts (Galvani *et al.,* 2021).

Interestingly, two more recent studies have shown recurrent spontaneous seizures in *Cdkl5* KO mice (Wang *et al.,* 2021; Terzic *et al.,* 2021). Using conditional KO mouse lines allowing Cdkl5 deficiency in glutamatergic or GABAergic neurons, Wang and colleagues demonstrated that mice that were Cdkl5-deficient in the glutamatergic neurons (Emx1- and CamK2α-derived *Cdkl5* cKO mice) manifest high-frequency spontaneous seizure activities recapitulating the epilepsy of CDD patients, which ultimately leads to sudden death in mice (Wang *et al.,* 2021). In contrast, Cdkl5 deficiency in GABAergic neurons does not generate such seizures.

Evidence of spontaneous seizure activity has recently been described in heterozygous Cdkl5 female mice (*Cdkl5* KO mice and CDKL5 R59X knock-in mice), but this phenotype appears only with aging, with a median onset at around 28 weeks of age (Terzic *et al.,* 2021). Similar seizure-like events are not observed in hemizygous KO male or homozygous KO female littermates, suggesting that X-linked cellular mosaicism is a driving factor underlying these seizure-like events.

Neuroanatomical features

Loss of Cdkl5 function causes severe dendritic hypotrophy. In *Cdkl5* KO mice with Cdkl5 exon 4 deletion, the total length of dendrites in CA1 pyramidal neurons of the hippocampus, cortex and granular cells of the dentate gyrus is significantly reduced compared to control mice (Amendola *et al.,* 2014; Fuchs *et al.,* 2014; Fuchs *et al.,* 2015). In another line of *Cdkl5* KO mice (with the deletion of exon 6), the dendritic complexity of the CA1 pyramidal neurons was decreased, but the total length of the dendrites remained unchanged compared to control mice (Tang *et al.,* 2017). This suggests that the presence of the Cdkl5 protein was not only necessary but also sufficient to promote the growth of dendrites. In fact, when Cdkl5 is over-expressed in neuronal cultures, an increase in the total dendritic length occurs (Chen *et al.,* 2010). Thus, CDKL5 appears to play a role in the signaling pathway that controls dendritic growth, but the mechanism by which it carries out this control on dendrite morphogenesis is not yet fully understood (Zhu & Xiong, 2019). Furthermore, *Cdkl5* KO mice show changes in the organization and stability of dendritic spines, as well as in the density of PSD-95 dendritic clusters in several brain structures (somatosensory and visual cortex, and hippocampus) (Della Sala *et al.,* 2016; Fuchs *et al.,* 2015; Trazzi *et al.,* 2016; Pizzo *et al.,* 2016), suggesting that CDKL5 deficiency leads to alterations of structural synaptic plasticity in excitatory circuits. In particular, repeated in vivo imaging shed light on the mechanisms underlying dendritic spine alterations in *Cdkl5* KO male mice (Della Sala *et al.,* 2016). Della Sala and colleagues showed that reduced spine density in Cdkl5 mutants is primarily due to an imbalance in the processes of spine formation and spine elimination. *Cdkl5* mutant mice are characterized by an enhanced spine elimination, starting from early postnatal stages to adulthood, suggesting that CDKL5 is important for synaptic stabilization throughout the entire lifespan (Della Sala *et al.,* 2016). However, in conditional KO mice, in which *Cdkl5* was specifically deleted in excitatory neurons of the forebrain, a trend toward increased density and volume of

dendritic spines was observed (Tang *et al.,* 2017). The cause of this discrepancy is unclear: it is possible that gene deletion in large cell clusters may trigger compensatory mechanisms that complicate phenotype analysis following loss-of-function mutations in single cells (Zhu & Xiong, 2019). In conclusion, the deficits in dendritic spine formation observed in mice that are KO for Cdkl5 collectively indicate the role of Cdkl5 in both dendritic development regulation and synapse formation. Importantly, CDKL5 deficiency affects synaptic organization and experience-dependent plasticity.

Few studies have investigated the functional consequences of the morphologic changes described above *in vivo* (Della Sala *et al.,* 2016; Okuda *et al.,* 2017; Ren *et al.,* 2019). In *Cdkl5* KO mice, long term potentiation (LTP) and the frequency of miniature excitatory postsynaptic currents, an indicator of the level of excitatory synaptic transmission, are altered (Della Sala *et al.,* 2016; Ren *et al.,* 2019). Recent immunohistochemical studies have revealed changes in both excitatory and inhibitory synaptic marker density (Pizzo *et al.,* 2016; Sivilia *et al.,* 2016; Gennaccaro *et al.,* 2021b). The higher number of GABAergic terminals in the cortex of *Cdkl5* KO compared to wild-type mice suggests that increased inhibitory transmission might contribute to LTP impairment (Gennaccaro *et al.,* 2021b). Interestingly, the recent finding that CDKL5 is involved in sensory-induced plasticity of both excitatory and inhibitory synapses in the barrel cortex (Pizzo *et al.,* 2020) indicates that CDKL5 deficiency alters both excitation and inhibition and suggests that the delivery of sensory inputs to the cortex might be less efficient in CDD.

CDKL5 has been shown to regulate both in vitro and in vivo cell survival (Loi *et al.,* 2020; Fuchs *et al.,* 2019; Fuchs *et al.,* 2014). It has been demonstrated that in the postnatal developing mouse hippocampus, loss of Cdkl5 increases the proliferation rate of neuronal precursors but causes the death of immature newborn neurons, thereby modulating the intricate balance between precursor proliferation and survival (Fuchs *et al.,* 2014). CDKL5 deletion in human neuroblastoma cells induces an increase in cell death and in DNA damage-associated biomarkers (Loi *et al.,* 2020). During brain aging, loss of Cdkl5 was found to decrease neuronal survival in different brain regions such as the hippocampus, cortex, and basal ganglia in *Cdkl5* KO mice, and this was paralleled by an increased neuronal senescence (Gennaccaro *et al.,* 2021a). Moreover, it was demonstrated that CDKL5 deficiency increases the vulnerability of neural cells to different neurotoxic/excitotoxic stimuli, suggesting that *CDKL5* mutations have an endangering

action that is likely to sensitize neurons in the brain to neurotoxic conditions known to promote neuronal death.

Neuroinflammatory processes are known to contribute to neuronal dysfunction and death. When over-activated in response to neuronal damage and to genetic or environmental factors, microglia, the brain macrophages (Ginhoux *et al.,* 2013), cause widespread damage to neighboring neurons. Recently, a major cytokine dysregulation proportional to clinical severity, inflammatory status, and redox imbalance was evidenced in plasma from CDD patients (Leoncini *et al.,* 2015; Cortelazzo *et al.,* 2017), suggesting a subclinical chronic inflammatory status in children affected by this pathology. However, to date, it is unknown whether such an inflammatory state is even mirrored at the cerebral level and whether it may contribute to the pathophysiology of CDD.

In 2021 Galvani and colleagues showed evidence of a microglia over-activation status in the brains of *Cdkl5* KO mice, characterized by alterations in microglia cell number/morphology and increased pro-inflammatory gene expression. They found that microglia over-activation is already present in the postnatal period in *Cdkl5* KO mice and worsens during aging. Importantly, by restoring microglia alterations, treatment with luteolin, a natural anti-inflammatory flavonoid, counteracts hippocampal neuron cell death in both adult and aged *Cdkl5* KO mice, and rescues NMDA-induced excitotoxic damage in *Cdkl5* KO mice. These findings bring new insight to the CDD pathophysiology and provide the first evidence that therapeutic approaches aimed at counteracting neuroinflammation could be beneficial in CDD (Galvani *et al.,* 2021).

2.4 Therapeutic strategies

There is currently no targeted therapy for CDD that is able to address the underlying problems of the disorder. Patients are completely dependent on medical care and require continuous medication throughout their lives (Demarest *et al.,* 2019; Olson *et al.,* 2019). The therapeutic methods implemented in patients with CDD are essentially based on the symptomatic use of drugs, in order to control the most problematic symptoms that increase disability and to ensure that patients have a chance for development. Epilepsy remains the symptomatic area of greatest interest, in which the greatest therapeutic effects could be obtained. It should be taken into account that resistance to antiepileptic

drugs in CDD reaches 84% (Frullanti *et al.,* 2019), and in addition, the effectiveness of these drugs decreases over time.

Various studies have been conducted by different research groups to develop a therapy aimed at the biological, metabolic, and genetic basis of CDD. Many of these therapeutic approaches tested on *Cdkl5* KO mice have been shown to be effective in ameliorating some neuroanatomical and behavioral defects.

2.4.1 Pharmacological approaches

Considering the strong impairment of dendritic spine stability observed in young *Cdkl5* KO mice, this phenotype was used by Della Sala and colleagues in 2016 to evaluate the effects of a treatment aimed at improving the condition of *Cdkl5* KO mice. Among other kinases, whose activation was found to be altered in the *CDKL5* KO mouse model, Ser240-244 phosphorylation of S6, a specific target of the AKT-mTOR pathway, is downregulated in CDKL5 mutants (Della Sala *et al.,* 2016). The AKT-mTOR pathway is an important molecular cascade involved in several neurodevelopmental disorders and is also hypofunctional in RTT models carrying the MeCP2 deletion. **Insulin-like growth factor 1 (IGF-1)** is an activator of the AKT-mTOR pathway, and treatment with IGF-1 has been found to improve spine dynamics and the behavioral phenotype in mouse models of RTT. Based on these considerations, Della Sala and colleagues treated young (P24-P27) and adult (P120-P124) *Cdkl5* KO mice with IGF-1, showing that this treatment is able to rescue S6 phosphorylation, spine deficits, and defective PSD-95 expression in *Cdk5* KO mice. In particular, the authors found that systemic IGF-1 treatment restored spine density and spine elimination rate. Interestingly, the increased spine density induced by IGF-1 was still present 20 days after the end of IGF-1 treatment, suggesting that the spines induced by IGF-1 are long-lasting (Della Sala *et al.,* 2016).

A further characterization of AKT-dependent pathways showed a disruption of AKT-GSK3β signaling in *Cdkl5* KO mice (Fuchs *et al.,* 2014; Fuchs *et al*., 2015). In 2014, Fuchs and colleagues found that the **lithium**-induced increase in GSK3β phosphorylation induced a complete restoration of survival and neuronal maturation of in vitro neuronal cultures from *Cdkl5* KO mice (Fuchs *et al.,* 2014). Another group of GSK3 inhibitors is represented by synthetic inhibitor compounds such as purine analogues, aminopyrimidine, and ATP-competitive GSK3 inhibitors (Ring *et al.,* 2003). However, the affinity of these ATP-

competitive compounds for more than one kinase is a limiting factor for their use in a therapeutic manner. A high toxicity of this type of drug prevents its use in the clinical phase, and may result in a failure in clinical trials (Eldar-Finkelman & Martinez, 2011). The compounds SB-216763 and SB-415286 (Coghlan *et al.,* 2000) are two structurally distinct ATP-competitive GSK3 inhibitors with similar potency, with no effects on activity of the major protein kinase in the cells (Coghlan *et al.,* 2000). These compounds acutely reduce cellular GSK3β activity as assessed by activation of glycogen synthase (Coghlan *et al.,* 2000) and inhibit GSK3β activity by enhancing Ser9 phosphorylation (Fuchs *et al.,* 2015). Fuchs and colleagues found that treatment with **SB216763**, improves several defects, including dendritic development and hippocampus-dependent learning and memory in *Cdkl5* KO mice (Fuchs *et al.,* 2015). Finally, ATP non-competitive GSK3 inhibitors are more selective compounds, because they do not simply block ATP entrance in the catalytic domain, but bind a specific region in the kinase domain, thus providing a more efficient modulation of GSK3 activity.

The first reported ATP non-competitive GSK3 inhibitor family was the small heterocyclic thiadiazolidinone (TDZD) family (Eldar-Finkelman & Martinez, 2011) which includes NP031112, also termed **NP-12 or Tideglusib**. This compound is a brain-permeable small molecule currently used in clinical trials for Alzheimer disease and autism spectrum disorders, in which it prevents neuronal loss and improves learning and memory (Domínguez *et al.,* 2012; Serenó *et al.,* 2009). Moreover, administration of NP12 compound promotes hippocampal neurogenesis via proliferation and differentiation in the subgranular zone of adult rats (Morales-Garcia *et al.,* 2012). Importantly, pharmacological inhibition of GSK-3β activity by NP12 rescues dendritic morphogenesis and synapse development in the *Cdkl5* KO mouse (Fuchs *et al.,* 2018). However, inhibition of GSK-3β activity has been shown to have positive effects in juvenile but not in adult *Cdkl5* KO mice (Fuchs *et al.,* 2018), suggesting that pharmacological interventions aimed at normalizing only impaired GSK-3β activity might not be sufficient to restore the defects of a complex disease such as CDD.

Histone deacetylases are important therapeutic targets for many diseases, including neurological disorders and epilepsy. The pan-HDAC inhibitor valproic acid, used for seizure control for decades, has been shown to block neurogenesis and differentiation of hippocampal progenitor cells, with increased histone acetylation (Hsieh *et al.,* 2004).

Preliminary human cancer studies have shown that pan-HDAC and selective class I inhibitors can cause numerous side effects, including bone marrow depression, weight loss, taste disturbances, electrolyte disturbances, disordered clotting, fatigue, and cardiac arrhythmias (Thurn *et al.,* 2011). These results highlight the need to use inhibitors that target the HDACs specifically involved in a given pathology, in order to reduce the side effects due to non-specific inhibitions. The new discovery of the **HDAC inhibitor**, **LMK235,** which shows a selectivity profile of the HDAC isoform with a preference for HDAC4 and HDAC5 (Marek *et al.,* 2013), provides an important tool for treating pathologies due to aberrant HDAC4/HDAC5 activity. In 2016, Trazzi and colleagues found that the histone deacetylase 4 (HDAC4) is a direct substrate of CDKL5 (Trazzi *et al.,* 2016). The authors showed that HDAC4 is a direct phosphorylation target of *CDKL5* and that *CDKL5*-dependent phosphorylation promotes HDAC4 cytoplasmic retention. Trazzi and colleagues found that LMK235 inhibited HDAC4 activity through its sequestration in the cytoplasm, and restored the normal gene transcription (Trazzi *et al.,* 2016). Importantly, pharmacological restoration of HDAC4 activity restores postmitotic neuronal maturation and hippocampus-dependent memory in *Cdkl5* KO mice, suggesting potential pharmacological interventions targeting HDAC.

Reduced expression of the GluA2 subunit of the AMPA-R was identified in *Cdkl5* KO mice (Tramarin *et al.,* 2018). Tramarin and colleagues found that treatment of *Cdkl5* KO mice with the antidepressant **tianeptine** normalized the expression of membrane inserted AMPA-Rs containing GluA2 (Tramarin *et al.,* 2018). Since AMPA-R derangement is likely to contribute, at least in part, to the altered synaptic functions and cognitive impairment linked to loss of Cdkl5, the authors suggest tianeptine's therapeutic potential for patients with mutations in CDKL5. GluA2-AMPA receptor levels were restored in the perirhinal cortex of *Cdkl5* KO mice by means of an *in vivo* treatment with a TrkB agonist (the **7,8-DHF prodrug R13**). R13, by triggering the TrkB/PLCγ1 pathway, rescued defective LTP, and restored visual recognition memory in *Cdkl5* KO mice (Ren *et al.,* 2019). In the wake of alterations involving glutamate receptors, Tang and colleagues demonstrated that altered NMDAR expression and signaling underlies autistic-like features in mouse models of CDD (Tang *et al.,* 2019). They found that an acute, low-dose inhibition of NMDAR signaling with **memantine** ameliorates autistic-like behaviors in a novel mouse model bearing a CDD-

associated nonsense mutation, CDKL5 R59X. This study provides evidence supporting a new therapeutic avenue for the treatment of CDD-related symptoms.

In 2020, Trovò and colleagues treated *Cdkl5* KO mice with **epigallatocathechin-3-gallate (EGCG)** (Trovò *et al.,* 2020), the major polyphenol of green tea. EGCG, a powerful antioxidant, appears to have many actions on the brain, preventing oxidative damage in healthy cells. It also affects a wide array of pro-survival/differentiation signal transduction pathways, including ERK, PI3K/AKT, and DYRK1A (Shankar *et al.,* 2007). Therefore, over the past few years it has garnered significant scientific interest as a therapeutic option for several neurological disorders (Granja *et al.,* 2017). Trovò and colleagues found that defective synaptic maturation in the hippocampi and cortices of adult *Cdkl5* KO mice can be rescued through the intraperitoneal administration of EGCG; however, this is not sufficient to normalize behavioral CDKL5-dependent deficits (Trovò *et al.,* 2020). The authors concluded that dietary supplementation of EGCG, in combination with the standard pharmacological intervention, may have a positive impact on CDKL5-related neurological defects, although additional studies will be required to further investigate its therapeutic potential.

Studies in mouse models have linked CDKL5 deficiency to disruption of the excitatory/inhibitory balance (Lupori *et al.,* 2019; Pizzo *et al.,* 2016). Increased density of GABAergic synaptic terminals in the cortex of *Cdkl5* KO mice suggests increased GABAergic transmission. In 2021, Gennaccaro and colleagues found that an acute in vivo treatment with **CGP55845**, a GABAB receptor antagonist, increased density and maturation of dendritic spines in the perirhinal cortex, and restored novel object recognition memory in *Cdkl5* KO mice. This data showed the efficacy of limiting excessive GABAB receptor-mediated signaling, leading to improved synaptic plasticity and cognition in CDD mice (Gennaccaro *et al.,* 2021b).

The recent finding of a generalized status of microglia over-activation in the brain of a mouse model of CDD (Galvani *et al.,* 2021) prompted the authors to use an anti-inflammatory drug to treat *Cdkl5* KO mice. Galvani and colleagues found that treatment with **luteolin** (a natural anti-inflammatory flavonoid) is able to recover impaired neuronal survival and maturation in *Cdkl5* KO mice, suggesting that a hyperactive state of microglia plays a causative role in the CDD phenotype.

Combinatorial therapies recently became one of the most successful drug development strategies for complex diseases. Simultaneous intervention on two targets relevant to a disease has shown improved therapeutic efficacy; there has been a move toward multiple target drugs (Korcsmáros *et al.,* 2007). Very recently Loi and colleagues hypothesized that, due to the complexity of CDD, a combined inhibition of GSK-3β and HDACs by a multi-target drug might be more efficient then a single-target therapy. In support of this hypothesis, it was reported that the combined inhibition of GSK-3β and HDACs induces synergistic effects compared to the single drug, with a potential improved therapeutic selectivity (Sharma & Taliyan, 2015). Loi and colleagues used a recently described **first-in-class GSK-3β/HDAC dual inhibitor, compound 11** (C11), that efficiently inhibits GSK3β and HDACs even at low doses (De Simone *et al.,* 2019). This study provides novel evidence that, in *in vitro* experimental models of CDD, the GSK-3β/HDAC6 dual inhibitor C11 is more effective at recovering neuronal survival than treatment with a single inhibitor that is selective for GSK-3β. Importantly, *in vivo* treatment with C11 restored synapse development, neuronal survival, and microglia over-activation, and improved motor and cognitive abilities of *Cdkl5* KO mice. Overall, data suggest that a GSK-3β/HDAC6 dual inhibitor therapy may engender a more effective strategy with which to achieve therapeutic benefits in CDD patients (Loi *et al.,* 2021).

2.4.2 Protein therapy

Since mutations in the CDKL5 gene lead to a lack of functional CDKL5, delivery of a functional CDKL5 protein to the brain may represent a therapeutic approach of choice. The failure of proteins to penetrate the cell membrane prevents their use as a therapeutic tool in a variety of monogenic disorders caused by the lack of function of a single protein. Recently, protein transduction domains (PTDs) have been shown to promote the delivery of proteins into living cells and through the blood brain barrier. PTDs are small peptides that are able to ferry much larger molecules into cells independently, by classical endocytosis (Bolhassani *et al.,* 2017). The HIV-1 transactivator of transcription (TAT) protein is the best characterized viral PTD-containing protein. Earlier experiments with the TAT-PTD protein domain demonstrated successful transduction of fusion proteins up to 120 kDa into murine cells (Nagahara *et al.,* 1998, Schwarze *et al.,* 1999, Xia *et al.,* 2001). Schwarze *et al*. reported that a recombinant TAT-β-galactosidase protein, injected

intraperitoneally into mice, was distributed to all tissues, including the brain, and retained its biological activity. Importantly, the TAT-PTD has not been reported to have any toxic effects or immunogenicity problems so far (Bolhassani *et al.,* 2017). Recently, Trazzi and colleagues engineered the human CDKL5 protein by binding the TAT peptide to it. This small protein sequence, derived from the HIV virus, has the ability to promote the transduction of proteins in cells, and to promote their transport across cell membranes and the blood brain barrier. In this way the TAT-CDKL5 fusion protein, once systemically injected into *Cdkl5* KO mice, is able to cross the blood–brain barrier and diffuse into brain cells, preserving its biological activity and improving many of the neuroanatomical and cognitive defects that characterize *Cdkl5* KO mice. Trazzi and colleagues found that protein treatment restored the correct morphology of hippocampal neurons, through an increase in the branching of the dendritic tree and in the density of the dendritic spines, resulting in a significant improvement in hippocampal-dependent functions, and also reduced the onset of obstructive sleep apnea and stereotyped behaviors in treated mice (Fig. 7). These promising results suggest that a protein substitution therapy with a TAT-CDKL5 fusion protein may be a successful therapy for CDKL5 disorder (Trazzi *et al.,* 2018).

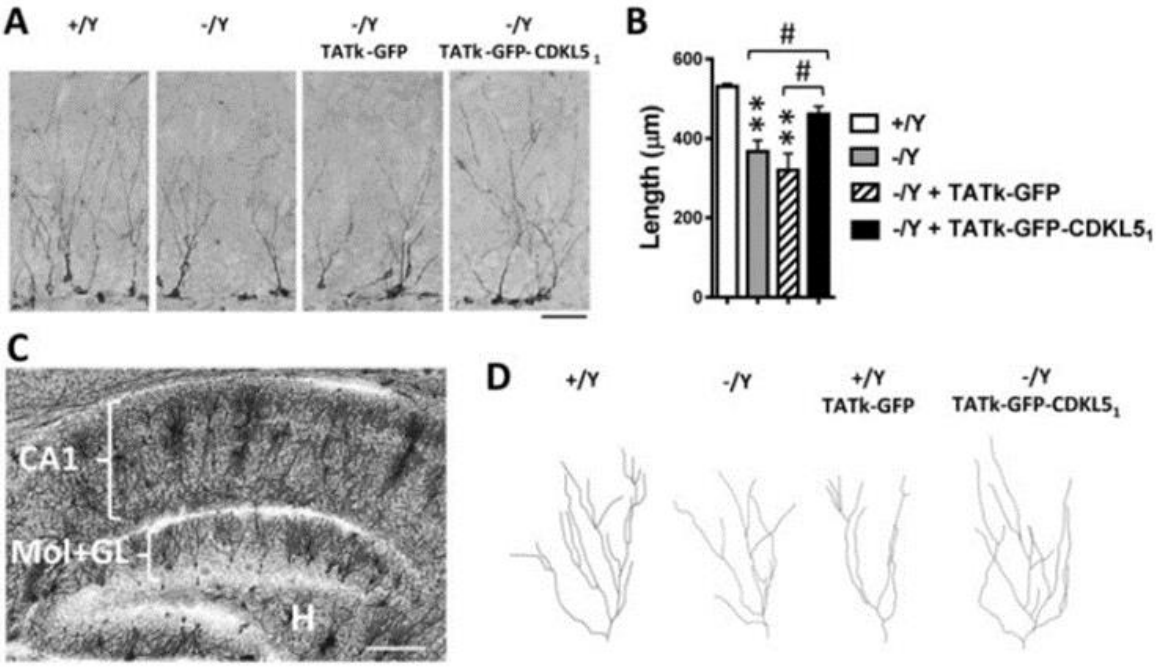

Fig. 7: Effect of TATk-CDKL5 protein therapy on dendritic morphology. (A) Examples of sections processed for DCX immunostaining from the DG of untreated *Cdkl5* +/Y and *Cdkl5* -/Y mice, and of *Cdkl5* -/Y mice treated with TATk-GFP or TATk-GFP-CDKL5$_1$. (B) Mean total dendritic length of newborn granule cells of untreated *Cdkl5* +/Y and *Cdkl5* -/Y mice, and of *Cdkl5* -/Y mice treated with TATk-GFP or TATk-GFP-CDKL5$_1$. (C) Example of a Golgi-stained hippocampal slice. Abbreviations: GL, granule cell layer; H, hilus; Mol, molecular layer. Scale bar: 250 µm. (D) Examples of the dendritic tree of Golgi-stained granule cells of 1 animal from each experimental group (Trazzi *et al.,* 2018).

2.5 Gene Therapy

Gene therapy consists in the transfer of genetic material to a patient with the aim of treating a disease. Although this concept has existed for many decades, clinical investigation began in 1990 when the first clinical trial for a rare immunodeficiency disorder was undertaken in the United States. Since that time, more than 2,500 gene therapy clinical trials have been initiated to treat a variety of monogenic diseases, infectious diseases, complex neurodegenerative disorders, and even cancer (Anguela *et al.,* 2019).

The goal of gene therapy for genetic diseases is to achieve a durable expression of the therapeutic gene or “transgene” at a level that is sufficient to ameliorate or cure the

disease symptoms with minimal adverse events (gene augmentation) (Fig. 8A). There are two basic strategies: an integrating vector is introduced into a precursor or stem cell and then the gene is passed to every daughter cell (the vector is designed to integrate at one or more loci in the patient's chromosomes) or the gene is delivered in a non-integrating vector to a long-lived postmitotic or slowly dividing cell, ensuring the expression of that gene for the life of the cell. In the latter case, integration of the therapeutic DNA into the chromosomes of the patient's cells is not required; instead, the transferred DNA is stabilized extrachromosomally. Transduction of stem cells with an integrating vector is generally an *ex vivo* process, whereas delivery to long-lived postmitotic cells is usually achieved through *in vivo* gene delivery (High *et al.,* 2019).

However, it is also possible to suppress the expression of a harmful gene by using RNA interference: in some diseases, in fact, cellular function is lost due to the toxic accumulation of a defective protein. In these cases, gene suppression aims to restore cellular functionality by reducing the expression of the mutated gene through RNA interference (Fig. 8B). It is also possible to use genome editing techniques (Fig. 8C) to correct a mutated gene in its precise genomic position by exploiting the formation of a break in the DNA double strand and leaving the repair of the break to the host cell's own repair systems: the result of this process will determine its gene modification (Anguela *et al.,* 2019).

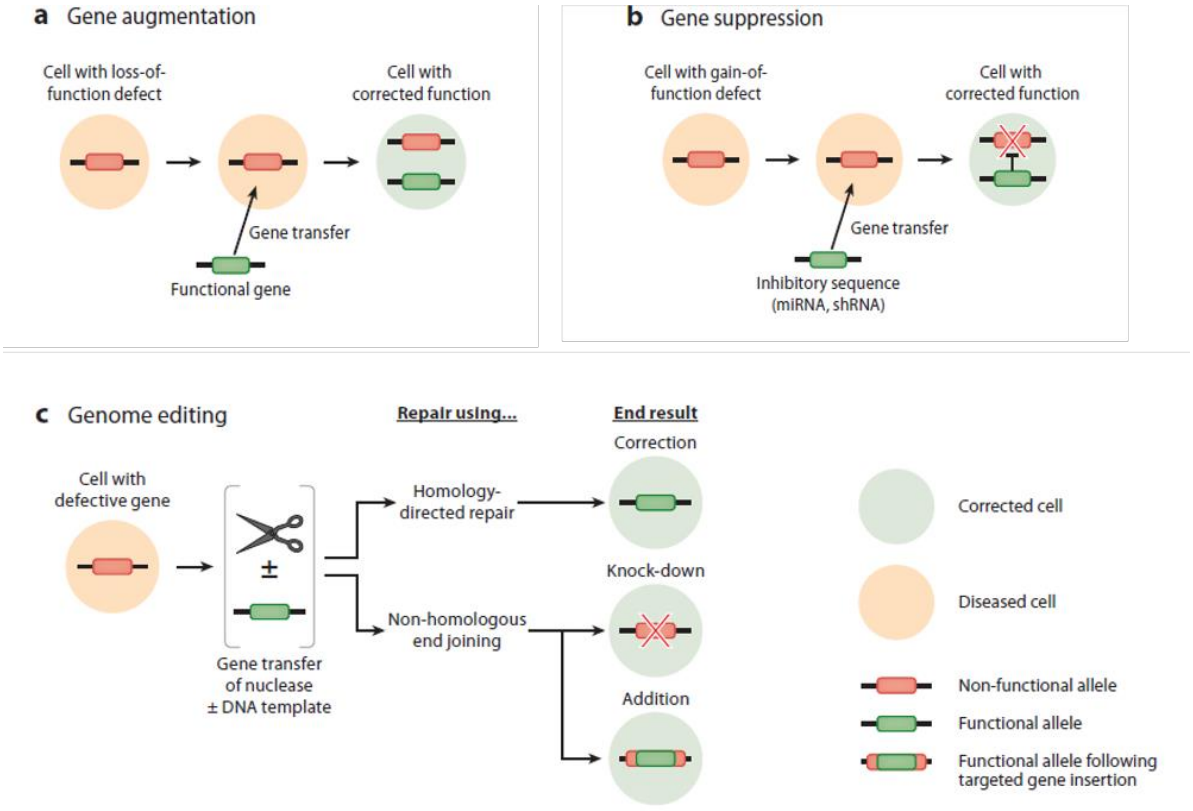

Fig. 8: (a) Gene augmentation: normal cell function can be restored by providing a functional copy of a gene. (b) Gene suppression: aims to reduce the expression of the mutated gene through RNA interference. (c) Genome editing: consists in the induction of a break in the double strand of DNA at the target site. The choice of one DNA repair mechanism over another will determine the outcome of the gene modification (Anguela *et al.,* 2019).

2.5.1 Viral vectors

One of the main differentiating factors for *in vivo* versus *ex vivo* gene therapy is the choice of vectors. Vectors can be divided according to their ability to integrate into the host genome. Indeed, when introducing genetic material into stem cells, it is crucial to use vectors that can integrate. For *in vivo* gene therapy, on the other hand, no integrating viruses are required as they often target post-mitotic cells, which are no longer dividing. In these cells, long-term expression can be obtained as long as the transferred DNA remains stable in the cell in an episomal form so as to promote the expression of the transgene for the entire cellular lifespan. Currently, most gene therapy strategies for the treatment of genetic diseases focus on two types of vectors: lentiviral vectors for *ex vivo* gene transfer into hematopoietic cells (or other stem cells) (Naldini *et al.,* 2011), and

adeno-associated viral (AAV) vectors for *in vivo* gene transfer in post-mitotic cells (Mingozzi *et al.,* 2011).

Both types of viral vectors have disadvantages: lentiviral vectors with integration capabilities present the risk of insertional mutagenesis, while for the administration of the vectors *in vivo*, the risk is mostly related to deleterious immune responses. The first successful attempts of gene therapy concern in *ex vivo* applications using hematopoietic stem cells (HSC) for the treatment of primary immunodeficiencies. However, over the years, *in vivo* gene therapies through the use of AAV vectors (adenoassociated-virus) have also achieved success (Anguela *et al.,* 2019). In particular, AAV vectors have proven to be reliable for the treatment of disorders of the nervous system, although many aspects remain to be clarified. The main difficulty encountered, which is due to the anatomical and functional complexity of the human brain, is the existence of the blood-brain barrier that limits the distribution of the vector in the central nervous system (Anguela *et al.,* 2019).

New serotypes and different infusion techniques have been tested to improve vector distribution in the central nervous system. The administration of AAV vectors into the cerebrospinal fluid, via intraventricular infusion or intrathecal administration, is the most efficient way to obtain a global distribution of the vector, but is also related to major side effects due to the invasiveness of the administration (Davidson *et al.,* 2000). Adeno-associated vectors (AAVs) are the primary delivery systems for the treatment of many human diseases. Preclinical and clinical achievements in AAV-mediated gene therapy have resulted in it gaining popularity as an ideal therapeutic vector (Wang *et al.*, 2019).

AAV occurs naturally in several serotypes, the most widely characterized and used being serotype 2 (AAV2). Nonetheless, the most promising serotype is AAV9, isolated from human liver tissue (Gao *et al.,* 2004), which has demonstrated its ability to cross the blood-brain barrier, making it a leading capsid for transduction into the central nervous system (CNS) via systemic administration. In fact, since the brain is very complex, direct intraparenchymal injections of rAAV determine a localized distribution and are ideal for the treatment of CNS diseases affecting a defined region of the brain. On the other hand, the release of the vector into the cerebrospinal fluid via intrathecal injection can achieve a wider distribution in the CNS. Unfortunately, these routes of administration can be invasive and carry substantial risks. Alternatively, the systemic administration of vectors such as AAV9, capable of crossing the blood-brain barrier to transduce neurons and glia

(Foust *et al.,* 2009; Zhang *et al.,* 2011), has demonstrated its therapeutic efficacy in several studies for the treatment of CNS diseases.

The current exponential growth of clinical trials using AAV vectors suggests the enormous potential of these viruses as ideal programmable vectors for the treatment of human diseases. Gene therapy represents one of the last frontiers for the treatment of human genetic diseases: the power and versatility of gene transfer strategies are such as to make approaches of this type increasingly relevant over time.

2.5.2 Gene therapy applications in human disorders

Despite years of preclinical work, it was not until the early 1990s that the first gene therapies were studied in humans, albeit with mixed results. The first clinical trial to gain approval for transfer of a foreign gene into humans was conducted at the National Cancer Institute in Bethesda, Maryland, in 1990. This trial used a retroviral vector to insert the gene encoding the cytokine, inteleukin-2 (IL-2) into patient-derived tumor-infiltrating lymphocytes (TILs). The genetically modified TILs were then infused back into patients with advanced melanoma. Although the results regarding efficacy were disappointing — all 5 patients treated ultimately died of progressive disease — TILs from 4 out of the 5 patients displayed in vivo expansion without significant toxicity (Rosenberg *et al.,* 1990).

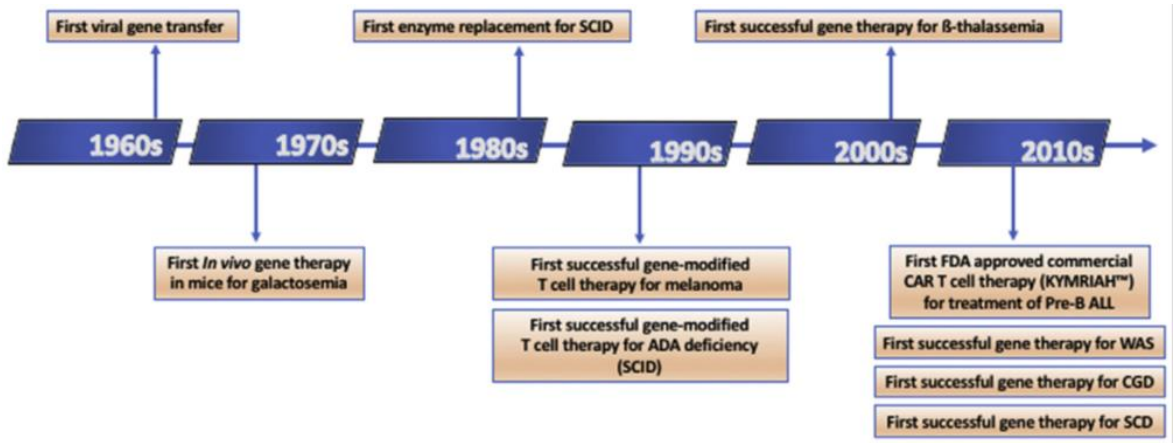

Fig. 9: Timeline depicting key milestones in preclinical research and clinical trials in gene therapy from the 1960s to the present day. CGD, Chronic granulomatous disease; SCD, sickle cell disease; WAS, Wiskott-Aldrich syndrome (Steffin *et al.,* 2019).

Although there was a plateau in clinical progress in the 1990s, over the last 20 years there has been a resurgence of research committed to improving cell therapies, with significant progress (Fig. 9). Gene therapy has also become a viable therapeutic option for several inherited hematologic diseases, for example b-Thalassemia major (Galanello *et al.,* 2010). In addition to providing a possible therapeutic option for inherited immunodeficiencies and inherited haematological diseases, gene therapy is generating a great deal of interest and is also emerging as a treatment with wide applicability for neurological disorders.

Despite preclinical data showing the feasibility of AAV-based gene therapy to treat CNS disorders, the number of clinical trials with encouraging results is relatively small. This is in part due to the anatomical and functional complexity of the human brain, including the existence of the blood–brain barrier, which limits biodistribution of the vector into the CNS. Even assuming that successful delivery of the vector takes place (e.g., via direct intraparenchymal, intrathecal, intracerebroventricular, or systemic administration), it is challenging to target a sufficient number of cells, either within a particular region or globally in the CNS, to achieve an adequate level of gene augmentation or gene suppression within a safe and therapeutic window.

The first clinical studies utilizing AAV vectors to mediate gene delivery in the human CNS were for the treatment of Canavan disease (McPhee *et al.,* 2006), Parkinson's disease (Kaplitt *et al.,* 2007), and late infantile neuronal ceroid lipofuscinosis (Worgall *et al.,* 2008). All these trials utilized AAV2 vectors delivered locally to certain areas of the brain; the expression was confined to areas close to the injection sites, a desirable goal for Parkinson's but not for the other indications. Novel serotypes and different infusion techniques have been tested to improve vector distribution for those CNS indications that require global distribution of the vector. Delivering AAV vectors into the cerebrospinal fluid, via either intracerebroventricular or intrathecal administration, has been proposed as a more efficient way to achieve global distribution (Davidson *et al.,* 2000). A breakthrough study by Foust and colleagues demonstrated successful targeting of spinal motor neurons after systemic administration of AAV9 in neonatal mice (Foust *et al.,* 2009). Using the same systemic intravenous administration of AAV9, these investigators subsequently showed robust efficacy in a phase I trial for the treatment of spinal muscular atrophy type 1 (SMA1) in 15 patients (Mendell *et al.,* 2017). SMA1 is the most common genetic cause of death during infancy, with less than 20% of patients alive and free of

ventilatory support at 20 months of age. The patients demonstrated improvements in motor function and survival that were significantly different from the expected course of the disease, using natural history as a comparator (Finkel *et al.,* 2016).

Some challenges in the development of successful CNS-directed therapies include the need for careful monitoring of potential immune responses, especially against the transgene product, and improved vector tropism in order to target higher numbers of cells at lower doses, as well as a more precise targeting of specific cell types in different regions of the brain.

Identification of the precise causative mutations for most neurologic disorders has aided in the ability of researchers to develop targeted gene therapies to combat them. AAV gene therapy enables both gene replacement to address loss-of-function mutations and gene silencing to address gain-of-function mutations.

Both strategies have been used in preclinical and clinical studies for neurologic diseases. For example, survival motor neuron (SMN) protein has been replaced to treat spinal muscular atrophy (SMA), while superoxide dismutase 1 has been silenced to treat amyotrophic lateral sclerosis, as has Huntington for Huntington disease. The FDA recently approved the drug Spinraza, which increases production of SMN protein, after it showed promising results in patients with SMA. In an expanded access program in Europe, 61 children with SMA were treated with Spinraza and experienced a substantial improvement in motor function after only 6 months (Steffin *et al.,* 2019).

In summary, this is an exciting time for the ever-growing field of gene therapy. Successful translation of preclinical discoveries to clinical trials has yielded promising results in several historically devastating diseases. Although some techniques are in their third decade of use and require only optimization, others, such as genome editing, are in their infancy. Like many novel therapies, the future of gene therapy requires a revisitation of the past attention to safety, efficacy, and cost, and ethical concerns must be addressed in order for the promise of this therapy to become reality.

2.5.3 Gene therapy in CDD

In 2020, Gao and colleagues published the first study that demonstrates that a gene therapy with AAV-CDKL5vector ameliorates deficits in both mouse and iPSC models of CDD (Gao *et al.,* 2020). They used the AAV vector serotype PHP.B in adult mice to transduce

neurons and astrocytes throughout the brain more efficiently than serotype 9. They found that replacement of the human isoform of *CDKL5* 1 (hCDKL5_1) (Hector *et al.*, 2016) significantly improved motor coordination in *Cdkl5* KO mice. The cerebellum, with its key role in motor coordination, was the region of the brain with the highest transduction efficiency. Unfortunately, other brain regions showed far lower transduction rates and, consequently, the behavioral improvement was very moderate or absent (Gao *et al.,* 2020). The work by these authors is the first such proof-of-concept study for gene replacement therapy in CDD and represents a small step toward demonstrating the utility of virus-mediated gene transfer in this disorder. Further studies are now needed to test the efficacy of such an approach and to decide on its translational applicability.

3. MATERIAL AND METHODS

3.1 Cloning and production of AVV vectors

To express the TATκ-CDKL5, CDKL5, TATκ-GFP and GFP proteins by means of AAV vector-mediatedgene delivery, the IgK-TATk-hCDKL5$_1$, hCDKL5$_1$, IgK-TATk-eGFP or eGFP gene expression cassette have been subcloned in the backbone of pAAV-CBh-DIO-EGFP (plasmid #87168, Addgene). The designed viral cassettes between the two AAV2 inverted terminal repeats (ITRs) contain a CBh promoter (~0,8 kbp), the IgK-TATκ-CDKL5$_1$ (~3.06 kbp) or CDKL5$_1$ (~2.9 kbp) or IgK-TATk-eGFP (~0,8 kbp) or eGFP (~0,7 kbp) open reading frame, followed by a WPRE and SV40 polyadenylation signal (~0,4 kbp) (Fig. 10). The TATk-CDKL5 and CDKL5 proteins were tagged with a haemagglutinin (HA)-tag to monitor delivered protein expression levels. The vectors thus obtained were controlled by enzymatic digestion and sequencing.

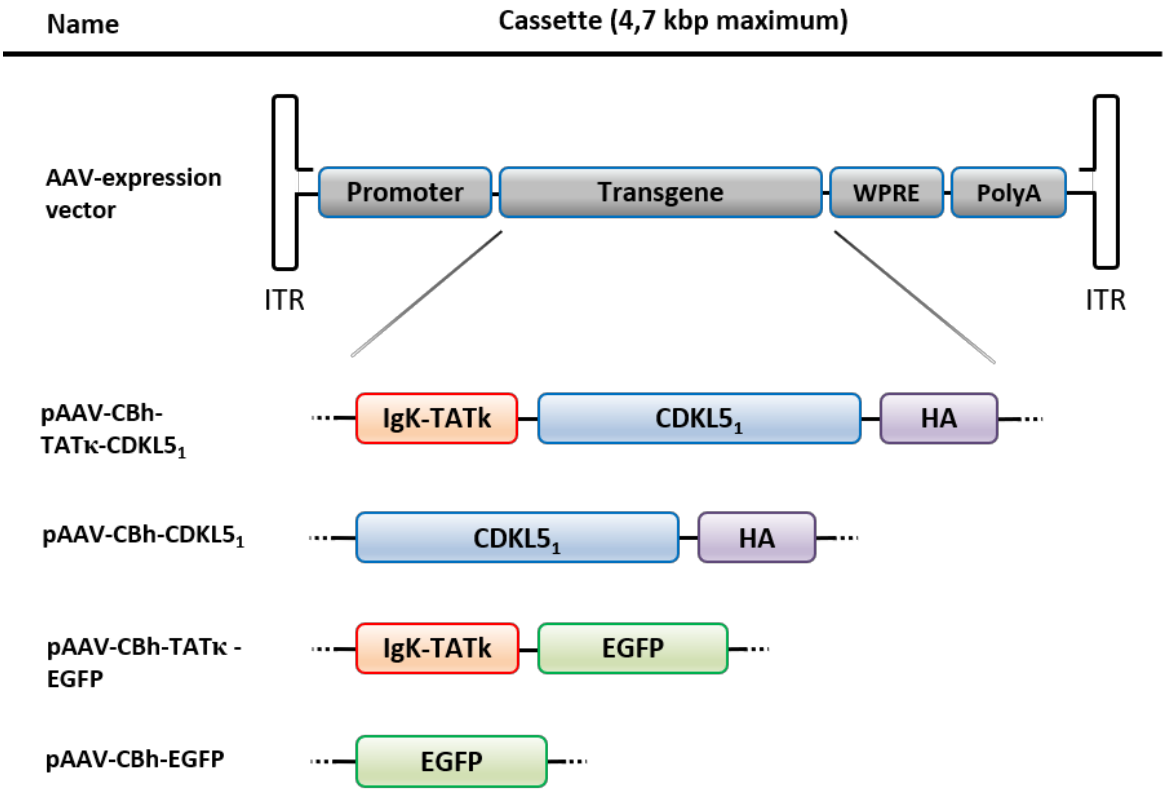

Fig. 10: Schematics depicting transgene cassettes cloned into the AAV vector genome. Expression of haemagglutinin (HA)-tagged *Igk-TATk-hCDKL5$_1$*, (HA)-tagged *hCDKL5$_1$*, *Igk-TATk-EGFP* and *EGFP* were driven by a CBh promoter. CBh = a hybrid form of CBA promoter; ITR = inverted terminal

repeat; WPRE = woodchuck hepatitis virus post-transcriptional regulatory element; polyA = SV40 poly-adenilation signal.

AAV vectors were produced in HEK293 cells using an adenovirus-free plasmid transfection method with modification on a scale of 1 to 2-liter culture. In brief, HEK 293 cells were grown in Dulbecco's modified Eagle's medium (DMEM) supplemented with 10% fetal bovine serum (FBS), L-glutamine, and penicillin-streptomycin. Immediately before plasmid DNA transfection, the culture media were changed to serum-free media. The following three plasmids were transfected at a 1:1:1 ratio in HEK293 cells using the standard polyethyleneimine (PEI) (1 mg/mL) DNA transfection procedure at a DNA:PEI weight ratio of 1:2. The three plasmids used for AAV vector production were: (1) pHELPER (an adenovirus helper plasmid from Agilent), (2) pHLP-AAV-PHP.B (an AAV helper plasmid supplying AAV2 Rep and AAV-PHP.B capsid proteins, constructed based on an AAV9 helper plasmid obtained from James M. Wilson, University of Pennsylvania), and (3) an AAV vector plasmid containing a transgene expression cassette placed between the two AAV2 inverted terminal repeats (ITRs), constructed based on an AAV vector plasmid obtained from Avigen Inc. Five days after transfection, both media and cells were harvested. The harvested media and cells underwent one cycle of freezing and thawing and the cell debris was removed by centrifugation. The culture medium supernatants were made to 8% polyethylene glycol (PEG) 8000 and 0.5 M NaCl, incubated on ice for 3 h, and spun at 10,000 × g for 30 min to precipitate viral particles. The pellets were resuspended in a buffer containing 50 mM Tris-HCl (pH 8.5) and 2 mM MgCl2, treated with Benzonase (EMD Millipore, Darmstadt, Germany) at a concentration of 200 units per mL for 1 h, and subjected to purification by two rounds of cesium chloride (CsCl) density-gradient ultracentrifugation, followed by dialysis with phosphate-buffered saline (PBS) with 0.001% Pluronic F68. The final viral preparations were made in PBS/5 % sorbitol/0.001% Pluronic F68 and stored at -80oC until use. The AAV vector titers were determined through a quantitative dot blot assay.

3.2 Cells cultures

3.2.1 HEK293T cell line and transient transfection

HEK293T cells were grown in DMEM (Dulbecco's modified Eagle's medium, with the addition of 2 mM of glutamine, 10% of FBS, and the antibiotics penicillin, 100 U/ml, and streptomycin, 100 µg/ml) in an incubator at 37 °C with 5% CO2. Cell medium was replaced every 3 days and the cells were sub-cultured once they reached 90% confluence. Cells were plated in 24-well plates and grown adherent to the well for western blot analysis or plated on poly-lysinated coverslip for immunocytochemical analysis. Twenty-four hours after plating, cells were transfected with the viral plasmids with METAFECTENE® EASY + (Biontex). The ratio 4 µl : 2 µg between METAFECTENE EASY and DNA was used. METAFECTENE EASY was mixed with 50 µl 1 x EASY buffer and then with the DNA. After 15 minutes of incubation time at room temperature, the mixture was added to the cell medium. Forty-eight hours after transfection, cells were washed with PBS and collected in a cell pellet for total protein extraction or fixed with 4% paraformaldehyde for immunocytochemistry. Cell medium was also collected and concentrated 200x for western blot analysis (Trazzi *et al.,* 2018).

3.2.2 Hippocampal neurons

Primary hippocampal neuronal cultures were prepared from 1-day-old (P1) wild-type and *Cdkl5* KO. Briefly, hippocampi were dissected from mouse brains under a dissection microscope and treated with trypsin (Gibco) for 15 min at 37°C and DNase (Sigma-Aldrich) for 2 min at room temperature before being triturated mechanically with a fire-polished glass pipette to obtain a single-cell suspension. Cells were plated on coverslips coated with poly-L-lysine in 6-well plates and cultured in Neurobasal medium (Gibco) supplemented with B27 (Invitrogen) and glutamine (Gibco). Cells were maintained in vitro at 37°C in a 5% CO2-humified incubator (Loi *et al.,* 2021; Trazzi *et al.,* 2016).

3.2.3 In vitro neuronal AAV transduction and co-culture

Primary hippocampal neurons were infected with AAV-PHP.B_IgK-TATk-CDKL5 and AAV-PHP.B_CDKL5 (MOI 10^6) at DIV2, fixed at DIV7 with 4% paraformaldehyde + 4% sucrose in 100 mM phosphate buffer pH 7.4. Fixed cells were stained with the primary and secondary antibodies. Nuclei were counterstained with Hoechst-33342 (Sigma-Aldrich) and

fluorescent images were acquired using a Nikon Eclipse Te600 microscope equipped with a Nikon Digital Camera DXM1200 ATI system (Nikon Instruments, Inc. Melville, NY, USA).
For co-culture experiment, HEK293T cells were plated in a 6-well plate adherent to the well, while primary hippocampal neurons were plated on coverglass. Twenty-four hours after plating, HEK293T were transfected with viral plasmids. Twenty-four hours after transfection, the co-culture was prepared as follow: HEK293T cells were washed with neuronal culture fresh medium. Coverglass with primary hippocampal neurons (DIV5) were transferred in the HEK293T 6-well plate in an elevated position thanks to gel supports underneath. Wells were then filled with half the medium of the neuronal culture and half fresh neuronal medium. After 48h of co-culturing, neurons were washed in PBS and fixed with 4% paraformaldehyde + 4% sucrose in 100 mM phosphate buffer pH 7.4 for immunocytochemistry.

3.2.4 Immunocytochemistry

Immunocytochemical analysis were performed on HEK293T cells transfected with viral plasmids, on neuronal primary culture infected with AAVPHP.B viruses and on hippocampal neurons co-cultured with HEK293T cells. For proteins expression evaluation, an anti-HA antibody (1:500, for HEK293T and 1:200, for neurons; Cell Signaling Technology), anti-GFP antibody (1: 500, Invitrogen), anti-TubJ (1:100, Sigma) were used as primary antibody and a secondary anti-rabbit IgG conjugated with CY3 (1:200; Jackson ImmunoResearch), anti-rabbit IgG conjugated with FITC (1: 200; Jackson ImmunoResearch) or anti-mouse IgG conjugated with FITC (1: 200; Jackson ImmunoResearch) were used (Table 1). Cellular nuclei were counterstained with Hoechst-33342 (Sigma-Aldrich). Fluorescence images were acquired using a Nikon Eclipse TE600 microscope equipped with an ATI Nikon Digital Camera DXM1200 system (Nikon Instruments Inc.).

3.3 Animal handling

3.3.1 Animal housing and Genotyping

Mice for testing were produced by crossing CDKL5 KO +/− females with CDKL5 KO -/Y males and CDKL5 KO +/− females with +/Y males. Littermate controls were used for all experiments. The day of birth was designed as postnatal day (P) zero and animals with 24 hours of age were considered as 1-day-old animals (P1). After weaning, mice were housed three to five per cage on a 12-hours light/dark cycle in a temperature-controlled environment with food and water provided *ad libitum*. Experiments were performed in accordance with the Italian and European Community law for the use of experimental animals and were approved by Bologna University Bioethical Committee. In this study all efforts were made to minimize animal suffering and to keep the number of animals used to a minimum.

Genomic DNA extraction

Genomic DNA extraction and purification were performed from tail biopsies of newborn mice, using the NucleoSpin®Tissue Kit (Macherey-Nagel, Düren, DE) extraction kit. The initial step involves the lysis of the tails, obtained by incubating the samples at 56 ° C, for 1-3 hours or overnight, with the T1 buffer (180 µl) and the proteinase K (25 µl), contained in the kit. At the end of the incubation period, to complete the lysis, 200 µl of buffer B3 (10 minutes at 70° C), also contained in the kit, were added to each sample. At the end of the lysis, 210 µl of ethanol (96-100%) are added to the lysate, which allows the DNA to precipitate and bind to the silica membrane of the column, where the cell lysate is contained (centrifuge one minute at 11,000 x g). Two washes are carried out with buffer BW (500 µl) and B5 (600 µl), which allow to eliminate the protein residues and possible contaminants that could compromise the purity of the sample (centrifuge 2 times for one minute at 11,000 x g). A further centrifuge (one minute at 11,000 x g) is performed to remove residual ethanol and the genomic DNA is eluted by means of a slightly alkaline BE buffer (100 µl) (incubate for one minute at room temperature and then centrifuge to one minute at 11,000 x g). All buffers used in the DNA extraction protocol are supplied with the extraction kit, with the exception of ethanol. The DNA obtained is quantified using a

NanoDrop ND-1000 spectrophotometer (NanoDrop Technologies, Wilmington, DE, USA) which also provides the values corresponding to the purity of the samples.

Genotyping

The mice were genotyped using an end-point PCR to detect the presence of the knockout allele for Cdkl5 containing the loxP region in the vicinity of exon 4 (Amendola *et al.,* 2014). The primers used in the reaction are: 108F: 5'-ACGATAGAAATAGGATCAACCC-3 ', 109R: 5'-CCCAAGTATACCCCTTTCCA-3 ', 125R: 5'-CTGTGACTAGGGGCTAGAGA-3 '.

The PCR reaction was performed according to the following protocol: initial denaturation at 94 °C for 4 minutes, 33 denaturation cycles (94 °C/40s), pairing (59 °C/30s), extension (72 °C /40s), final step at 72 °C for 7 minutes. The product of the PCR reaction gives rise to a fragment of 240 bp for the wild type allele and 344 bp for the knockout allele.

3.3.2 Intravenus injections

Prior to injection, mice (three months old) were warmed for 5-10 minutes using an overhead heat lamp to dilate the veins. The animals were then placed in a restraint device of the appropriate size. The tail was wet with ethanol to improve tail vein visualization. A syringe with an appropriate needle (small gauge, 27-30) was prepped with the viral solution, avoiding the presence of air bubbles. The injection was performed by inserting the needle, bevel up, into the later vein and by slowly injecting the solution. Mice were injected with a dose of $5x10^{11}$ vg/mouse. The needle was removed and gentle compression of the tail was applied immediately after until bleeding had stopped. The needle and restraint device were washed with ethanol between each mouse injection.

3.3.3 Intracarotid injections

Surgery was performed on mice (three months old) under general anesthesia (ISOFLO, Esteve Spa, Milano. Italy,1.8- 2.4% in oxygen, inhalation route) with the mouse's body temperature maintained at 37°C by using a heating pad and intra-operative analgesia (10 µL of Norocarp dissolved in 1 ml of saline; 0.2 ml subcutaneously, Pfizer, Italy, Latina). All procedures were performed in sterile conditions; the surgical tools were sterilized for 15 minutes at 121°C in an autoclave (Beta 35 Easy-lock, PBI, Milano, Italy), the catheter was sterilized in Ethanol 99% and flushed with sterile saline. The tip of the catheter was flushed

with sterile heparin. The catheter was then pre-filled with sterile saline; an air bubble was introduced at the end of the catheter. Then the catheter was filled with the solutions containing the viral vector. The bubble avoids mixing of the two solutions and allows the technicians to follow the correct infusion during surgery. The mouse's neck was shaved and sterilized with iodine solution. The mouse was positioned on its back, with the tail facing toward the surgeon. The forepaws were secured to surgical table with adhesive tape to keep the mouse steady.

Isolation of carotid artery

A one cm longitudinal cut slightly to the right of the midline of the neck was made, using forceps to separate fat and muscle to expose the trachea. Then the carotid artery was located running parallel to the trachea and forceps were used to separate the fascia overlying the artery. At this point the vagus nerve was lightly pulled aside from the carotid, and forceps were inserted into the space in between. Last, the forceps were opened to create a gap in the fascia, and the nerve was carefully pulled away from the artery, from the fork in the artery near the larynx (anterior end), up (posterior) as far as possible (at least 3 mm). A drop of saline was added to the surgery area occasionally to keep tissue moist, and thus less brittle and less prone to random tearing (Jacobs *et al.,* 2014).

Suture placement and artery preparation for catheter insertion

Once isolated, two silk suture threads (Softsilk 5-0, United States 47 Surgical, CT, USA) were proximally and distally placed below the arterial segment of interest. The proximal thread (posterior, close to the heart) was permanently knotted and tied while the distal one (near the bifurcation of the carotid) was pulled by another operator to temporarily close off the artery and to keep the artery remaining slightly taut during the insertion of the catheter.

Catheter insertion

The catheter was inserted between the suture threads, close to the proximal thread, through a hole made by a 90° bent needle (25 G). After the tip of the catheter was inserted, the infusion began, with 50 □l/min speed to infuse all the solution. Mice were injected with a dose of $1x10^{12}$ vg/mouse. The bubble was to flow smoothly inside the catheter. When the whole amount of the solution was infused, the infusion was stopped and the catheter was gently pulled out. The threads were both tied. Finally, suture stitches and an antiseptic

ointment (Betadine 10%, Viatris, Milan, Italy) were applied to the skin incision. At the end of the surgical procedure, an antibiotic solution (30 µL of Veterinary Rubrocillin, Intervet, Schering-Plow Animal Health, Milan – Italy, dissolved in 0.8 ml of sterile saline) was administered subcutaneously to prevent infections and to rehydrate the animal.

3.4 Behavioral testing

Behavioral tests were performed 2 months after the injection. An hour before each test, the animals were placed in the room for the "acclimatization" phase which allows for better adaptation to the new environment. The tests were always carried out in the same hours to minimize the variability of performance due to time changes and therefore cause less stress to the animals. Operators were blinded to genotypes and injections.
A total of 87 animals divided into three independent test cohorts were used. The first test cohort consisted of 34 animals (*Cdkl5* +/Y + vehicle n = 10, *Cdkl5* -/Y + vehicle n = 6, *Cdkl5* -/Y + AAVPHP.B_CDKL5 n = 10, and *Cdkl5* -/Y + AAVPHP.B_Igk-TATk-CDKL5 n = 8) that were tested with the following assays: marble burying, nesting test, hindlimb clasping, open field, Barnes maze. The second cohort consisted of 34 animals (*Cdkl5* +/Y + vehicle n = 4, *Cdkl5* -/Y + vehicle n = 10, *Cdkl5* -/Y + AAVPHP.B_CDKL5 n = 10, and *Cdkl5* -/Y + AAVPHP.B_Igk-TATk-CDKL5 n = 10) that were tested with the following assays: marble burying, nesting test, hindlimb clasping, open field. The third cohort consisted of 19 animals (*Cdkl5* +/Y + vehicle n = 6, *Cdkl5* -/Y + AAVPHP.B_CDKL5 n = 6, and *Cdkl5* -/Y + AAVPHP.B_Igk-TATk-CDKL5 n = 7) that were tested with the following assays: marble burying, nesting test, hindlimb clasping, open field and Barnes maze.

3.4.1 Innate behaviors

Marble Burying **-** The Marble Burying test is a commonly used test to analyze repetitive and compulsive behaviors in mice (Angoa-Perez *et al.,* 2013). In this study, the protocol used was that described in Thomas' study (Thomas *et al.,* 2009). In short, 20 marbles are placed in 4 rows of 5 to 4.5 cm of litter inside standard rat cages (20 cm x 45 cm). Subsequently, the mice were positioned at the corner of the cages, in front of the marbles. Animals are given 30 minutes to explore the cages. After 30 minutes, the mice were removed from the cages and the number of “hidden” marbles was counted. A marble is considered hidden if more than 2/3 of its surface is covered by the litter. At least two

operators, unaware of the genotype, evaluated the number of hidden marbles and the assigned scores were averaged to avoid individual bias.

Nesting test **-** The ability to build the nest was evaluated as proposed by Deacon (Deacon *et al.,* 2006). The animals were placed in individual cages with standard bedding and a standard piece of absorbent paper (23 cm × 23 cm) was provided. The nests were independently assessed at 24h by two operators using the following scoring system: 0 - no nest, 1 - primitive flat nest (cushion-shaped, consisting of a flat paper handkerchief that slightly raises a mouse above the litter) , 2 - more complex nest (includes biting the piece of paper and deforming it), 3 - neat and complex cup-shaped nest (with shredded paper woven to form the walls of the cup), 4 - complex nest with hood, with walls which form a ceiling so that the nest becomes a hollow sphere with an opening.

3.4.2 Motor and coordination

Clasping of the hind limbs **-** The reflex of the animal to bring the hind legs along the body while it is suspended upside down, held by the tail is normally defined as clasping (Fig. 11). This reflex is an indicator often used to identify neurological deficits in rodents (Lalonde & Strazielle, 2011). For this behavioral test, the animals were held by the tail, suspended upside down at a height of at least 50 cm from the ground for two minutes. The test was taken with a video camera. The clasping scores were independently assessed by two operators using the following scoring system: 0 - both hindlimbs were splayed outward away from the abdomen with splayed toes, 1 - one hindlimb was retracted or both hindlimbs were partially retracted toward the abdomen without touching it and the toes were splayed, 2 - both hindlimbs were partially retracted toward the abdomen and were touching the abdomen without touching each other, 3 - both hindlimbs were fully clasped and touching the abdomen (Zhu *et al.,* 2016) (Fig. 11).

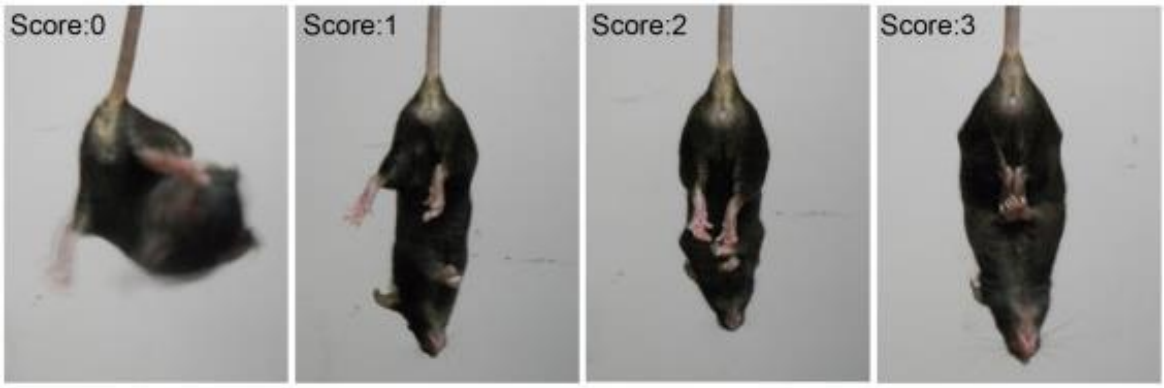

Fig. 11: Representative posture and scoring in the hindlimb clasping test (Zhu *et al.,* 2016).

Open Field test - In order to assess locomotion, the animals were placed in the center of a square arena (50 × 50 cm) and their behavior monitored for 20 min using a video camera placed in the center of the arena. Distinctive features of locomotor activity, including total distance traveled and average speed of locomotion were assessed by the EthoVision10XT software (Noldus Information Technology B.V., Netherlands). Test chambers were cleaned with 70% ethanol between tests.

3.4.3 Learning and memory

Barnes Maze - Mice were trained to locate the target hole (with an underneath escape box) from 20 holes (5 cm diameter) evenly spaced around the perimeter of an elevated (60 cm above the floor) circular open field (100 cm diameter) (Ugo Basile,). The escape box was designated as an analogue to the hidden platform in the MWM, containing a ramp under the target hole so that mice could enter the escape box easily. Mice were initially placed in the centre of the arena covered by a dark cylinder, which was removed 10 s after the start of a trial. All mice were trained with three trials per day for three consecutive days with an inter-trial interval of 30 min. Mice that initially failed to locate the target hole within 3 min were gently guided to the target by the operator. The mouse was left in the escape box for 1 min and then returned to its home cage before the next training trial. On the next day mice were tested for the 'probe trial' (trial duration 90 s) in which the escape box was removed. All training trials and probe trials were videotaped for 3 min and the latency to enter the escape box/target hole were automatically scored by EthoVision10XT software (Noldus Information Technology B.V., Netherlands).

3.4.4 Non-invasive assessment of sleep and breathing pattern

Hypnic and respiratory phenotypes of mice were assessed non-invasively with a validated technique based on whole-body plethysmography (WBP) (Bastianini *et al.,* 2017; Lo Martire *et al.,* 2017). Briefly, each mouse was placed inside a WBP chamber flushed with air at 1.5 l/h for the first 8 h of the light period. The respiratory (WBP chamber pressure) signal was continuously recorded together with chamber humidity and temperature, digitized, and stored at 128 Hz, 4 Hz, and 4 Hz, respectively. The system was calibrated with a 100 µl micro-syringe (Hamilton, Reno, USA) at the end of each recording. The states of wakefulness, non-rapid-eye-movement sleep (NREMS) and rapid-eye-movement sleep (REMS) were scored based on inspection of the raw WBP signal with the investigators blinded to the animal's genotype. Quantitative analysis of breathing was restricted to stable sleep episodes ≥ 12 s because of the frequent occurrence of movement artefacts during wakefulness. Apnoea's were automatically detected as breaths with instantaneous total breath duration (T_{TOT}) > 3 times; the average T_{TOT} for each mouse and sleep state, and detection accuracy were checked on raw recordings.

3.5 Histological Procedures

3.5.1 Tissue fixation

For immunohistochemical analysis, the animals were sedated with isoflurane (2% pure oxygen) and sacrificed for cervical dislocation. The brains were quickly removed and cut along the midline. The two hemispheres were fixed separately by immersion in a solution of 4% paraformaldehyde in 100 mM phosphate buffer (pH 7.4) for 48 hours and subsequently stored in 20% sucrose for another 24 hours, before being frozen in dry ice and stored at - 80 °C. The hemispheres were then cut with a freezer microtome into 30 µm thick coronal sections which were serially collected in a 96-well plate containing a freezing solution (30% glycerol, 30% ethylene glycol, 0.02% sodium azide in PBS1X).

3.5.2 Immunohistochemistry

Immunohistochemistry was carried out on free-floating sections for the frozen brains. One out of every eight free-floating sections from the hippocampal formation was washed three times for 10 minutes in PBS Triton 0.1%. Sections were blocked in bovine serum

albumin (BSA, 3%) blocking buffer 1X in PBS 1h at room temperature. After blocking, sections were incubated with the primary antibody, overnight at 4°C. The next day, sections were washed three time in PBS Triton 0.1% and then incubated with the secondary antibody, 2h at room temperature. After washing in PBS Triton 0.1% slices were mounted on Poly-L-Lysine coated glass cover slips; nuclei were counterstained with Hoechst 33342 (Sigma-Aldrich). The primary and secondary antibodies used are listed in Table 1. For HA immunostaining, after incubation with an HRP-conjugated secondary antibody, sections were incubated in the TSA Cyanine 3 Plus solution (Perkin Elmer), following the kit instruction.

	Target	Description	Dilution	Manufacturer
Primary Antibody	AIF-1	Rabbit polyclonal	IHC 1:300	ThermoFisher
	GFP	Rabbit polyclonal	IHC 1:500	Invitrogen
	HA	Rabbit monoclonal	IHC 1:500 ICC 1:200 WB 1:1000	Cell signalling Technology
	PSD95	Rabbit polyclonal	IHC 1:1000	Abcam
	TubJ	Mouse monoclonal	ICC 1:100	Sigma
	CDKL5	Sheep polyclonal	WB 1:500	University of Dundee
	P-EB2	Rabbit polyclonal	WB 1:1000	CovalAb
	EB2	Rabbit polyclonal	WB 1:1000	Abcam
Secondary Antibody	Goat anti-Rabbit IgG HRP-conjugated		WB 1:5000 IHC 1:1000	Jackson ImmunoResearch
	Goat anti-Sheep IgG HRP-conjugated		WB 1:5000	Jackson ImmunoResearch
	Goat anti-mouse IgG FITC-conjugated		ICC 1:200	Jackson ImmunoResearch
	Goat anti-rabbit IgG FITC-conjugated		IHC 1:200	Jackson ImmunoResearch
	Goat anti-rabbit IgG Cy3-conjugated		IHC 1:1000 ICC 1:200	Jackson ImmunoResearch

Table 1: Primary and secondary antibodies used.

For quantification of PSD-95 immunoreactive puncta, images from the CA1 layer were acquired using a LEICA TCS SL confocal microscope (LEITZ; Leica Microsystems, Wetzlar, Germany; objective 63X, NA 1.32; zoom factor = 8). Three to four sections per animal were analyzed and the number of PSD-95 immunoreactive puncta was expressed per μm^2.

The number of AIF-1-positive cells (cell density) in the cortex was manually counted using the point tool of the Image Pro Plus software and cell density was established as AIF-1-positive cells/mm^3. For the morphometric microglial cell analysis, starting from 20X

magnification images of AIF-1-stained cortical slices, AIF-1 positive microglial cell body size was manually drawn using the Image Pro Plus (Media Cybernetics, Silver Spring, MD, USA) measurement function, and expressed in μm^2. Fluorescence images were taken with an Eclipse TE 2000-S microscope equipped with a DS-Qi2 digital SLR camera (Nikon Instruments Inc.).

The number of Hoechst-positive nuclei and NeuN-positive neurons in the CA1 layer of the hippocampus was manually counted using the point tool of the Image Pro Plus software and cell density was established as cells/mm^3.

The number of GFP positive cells and Hoechst-positive nuclei, in the cortex (Cx), hippocampus (CA1 layer), and striatum (St) were manually counted using the point tool of the Image Pro Plus software. Density of GFP-positive cells was expressed as number of GFP-positive cells on total cell number.

3.5.3 Golgi staining

Brains were Golgi-stained using the FD Rapid Golgi StainTM Kit (FD NeuroTechnologies, Inc.) Brains were immersed in the impregnation solution containing mercuric chloride, potassium dichromate, and potassium chromate, and stored at room temperature in darkness for 3 weeks. Hemispheres were cut with a microtome in 90-mm-thick coronal sections that were mounted on gelatin-coated slides and were air dried at room temperature in the dark for 1 day. After drying, sections were rinsed with distilled water and subsequently stained in a developing solution (FD Rapid Golgi Stain Kit) (Guidi *et al.,* 2013). A light microscope (Leica Mycrosystems) equipped with a motorized stage and focus control system and a color digital camera (Coolsnap-Pro; Media Cybernetics) were used for neuronal tracing and to take dendritic spine images.

Measurement of the dendritic tree

Golgi-stained CA1 pyramidal cells were traced with dedicated software, custom-designed for dendritic reconstruction (Immagini Computer, Milan, Italy), interfaced with Image Pro Plus (Media Cybernetics, Silver Spring, MD, USA). The dendritic tree was traced live, at a final magnification of 500X, by focusing on the depth of the section. The operator starts with branches emerging from the cell soma and after having drawn the first parent branch goes on with all daughter branches of the next order in a centrifugal direction. At the end

of tracing the program reconstructs the total dendritic length, the mean length of branches and the number of segments.

Spine density/morphology

In Golgi-stained sections, apical spines of CA1 pyramidal neurons were counted using a 100X oil-immersion objective lens. Dendritic spine density was measured by manually counting the number of dendritic spines and expressed as the number of dendritic spines per 10 µm dendritic length. The number of dendritic segments counted per animal was 10–15.

3.6 Western blotting assay

Western blot analysis was first performed on total protein extracts of HEK293T cells transfected with viral plasmids and their corresponding medium. Cellular pellets were lysed with Laemmli buffer (2x) + Beta-mercaptoethanol, vortexed, sonicated for 10 ', and boiled at 95 °C 10'. Brainstems of treated mice were homogenized in ice-cold RIPA buffer (50 mM Tris–HCl, pH 7.4, 150 mM NaCl, 1% Triton-X100, 0.5% sodium deoxycholate, 0.1% SDS) supplemented with 1mM PMSF and 1% protease and phosphatase inhibitor cocktail (Sigma-Aldrich). Protein concentration for both cell and tissue extracts was determined using the Lowry method (Lowry *et al.,* 1951). Equivalent amounts of extract were subjected to polyacrylamide gel electrophoresis (SDS-page) and subsequently transferred to an ECL Hybond nitrocellulose membrane (GE Healthcare Life Sciences, Amersham, UK). The following primary anti-HA (1: 1000, Cell Signaling Technology) and anti-GFP (1: 1000, Invitrogen) antibodies were used for Western blot analysis. The following day, the membranes were incubated with an HRP-conjugated rabbit IgG secondary antibody (1: 5000; Jackson ImmunoResearch) (Table 1).

Signal detection was performed according to the protocol suggested by the supplier of the ECL kit (GE Healthcare Life Sciences). The densitometric analysis of the digitized images was performed with the ChemiDoc XRS instrument and with the Image Lab software (Bio-Rad Laboratories, Hercules, CA, USA).

3.7 Viral biodistribution and viral RNA expression

For biodistribution analysis animals were sedated with isoflurane (2% pure oxygen) and sacrificed for cervical dislocation. The brains were quickly removed and cut along the midline. The various brain regions were separated and stored at -80 °C.

For the quantification of viral DNA copies per cell, the genomic DNA was extracted with the NucleoSpin®Tissue Kit (Macherey-Nagel) extraction kit and used as a qPCR template. A portion of the viral promoter CBh and of the mouse Agouti gene was amplified for the quantification of the number of viral copies present in the sample and for their normalization, respectively. Copy number was interpolated using mean calibration curves for CBh (N = 9) and Agouti (N = 12) obtained from serial dilutions of the viral plasmid and a plasmid containing Agouti cDNA, respectively. The number of viral DNA copies per cell was finally calculated on the amount of genomic used as a template.

For the quantification of the viral RNA expression, the RNA was extracted following the indications of the GRS FullSample Purification Kit (GRISP) extraction kit, subjected to a DNaseI treatment (GRISP), and retro-transcribed to cDNA with the iScript™ kit cDNA Synthesis Kit (Biorad). A portion of the CDKL5 and GAPDH sequence was amplified respectively for the quantification of viral expression and for its normalization. The differential expression folds were calculated with the ΔΔCt method. Quantitative RT-PCRs were performed using SsoAdvanced Universal SYBR Green Supermix (Bio-Rad, CA, USA) in iQ5 Real-Time PCR Detection System (Bio-Rad).

Primers used: CBh = Fw 5'-TACTCCCACAGGTGAGCGG-3 ', Rev 5'-GGCAGGTGCTCCAGGTAAT-3'; mAgouti = Fw 5'-GGCGTGGTCAGTGGTTGTG-3 ', Rev 5'-TTTAGCTTCCACTAGGTTTCCTAGAAA-3'; GAPDH = Fw 5'-GAACATCATCCCTGCATCCA-3 ', Rev 5'-CCAGTGAGCTTCCCGTTCA-3'; m-hCDKL5 = Fw 5'-GACACAAGGAAACACATGAAATTG-3 ', Rev 5'-TCCACAATGTTTTCCTGCTTGA-3'; hCDKL5 (Fw 5’-GCAGACACAAGGAAACACATGA-3’, Rev 5’-CAACTTTCCCCTCCGACGAA-3’).

3.8 Statistical analysis

Data from single animals represented the unity of analysis. Results are presented as mean ± standard error of the mean (± SE), and n indicates the number of mice. Statistical analysis was performed using GraphPad Prism software (GraphPad Software, Inc., San Diego, CA). All datasets were analyzed using the ROUT method (Q=1%) for the

identification of significant outliers and the Shapiro-Wilk test for normality testing. Datasets with normal distribution were analyzed for significance using Student's t-test or an ordinary one-way analysis of variance (ordinary one-way ANOVA). *Post hoc* multiple comparisons were carried out using the Fisher least significant difference (Fisher's LSD) or a Tukey test. Datasets with non-parametric distribution were analyzed using the Kruskal-Wallis test. *Post hoc* multiple comparisons were carried out using Dunn's multiple comparison test or the Mann-Whitney U test. For the open field and the learning phase of the Barnes maze, statistical analysis was performed using a repeated measure two-way analysis of variance (RM two-way ANOVA). A probability level of $p<0.05$ was considered to be statistically significant.

4. RESULTS

4.1 Production of a secretable AAVPHP.B_Igk-TATk-CDKL5 vector for gene therapy

We took advantage of a novel system for the secretion of TAT recombinant proteins from mammalian cells (Flinterman *et al.,* 2009, Trazzi *et al.,* 2018). The success of this system is due to the identification and modification of the two furin sites present in the TAT peptide. Furin is mainly localized in the trans-Golgi network but can translocate between the trans-Golgi network and the cell surface (Denault & Leduc, 1996). Therefore, the presence of these furin sites in the TAT moiety results in the TAT peptide being cleaved from fusion proteins that are secreted via the constitutive pathway. Recently, Flinterman and colleagues introduced mutations to destroy the two furin cleavage sites without affecting TAT protein transduction ability. The modified TAT was named TATκ (Flinterman *et al.,* 2009). The TATκ-fusion gene containing a human CDKL5 or GFP was fused at the N-terminus to the murine Igκ chain leader sequence for protein secretion in culture medium. Due to the absence of a suitable anti-CDKL5 antibody, the TATκ-CDKL5 fusion protein was tagged with a HA epitope to monitor the expression levels and localization of the TATκ-CDKL5 fusion protein.

To express the IgK-TATκ-CDKL5, CDKL5, IgK-TATκ-GFP and GFP proteins by means of AAV vector-mediated gene delivery, an IgK-TATκ-CDKL5, CDKL5, IgK-TATκ-GFP and GFP gene expression cassette (Trazzi *et al.,* 2018), under the control of a strong, long-term, and ubiquitous CNS expression promoter (Gray *et al.,* 2010), was inserted into the AAV vector plasmid (Fig. 10, Materials and Methods section).

To confirm the efficiency of the newly-constructed AAV plasmids to express CDKL5, Igk-TATk-CDKL5, IgK-TATκ-GFP and GFP proteins, we transfected HEK293T cells with the AAV plasmids (Fig. 12A,B). As expected, CDKL5 expression resulted in even distribution of the protein between the nucleus and cytoplasm while TATκ-CDKL5 showed a more cytoplasmic distribution (Fig. 12B), due to the presence of protein secretion via the constitutive secretory pathways. Differently, as previously reported (Flinterman *et al.,* 2009), IgK-TATκ-GFP protein showed a different expression pattern compared to GFP with a speckled nuclear pattern (Fig. 12B).

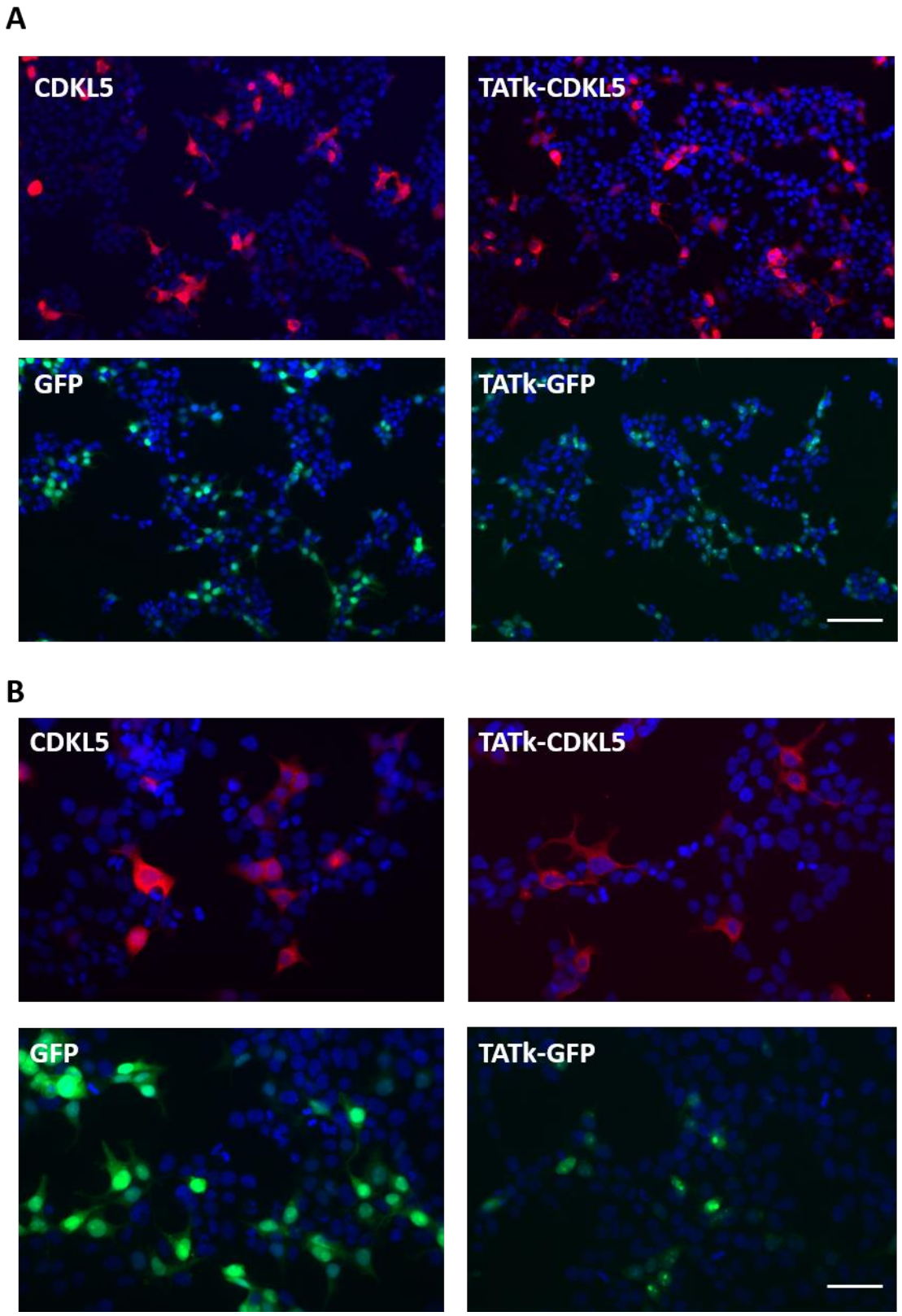

Fig. 12: (A,B) Representative fluorescence images of HEK293T cells transiently transfected with AAV-CBh_IgK-TATk-CDKL5, AAV-CBh_CDKL5, AAV-CBh_IgK_TATk-GFP or AAV-CBh_GFP plasmid (Fig. 10) as indicated in the Materials and Methods section. Cells were immunostained with an anti-

HA antibody (red) or an anti-GFP antibody (green) and nuclei were counterstained with Hoechst. Scale bar = 70 µm (A); = 25 µm (B).

To demonstrate efficient TATk-fusion protein secretion, HEK293T cells were transfected with the AAV plasmids and grown in serum-free medium. After 48 hours the medium was collected, diafiltered and concentrated with 50 kDa cut-off Amicon ultra centrifugal filters (Trazzi *et al.,* 2018). This method allows recovery and concentration of the secreted TATκ-fusion protein. We found an efficient TATk-CDKL5 protein secretion using western blot analysis (Fig. 13A). TATk-CDKL5, but not CDKL5 protein, was detected in the culture medium of HEK293 cells transfected with the AAV_Igk-TATk-CDKL5 or the AAV_CDKL5 plasmid (Fig. 13A). Differently, Western blot analysis detected high levels of both TATκ-GFP and GFP proteins in the culture medium 48 hours after transfection of HEK293T cells (Fig. 13A). This unexpected GFP secretion has been previously reported (Tanudji *et al.,* 2002; Flinterman *et al.,* 2009) and it is probably due to a non-classical secretion by which cells remove the excess of improperly folded, cytosolic GFP protein.

To evaluate whether neurons are transduced by the secreted TATκ-CDKL5 protein, hippocampal neurons were co-cultured, using transwells (Fig. 13B), with HEK293 cells transfected with the AAV-Igk-TATk-CDKL5 or the AAV-CDKL5 plasmid. We found that after 48 h of co-culture, TATk-CDKL5 protein was efficiently internalized by hippocampal neurons (Fig. 13B), while, as expected, no CDKL5-positive neurons were present (data not shown).

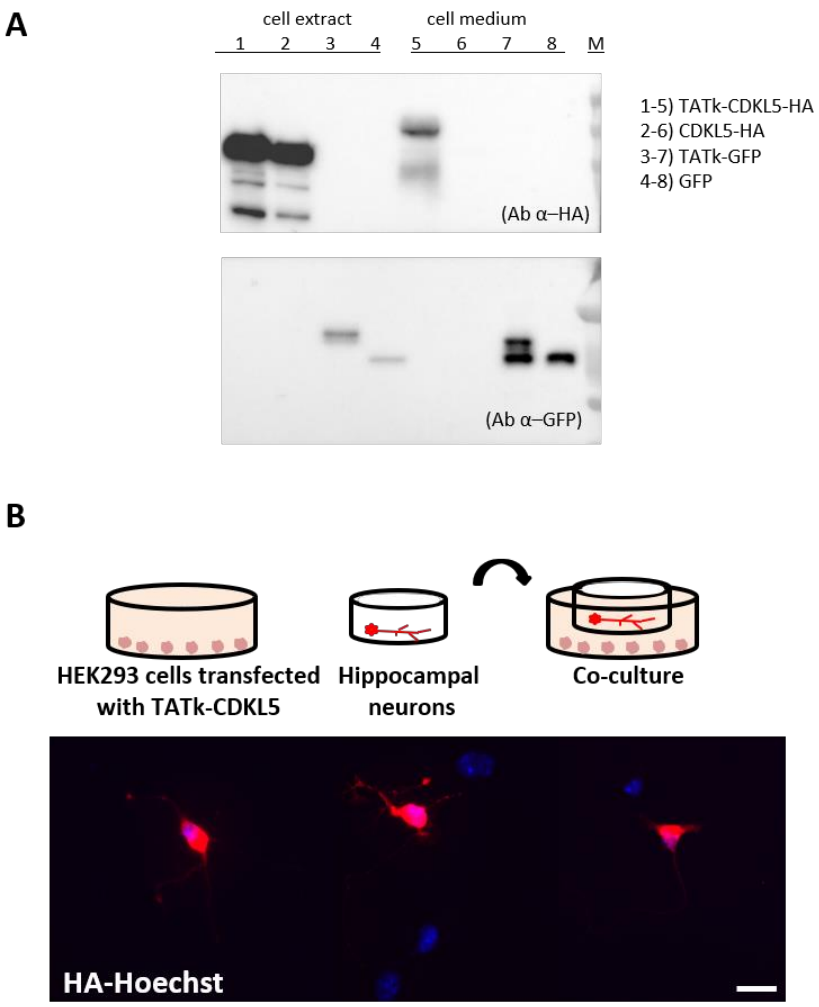

Fig. 13: (A) Western blot analysis using an anti-HA antibody and an anti-GFP antibody confirmed TATk-CDKL5, CDKL5, TATk-GFP and GFP protein expression in transfected HEK293T cells (cell extract, lanes 1-4), and TATk-CDKL5 and TATk-GFP protein accumulation in the concentrated culture medium (lanes 5, 7), indicating that the TATk-CDKL5 and TATk-GFP proteins were secreted from cells. Please note the presence of GFP in the culture medium (line 8) (B) Co-culture experimental design: HEK293T cells were transfected with the AAV vector plasmid containing the IgK-TATk-CDKL5 cassette. Twenty-four hours after transfection, cover glasses with 5-day (DIV5) differentiated primary hippocampal neurons were transferred to the HEK293T 6-well plate in an elevated position. Fluorescence microscopy images showing the presence of TATk-CDKL5 protein in differentiated primary hippocampal neurons from *Cdkl5* -/Y mice co-cultured for 48 h (DIV5-DIV7) with HEK293T cells transfected with AAV-CBh_Igk-TATk-CDKL5 plasmid. Neurons were immunostained with an anti-HA antibody (red) and nuclei were counterstained with Hoechst. Scale bar = 10 µm.

After confirming the secretory and transduction efficiency of the TATk-CDKL5 protein, we produced recombinant AAVPHP.B vector from the above-described AAV vector plasmids using the standard adenovirus-free three plasmid transfection system. The efficiency of the AAVPHP.B vector particles to infect neurons and express recombinant proteins was confirmed by primary hippocampal neuron infection (Fig. 14A,B). Interestingly, when expressed in post-mitotic neurons IgK-TATκ-GFP, similarly to Igk-TATk-CDKL5, showed a expression pattern with a more cytoplasmic distribution compared to GFP and CDKL5, respectively (Fig. 14A,B), suggesting protein secretion via the constitutive secretory pathways.

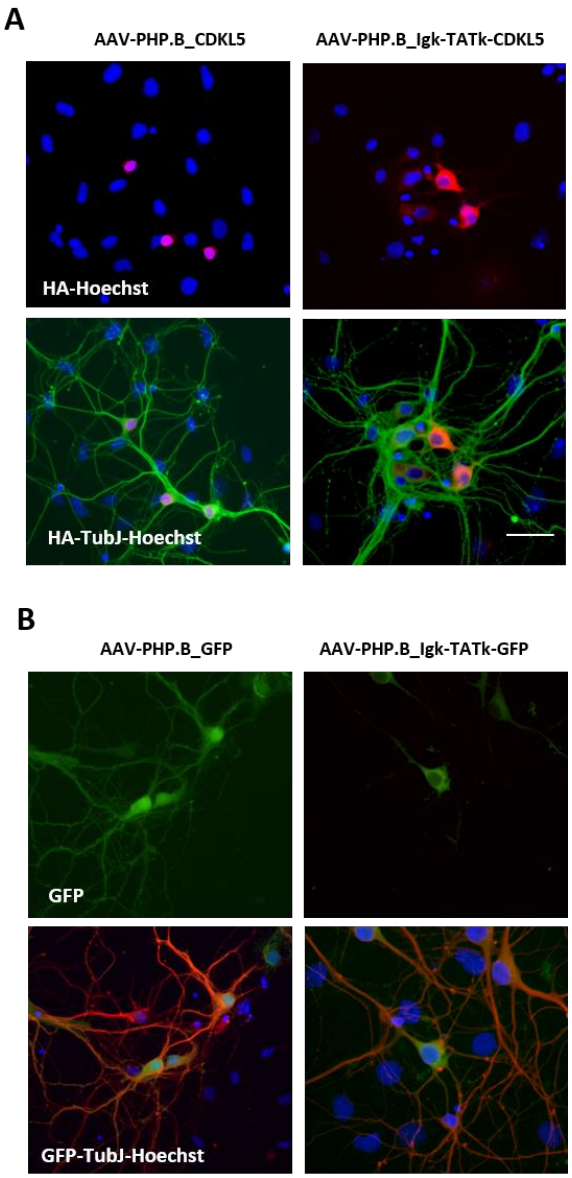

Fig. 14: (A,B) Two-day (DIV2) primary hippocampal neuronal cultures from *Cdkl5* -/Y mice were infected with the AAVPHP.B_Igk-TATk-CDKL5, AAVPHP.B_CDKL5, AAVPHP.B_Igk-TATk-GFP or the

AAVPHP.B_GFP vector (MOI 10^6) and fixed at DIV 7. CDKL5 and TATk-CDKL5 protein localization was assessed by immunostaining with an anti-HA antibody (red) and an anti-β III tubulin antibody (TubJ, green). GFP and TATk-GFP protein localization was assessed by immunostaining with an anti-GFP antibody (green) and an anti-β III tubulin antibody (TubJ, red). Nuclei were counterstained with Hoechst. Scale bar = 10 µm.

Next, we evaluated the efficiency of TATk-CDKL5 protein transduction *in vivo*. Three months old *Cdkl5* -/Y mice were intravenously injected with AAVPHP.B_Igk-TATk-CDKL5 (n=5) or AAVPHP.B_CDKL5 vector (n=5) (dose $5x10^{11}$ vg) and sacrificed 3 months after the injection. After qRT PCR analysis the AAVPHP.B_Igk-TATk-CDKL5 vector showed a similar infection efficiency in comparison with the AAVPHP.B_CDKL5 vector (Table 2A), and induced similar *CDKL5* mRNA levels in the brains and livers of treated mice (Table 2B). Localization of TATk-CDKL5 or CDKL5 was evaluated through immunohistochemistry using an anti-HA antibody and nuclei were counterstained with Hoechst. Given the small number of labeled cells, it was impossible to make a quantitative analysis of the number of positive labeled cells. However, we noticed the presence of less intense immunostained cells surrounding intense stained cells only in the TATk-CDKL5 samples (Fig. 15), suggesting that the AAVPHP.B_Igk-TATk-CDKL5 vector led to a higher CDKL5 protein replacement due to secretion and transduction of the TATk-CDKL5 protein into the neighboring cells (Fig. 15).

A

Intravenous injection

(dose 5x10^11 vg/mouse)

	CDKL5 (N=5)	TAT-CDKL5 (N=5)	p
Cerebellum	1.969 ± 0.345	3.874 ± 1.923	0.382
Cortex	0.604 ± 0.068	1.937 ± 1.242	0.344
Hippocampus	0.633 ± 0.048	0.989 ± 0.512	0.526
Striatum	1.956 ± 0.373	2.595 ± 0.927	0.580
Liver	33.900 ± 3.195	69.672 ± 22.796	0.192

B

Intravenous injection

(dose 5x10^11 vg/mouse)

	CDKL5 (N=4)	TAT-CDKL5 (N=4)	p
Cortex	318.4 ± 114.3	546.2 ± 327.9	0.536
Liver	224.6 ± 67.3	253.5 ± 94.4	0.820

Table 2: (A) Brain and Liver transduction following intravenous injection of AAVPHP.B_CDKL5 (n=5) and AAVPHP.B_Igk-TATk-CDKL5 (n=5) vectors. Vector genome dissemination was assessed using qPCR and expressed as viral genomes per diploid cell (vg/cell). (B) Expression of mRNA for CDKL5 in the cortex and liver of *Cdkl5* -/Y mice intravenously injected with AAVPHP.B_CDKL5 (n=4) and AAVPHP.B_Igk-TATk CDKL5 (n=5) vectors. Values are presented as means ± SE.

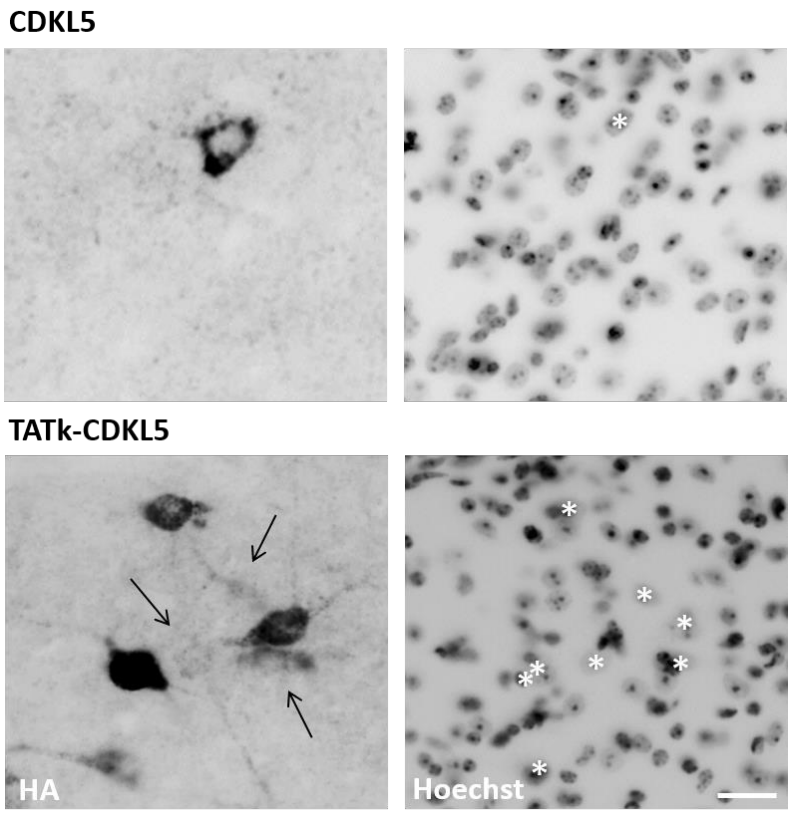

Fig. 15: Adult mice (3 months) were systemically treated (intravenous tail injection) with AAVPHP.B_CDKL5 or AAVPHP.B_Igk-TATk-CDKL5 vectors, and brain samples were collected 90 days post injection. Images show TATk-CDKL5 or CDKL5 protein localization in the striatum of treated mice 90 days post injection. Localization of TATk-CDKL5 or CDKL5 was evaluated through immunohistochemistry using an anti-HA antibody and nuclei were counterstained with Hoechst. Scale bar = 25 µm. The arrows indicate the cells that probably received TATk-CDKL5 by local diffusion; the asterisks indicate the nuclei of the immunolabeled cells.

4.2 Effect of gene therapy with AAVPHP.B_Igk-TATk-CDKL5 or AAVPHP.B_CDKL5 vector on behavior in *Cdkl5* KO mice

To compare the effects of a gene therapy with the AAVPHP.B_CDKL5 vector or the AAVPHP.B_Igk-TATk-CDKL5 vector, adult *Cdkl5* KO male mice were administered viral particles at the dose of $1x10^{12}$ vg via intracarotid injection. To compare the effectiveness of the two viral vectors, we used a viral dose that results in an average value of 15-35% infected cells in different brain regions (Fig. 16A).

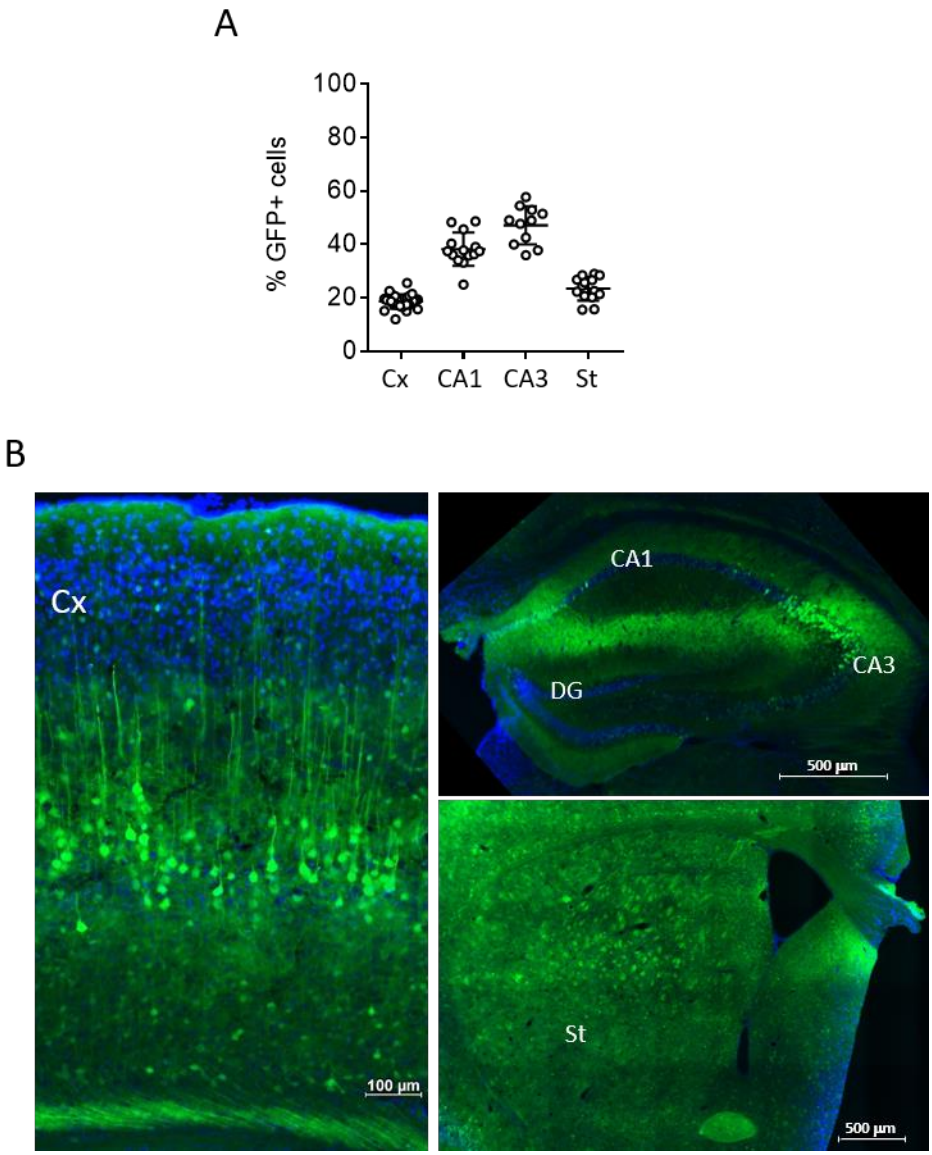

Fig. 16: (A) Quantification of GFP-positive cells in the cortex (Cx), hippocampus (CA1 layer), and striatum (St) of a Cdkl5 -/Y mouse that had undergone intracarotid injection with AAVPHP.B_GFP vector (dose $1x10^{12}$ vg). The brain was collected 90 days post injection. (B) Representative fluorescence images of brain sections processed for GFP immunohistochemistry of a Cdkl5 -/Y mouse treated with intracarotid injection with AAVPHP.B_GFP vector (dose $1x10^{12}$ vg).

To allow protein expression and consequent recovery of brain structure and function, the effects of treatment were evaluated starting from 60 days post-injection (Fig. 17A). The sequence of the tests was arranged to minimize the effect of one test influencing subsequent evaluation of the next test. A group of vehicle-treated *Cdkl5* KO (-/Y) and wild-type (+/Y) mice were used as controls for behavioral tests. Importantly, no changes in terms of body weight, sleep pattern or microglial cell number were observed in treated

Cdkl5 KO mice compared to age-matched vehicle-treated mice (Fig. 17B,C,D), indicating that viral infection and secreted CDKL5 protein did not affect animal well-being and/or cause an inflammatory response.

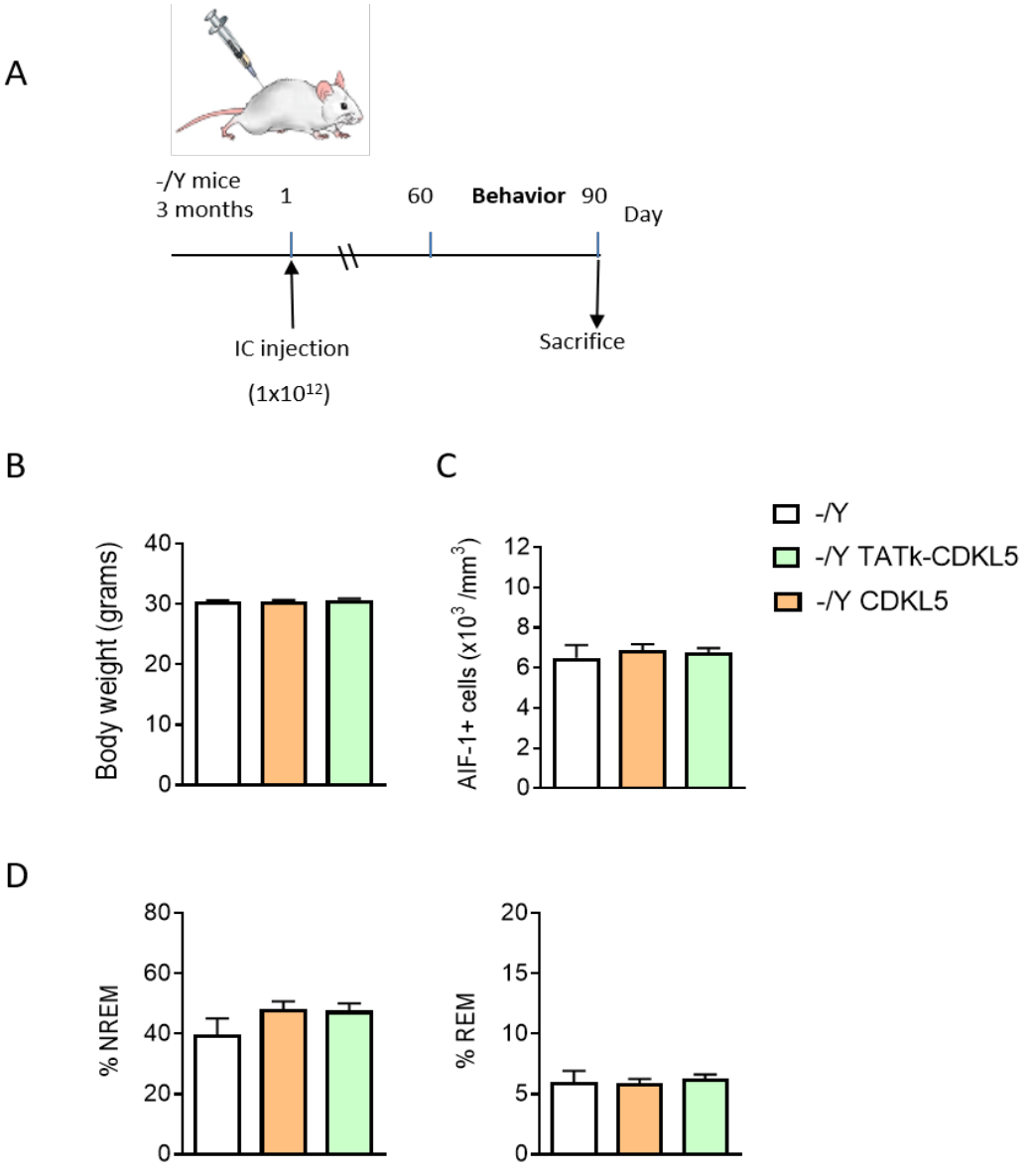

Fig. 17: (A) Experimental plan. Adult mice (3 months) were systemically treated (intracarotid injection; IC) with vehicle, or with either AAVPHP.B_CDKL5 or AAVPHP.B_Igk-TATk-CDKL5 vector, and brain samples were collected 90 days post injection. (B) Body weight (in grams) of vehicle-treated *Cdkl5* KO mice (-/Y; n = 10) and *Cdkl5* -/Y mice treated with AAVPHP.B_CDKL5 (n = 16) or AAVPHP.B_Igk-TATk-CDKL5 (n = 18) vectors according to the treatment schedule shown in A. Mice were weighed before the sacrifice at 90 days post injection. (C) Quantification of AIF-1-positive cells in the somatosensory cortex of vehicle-treated *Cdkl5* KO mice (-/Y; n = 3) and *Cdkl5* -/Y mice treated with AAVPHP.B_CDKL5 (n = 4) or AAVPHP.B_Igk-TATk-CDKL5 (n = 4) vectors. Values are presented as means ± SE. (D) Percentage of time spent in non-rapid-eye-movement sleep (NREMS)

and rapid-eye-movement sleep (REMS) during whole-body-plethysmography recordings of vehicle-treated *Cdkl5* KO mice (-/Y; n = 7) and *Cdkl5* -/Y mice treated with AAVPHP.B_CDKL5 (n = 16) or AAVPHP.B_Igk-TATk-CDKL5 (n = 16) vectors.

Loss of Cdkl5 function in *Cdkl5* KO mice is associated with autistic-like (ASD-like) phenotypes, analyzed through home-cage social behaviors (marble burying and nest building ability) (Fuchs *et al.,* 2018). *Cdkl5* KO (-/Y) mice buried a significantly lower number of marbles and showed a reduced nest building ability compared to wild-type (+/Y) mice (Fig. 18A,B). Sixty days after treatment with AAVPHP.B_Igk-TATk-CDKL5 vector *Cdkl5* KO mice buried a higher number of marbles compared to vehicle-treated and AAVPHP.B_CDKL5-treated *Cdkl5* KO mice (Fig. 18AA). Similarly, nest building ability was improved only in *Cdkl5* KO mice treated with AAVPHP.B_Igk-TATk-CDKL5 vector (Fig. 18B). Stereotypic movements characterize *Cdkl5* KO mice (Amendola *et al.,* 2014; Fuchs *et al.,* 2018) and CDD patients (Bahi-Buisson & Bienvenu, 2012). In order to examine the effect of gene therapy on motor stereotypies, mice were tested for hind-limb clasping (Fig. 18C). Unlike wild-type (+/Y) mice, vehicle-treated and AAVPHP.B_CDKL5-treated *Cdkl5* KO (-/Y) mice spent a lot of time in the clasping position (Fig. 18C). *Cdkl5* KO mice treated with AAVPHP.B_Igk-TATk-CDKL5 vector showed a decrease in clasping (Fig. 18C), indicating that gene therapy with Igk-TATk-CDKL5 has a greater positive impact on the stereotypic behavior that is due to loss of Cdkl5 expression.

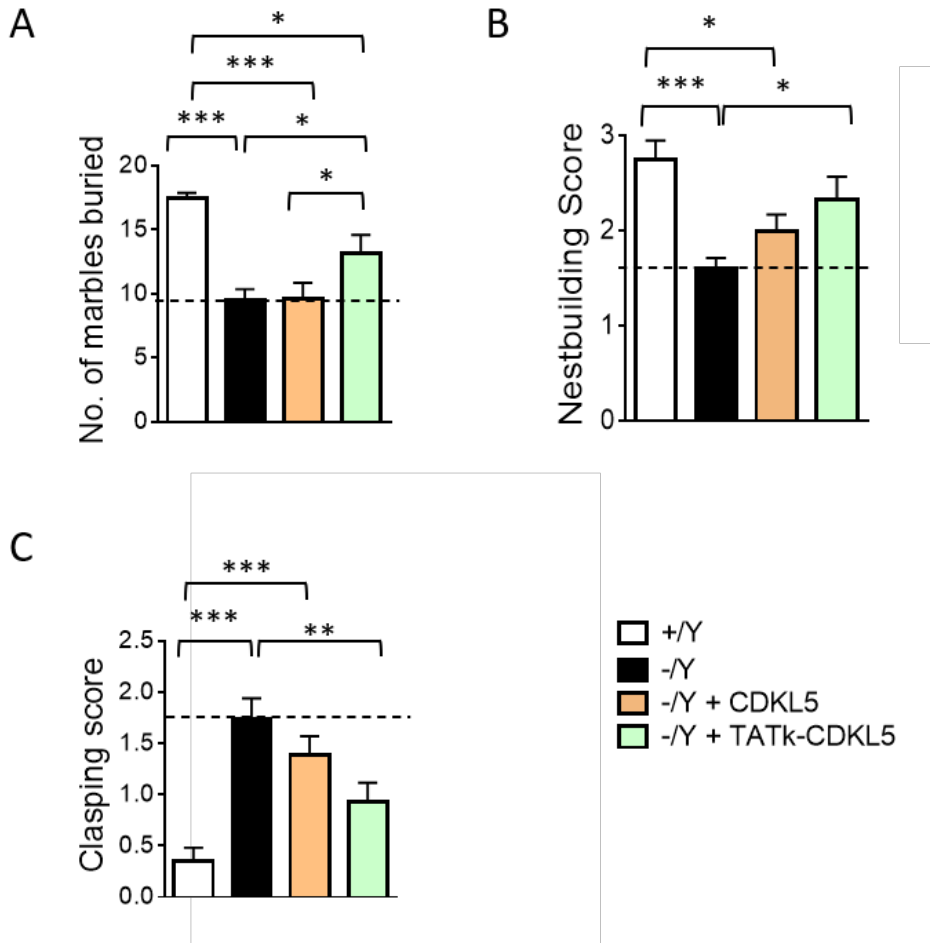

Fig. 18: (A, B) Autistic-like features in treated *Cdkl5* KO mice as in Fig. 17 A. Number of marbles buried (A) and nest quality (B) of wild-type mice (+/Y, n = 20) and *Cdkl5* KO mice (-/Y, n = 6 (A); n = 16 (B)) and of *Cdkl5* -/Y mice 60 days from treatment with AAVPHP.B_CDKL5 (n = 26) or AAVPHP.B_Igk-TATk-CDKL5 (n = 25). (C) Hind-limb clasping score during a 2 min interval in wild-type mice (+/Y, n = 20) and *Cdkl5* KO mice (-/Y, n = 16), and in *Cdkl5* -/Y mice 60 days after treatment with AAVPHP.B_CDKL5 (n = 26) or AAVPHP.B_Igk-TATk-CDKL5 (n = 25). Values are presented as means ± SE. *p < 0.05; **p < 0.01; ***p < 0.001 (Dunn's test after Kruskall-Wallis).

We assessed motor function of treated *Cdkl5* KO mice in the open-field test. The elevated locomotor activity (longer distance traveled with a higher average speed; Fig. 19B) that characterizes *Cdkl5* KO mice was improved by treatment with AAVPHP.B_Igk-TATk-CDKL5 vector (Fig. 19), while no improvement was observed in mice treated with AAVPHP.B_CDKL5 vector.

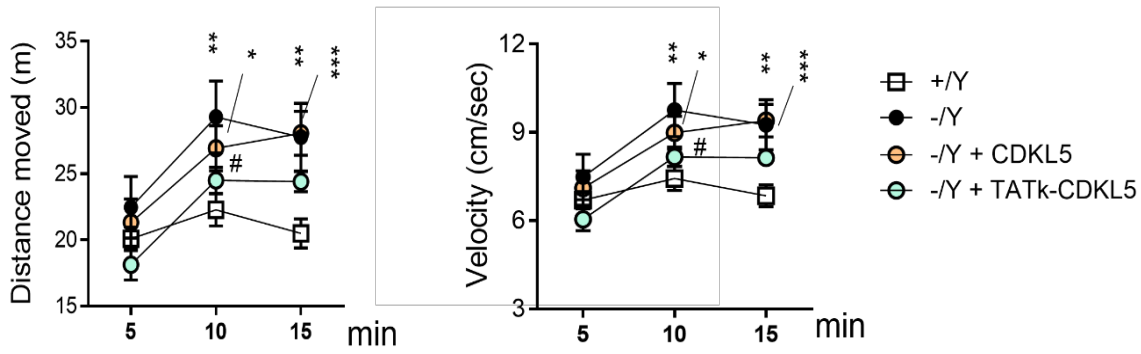

Fig. 19: Total distance traveled (left graph) and average locomotion velocity (right graph) of wild-type mice (+/Y, n = 20) and *Cdkl5* KO mice (-/Y, n = 16), and of *Cdkl5* -/Y mice treated with AAVPHP.B_CDKL5 (n = 26) or AAVPHP.B_Igk-TATk-CDKL5 (n = 25), during a 15 min open field test. Values are presented as means ± SE. *p < 0.05; **p < 0.01; ***p < 0.001 compared to the vehicle-treated wild-type condition; #p < 0.05 as compared to the vehicle-treated *Cdkl5* -/Y samples (Fisher's LSD test after RM two-way ANOVA).

Learning and memory were evaluated using the Barnes maze test, a cognitive paradigm in which *Cdkl5* KO mice are documented to be impaired (Okuda *et al.,* 2018). A significative improvement in learning was observed only in *Cdkl5* KO mice treated with AAVPHP.B_Igk-TATk-CDKL5 vector (Fig. 20A). The latency that animals have before finding the escape box were assessed by the probe trial on the 4th day, confirming the spatial memory impairment of *Cdkl5* KO mice (Fig. 20B). No memory improvement was observed in *Cdkl5* KO mice treated with AAVPHP.B_Igk-TATk-CDKL5 or AAVPHP.B_CDKL5 vector (Fig. 20B).

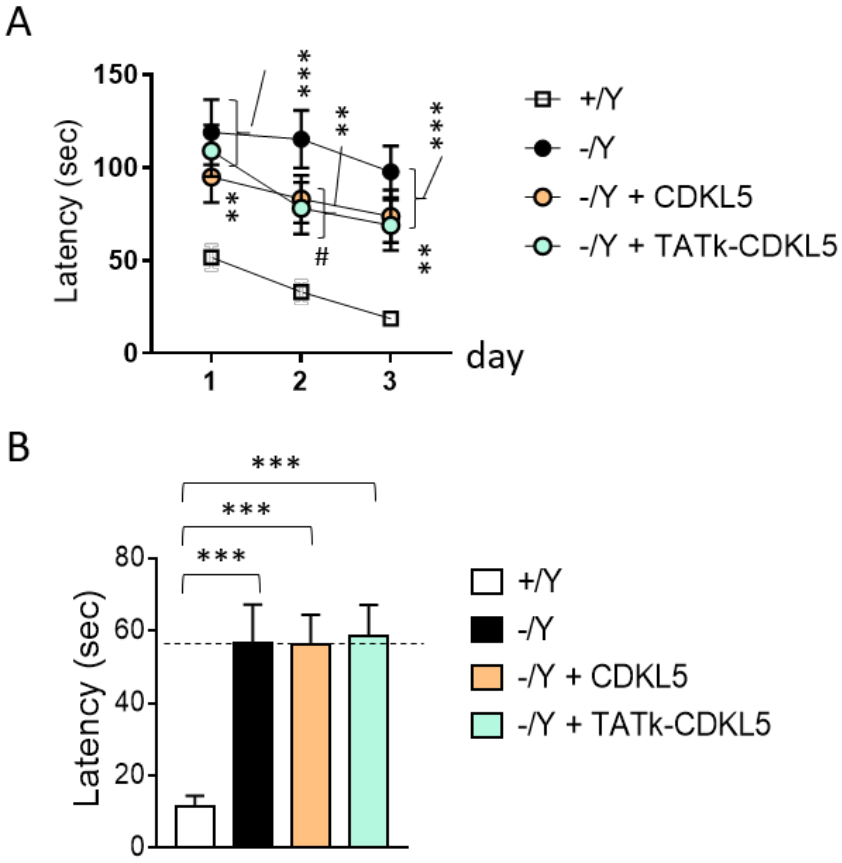

Fig. 20: Spatial learning and memory assessed using the Barnes Maze in wild-type mice (+/Y, n = 16) and *Cdkl5* KO mice (-/Y, n = 11), and in *Cdkl5* -/Y mice treated with AAVPHP.B_CDKL5 (n = 16) or AAVPHP.B_Igk-TATk-CDKL5 (n = 14). Graphs show the mean latency to find the target hole during the 3-day learning period (A) and the latency to find the target hole (B), on the probe day (day 4). Values are presented as means ± SE. **p < 0.01; ***p < 0.001 compared to the vehicle-treated wild-type condition; #p < 0.05 as compared to the vehicle-treated *Cdkl5* -/Y samples (Fisher's LSD test after RM two-way ANOVA, Fig. 20A; Dunn's test after Kruskall-Wallis, Fig. 20B).

A breathing disturbance during sleep in *Cdkl5* KO mice was recently described (Trazzi *et al.,* 2018; Fuchs *et al.,* 2018; Lo Martire *et al.,* 2017). Using whole-body plethysmography, we found that treatment with both AAVPHP.B_CDKL5 and AAVPHP.B_Igk-TATk-CDKL5 vectors led to a drastic reduction in the number of apneas during REM sleep that became similar to that of wild-type mice (Fig. 21). In contrast, an improvement was not achieved during NREM sleep (Fig. 21).

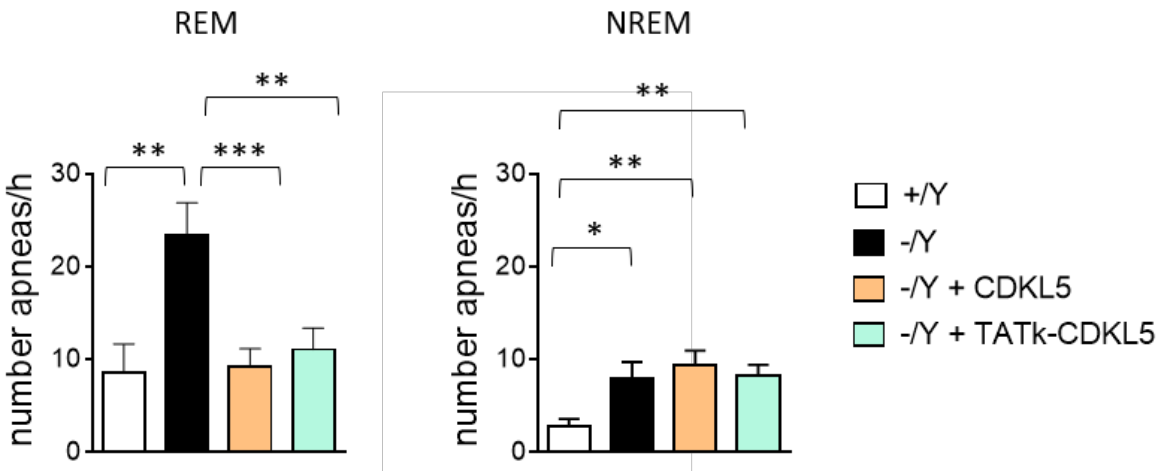

Fig. 21: Sleep apnea occurrence rate in treated *Cdkl5 KO* mice was assessed using whole-body plethysmography. Sleep apnea occurrence in vehicle-treated wild-type (+/Y, n = 9) and *Cdkl5* -/Y(-/Y, n = 7) mice, and in *Cdkl5* -/Y mice treated with AAVPHP.B_CDKL5 (n = 16) or AAVPHP.B_Igk-TATk-CDKL5 (n = 15), during rapid eye movement (REM) sleep and non-rapid eye movement (NREM) sleep. Values are presented as means ± SE. *p < 0.05; **p < 0.01; ***p < 0.001 (Fisher's LSD test after one-way ANOVA).

4.3 Effect of gene therapy with AAVPHP.B_Igk-TATk-CDKL5 or AAVPHP.B_CDKL5 vector on dendritic hypotrophy and connectivity in the hippocampus of *Cdkl5* KO mice

Dendritic arborization was found to be reduced in cortical and hippocampal pyramidal neurons of *Cdkl5* KO mice (Amendola *et al.,* 2014; Fuchs *et al.,* 2015; Trazzi *et al.,* 2016; Fuchs *et al.,* 2018). In addition, *Cdkl5* KO mice exhibit a deficit in dendritic spine structure and stabilization (Ricciardi *et al.,* 2012; Fuchs *et al.,* 2015; Della Sala *et al.,* 2016) and a reduction in the number of PSD-95-positive puncta (Trazzi *et al.,* 2016; Trazzi *et al.,* 2018), which indicates loss of excitatory synaptic contacts. In order to establish the effect of gene therapy on dendritic pattern, we evaluated the dendritic length and spine density of CA1 pyramidal neurons (Fig. 22). In *Cdkl5* -/Y mice treated with AAVPHP.B_Igk-TATk-CDKL5 vector the length of both apical and basal dendrites was recovered compared to vehicle-treated and AAVPHP.B_CDKL5-treated *Cdkl5* KO mice (Fig. 22C), an improvement which may be mainly attributable to a recovery in the number of branches (Fig. 22C).

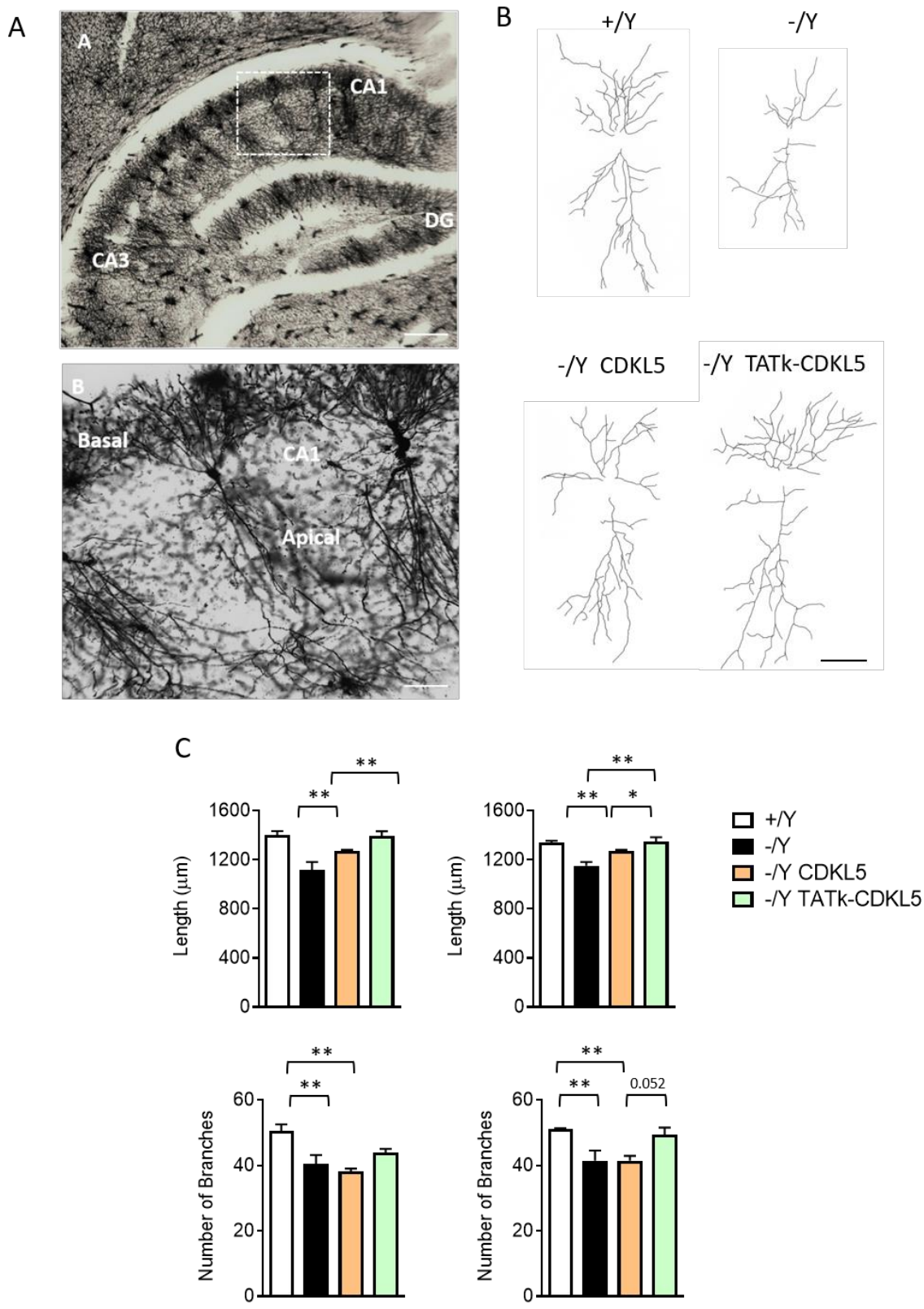

Fig. 22: (A) Example of a Golgi-stained slide at the level of hippocampus; magnification of the CA1 layer bounded by a white dashed rectangle is reported in the lower panel. Scale bar = 100 µm (upper panel), 30 µm (lower panel). (B) Example of the reconstructed apical and basal dendritic tree of Golgi-stained CA1 pyramidal neurons of 1 animal from each experimental group. Scale bar

= 40 µm (C) Apical (left graphs) and basal (right graphs) mean total dendritic length and mean number of dendritic segments of Golgi-stained CA1 pyramidal neurons of wild-type (+/Y, n = 3) and *Cdkl5* KO (-/Y, n = 3) mice and of Cdkl5 -/Y mice 90 days from treatment with AAVPHP.B_CDKL5 (n = 4) or AAVPHP.B_Igk-TATk-CDKL5 (n = 4). Abbreviation: DG, dentate gyrus. Values are represented as means ± SE. *P< 0.05; **P < 0.01 (Turkey's test after one-way ANOVA).

Unlike in AAVPHP.B_CDKL5-treated *Cdkl5* -/Y mice, we found a recovery of spine density in *Cdkl5* -/Y mice treated with AAVPHP.B_Igk-TATk-CDKL5 vector in comparison with vehicle-treated *Cdkl5* -/Y mice (Fig. 23A,B). The percentage of mature spines was restored in *Cdkl5* KO mice treated with AAVPHP.B_Igk-TATk-CDKL5 vector (Fig. 23B), and it was only partially recovered in *Cdkl5* KO mice treated with AAVPHP.B_CDKL5 (Fig. 23B).

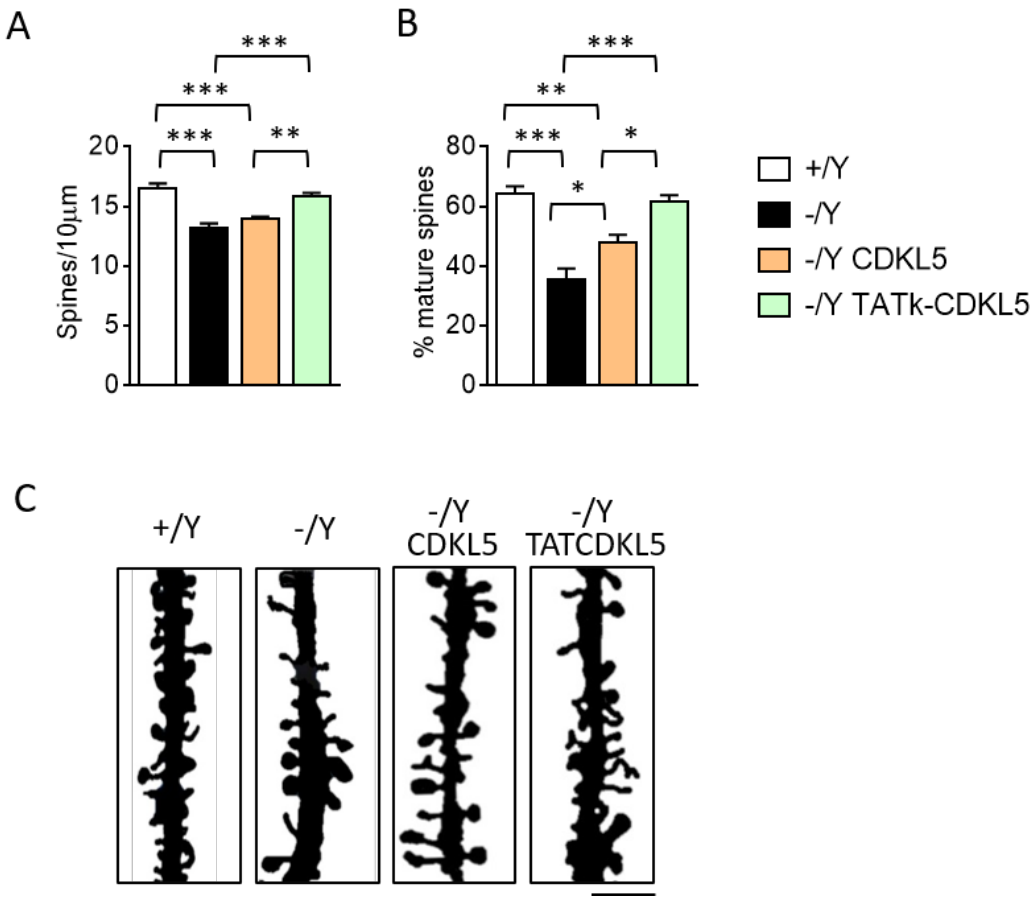

Fig. 23: Dendritic spine density (A) and percentage of mature spines in relation to the total number of protrusions (B) of CA1 pyramidal neurons from wild-type (+/Y, n = 3) and *Cdkl5* KO (-/Y, n = 3) mice and of *Cdkl5* -/Y mice treated with AAVPHP.B_CDKL5 (n = 4) or AAVPHP.B_Igk-TATk-CDKL5 (n = 4). (C) Images of Golgi-stained dendritic branches of CA1 pyramidal neurons of 1 animal from

each experimental group. Scale bar = 2 µm. Values are represented as means ± SE. *P< 0.05; **P < 0.01; ***P < 0.001 (Turkey's test after one-way ANOVA).

Similarly, the number of PSD-95 puncta was restored in AAVPHP.B_Igk-TATk-CDKL5 treated *Cdkl5* -/Y mice (Fig. 24A), while only a partial improvement was present in *Cdkl5* KO mice treated with AAVPHP.B_CDKL5 (Fig. 24A).

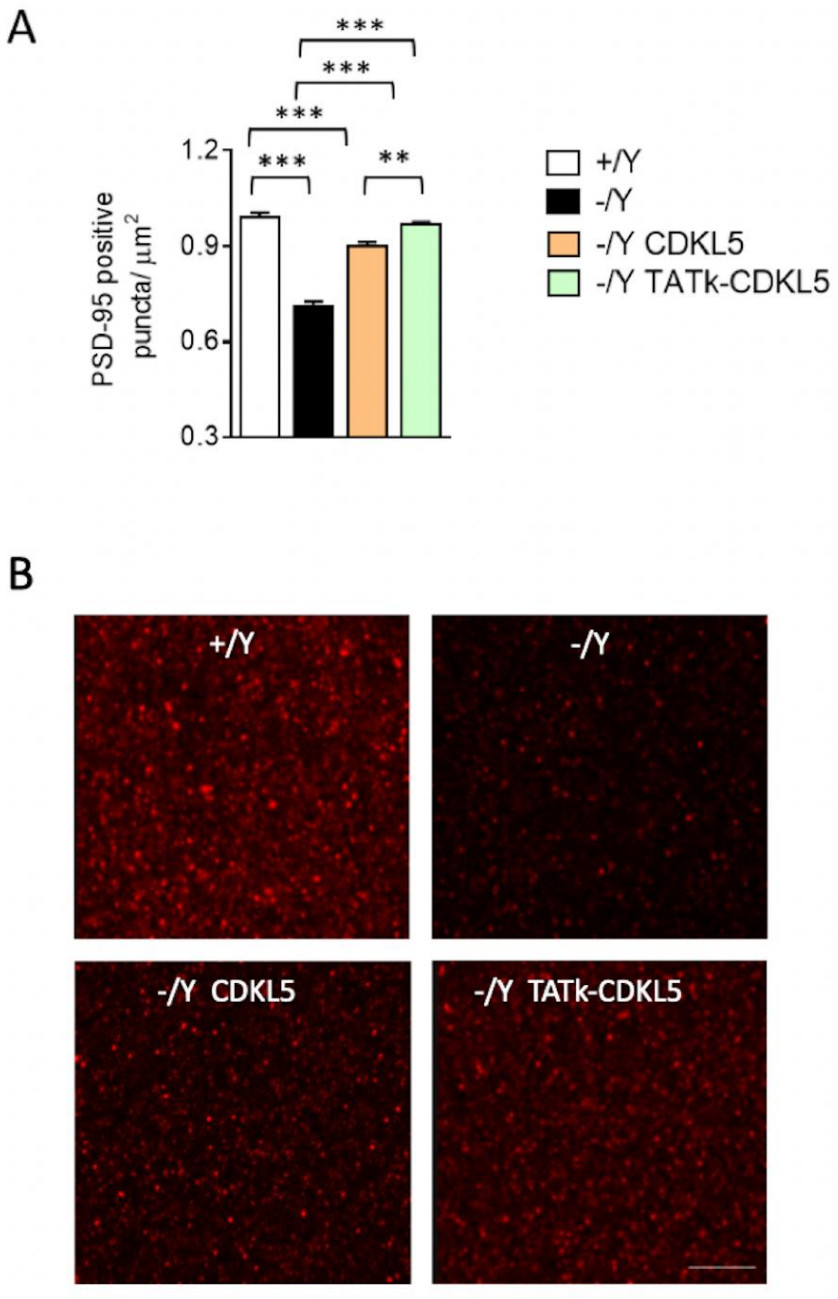

Fig. 24: (A) Number of fluorescent puncta per mm^2 exhibiting PSD-95 immunoreactivity in the CA1 layer of the hippocampus of wild-type (+/Y, n = 3) and *Cdkl5* KO (-/Y, n = 3) mice and of *Cdkl5* -/Y mice treated with AAVPHP.B_CDKL5 (n = 4) or AAVPHP.B_Igk-TATk-CDKL5 (n = 4). (B)

Representative fluorescence image of PSD-95 immunoreactive puncta in the hippocampus of 1 animal from each experimental group. Scale bar = 6 µm. Values are represented as means ± SE. **P < 0.01; ***P < 0.001 (Turkey's test after one-way ANOVA).

4.4 Effect of gene therapy with AAVPHP.B_Igk-TATk-CDKL5 or AAVPHP.B_CDKL5 vector on neuronal survival and microglia activation in the brain of *Cdkl5* -/Y mice

Cdkl5 KO mice are characterized by decreased survival of hippocampal neurons (Loi *et al.,* 2021; Gennaccaro *et al.,* 2021b), and by an increased microglial activation (Galvani *et al.,* 2021). *Cdkl5* KO mice treated with AAVPHP.B_Igk-TATk-CDKL5 vector showed a higher number of Hoechst-positive nuclei and NeuN-positive pyramidal neurons in the CA1 layer (Fig. 25A,B and 26) in comparison with vehicle- and AAVPHP.B_CDKL5-treated *Cdkl5* -/Y mice, indicating that a gene therapy with Igk-TATk-CDKL5 has a greater positive impact on the impaired neuronal survival that is due to loss of Cdkl5 expression.

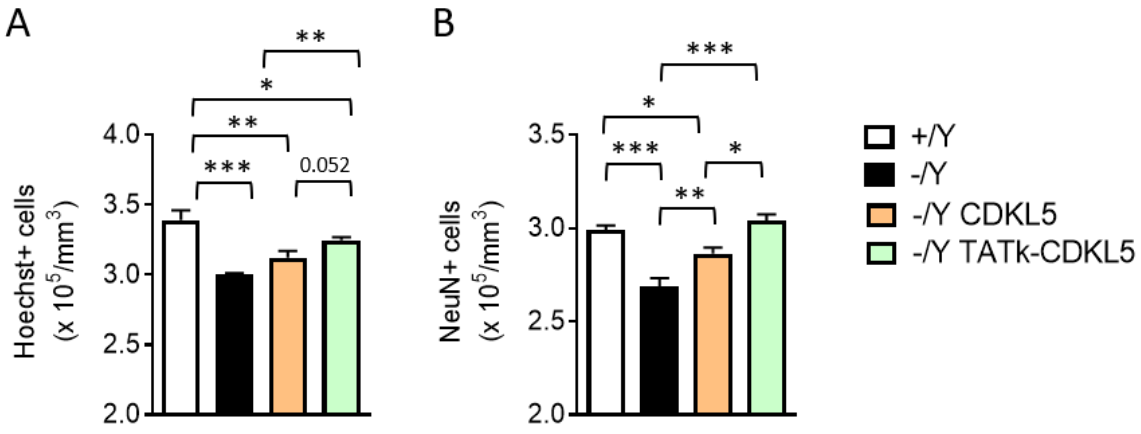

Fig. 25: Quantification of Hoechst-positive cells (A) and NeuN-positive cells (B) in the CA1 layer of hippocampal sections from wild-type (+/Y, n = 3) and *Cdkl5* KO (-/Y, n = 3) mice and from *Cdkl5* -/Y mice treated with AAVPHP.B_CDKL5 (n = 4) or AAVPHP.B_Igk-TATk-CDKL5 (n = 4). Values are represented as means ± SE. *P< 0.05; **P < 0.01; ***P < 0.001 (Fisher's LSD test after one-way ANOVA).

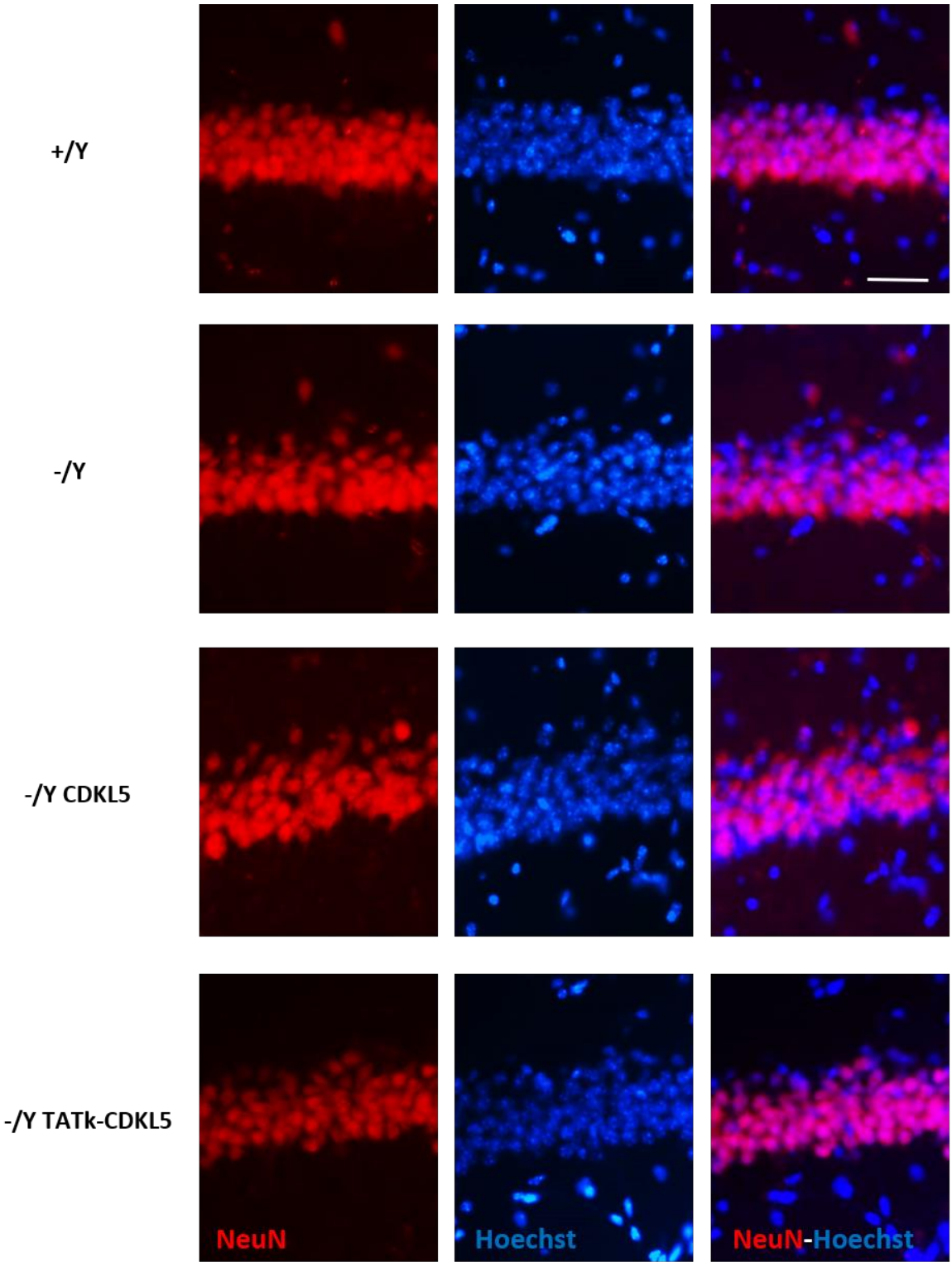

Fig. 26: Representative fluorescence images of sections that were immunopositive for NeuN (red) and counterstained with Hoechst (blue) in the hippocampal CA1 region of 1 animal from each group. Scale bar = 50 µm.

Similarly, a reversal of the inflammatory status, with a reduction in microglial soma size compared to the control levels, was present only in *Cdkl5* KO mice treated with AAVPHP.B_Igk-TATk-CDKL5 vector (Fig. 27).

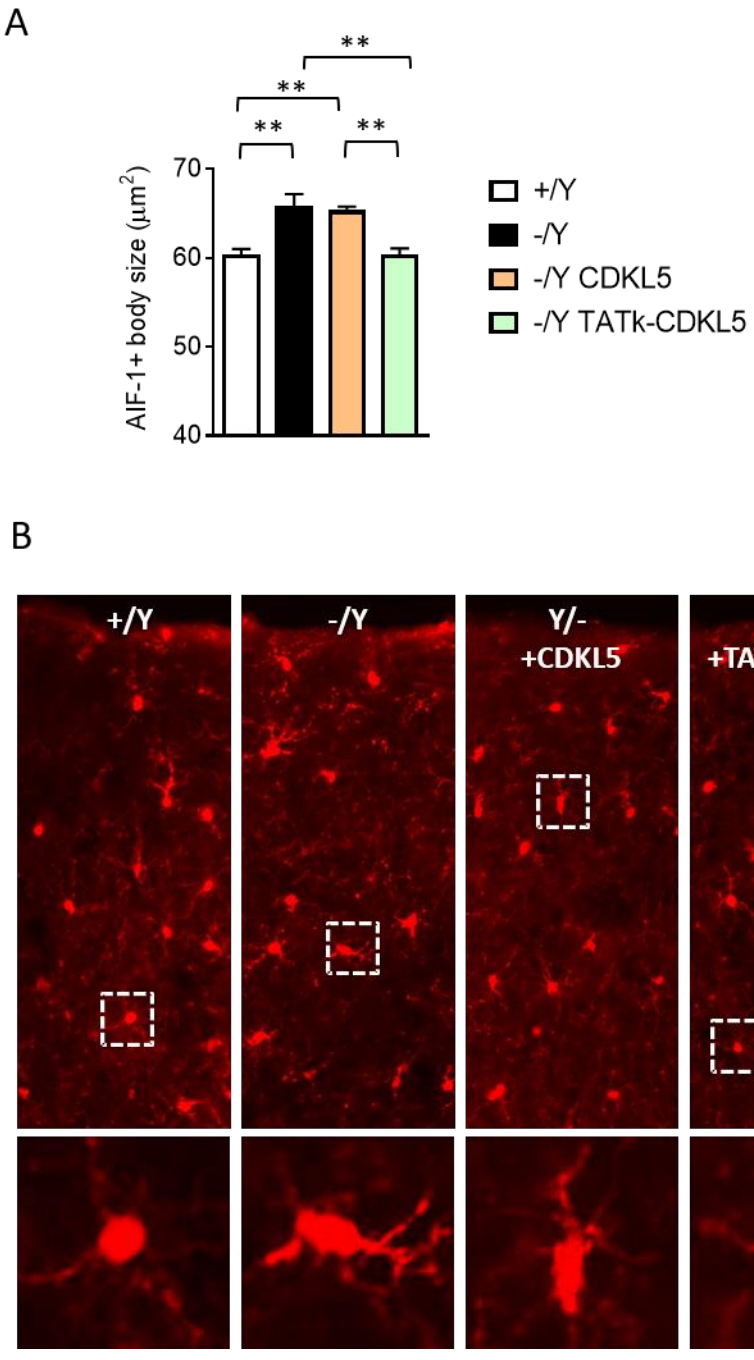

Fig. 27: (A) Mean of microglia cell body size in hippocampal sections from wild-type (+/Y, n = 3) and *Cdkl5* KO (-/Y, n = 3) mice, and from *Cdkl5* -/Y mice treated with AAVPHP.B_CDKL5 (n = 4) or AAVPHP.B_Igk-TATk-CDKL5 (n = 4). (C) Representative fluorescence images of hippocampal sections processed for AIF-1 immunohistochemistry of one animal from each group. The dotted boxes in the upper panels indicate microglial cells shown in magnification in the lower panels. Scale

bar = 30 µm (low magnification), 10 µm (high magnification). Values are represented as means ± SE. **p < 0.01 (Fisher's LSD test after one-way ANOVA).

4.5 Evaluation of the efficiency of AAV vector transduction and CDKL5 protein biodistribution

To quantify and compare the efficiency of gene transfer between AAVPHP.B_Igk-TATk-CDKL5 and AAVPHP.B_CDKL5 vectors vectors, we assessed vector genome copy numbers per cell in several brain regions via qPCR. We found that AAVPHP.B_Igk-TATk-CDKL5 and AAVPHP.B_Igk-TATk-CDKL5 vectors had the same brain transduction efficiency, regardless of the tropism of various brain regions (Fig. 28A).

By comparing the *CDKL5* mRNA levels in treated *Cdkl5* KO mice versus those of wild-type mice we found that the levels in treated mice were much lower than those of wild-type mice in almost all the brain regions analyzed (Fig. 28B), indicating only a partial recovery of CDKL5 expression in *Cdkl5* KO mice. Only in the brainstem, a brain structure with relatively low CDKL5 physiological levels (Fig. 28B), did the *CDKL5* mRNA reach the levels of wild-type mice, even exceeding them (Fig. 28B), suggesting a full recovery of CDKL5 expression in this brain region. The low level of *CDKL5* expression in the brains of treated *Cdkl5* KO mice was confirmed by western blot analysis (Fig. 28C).

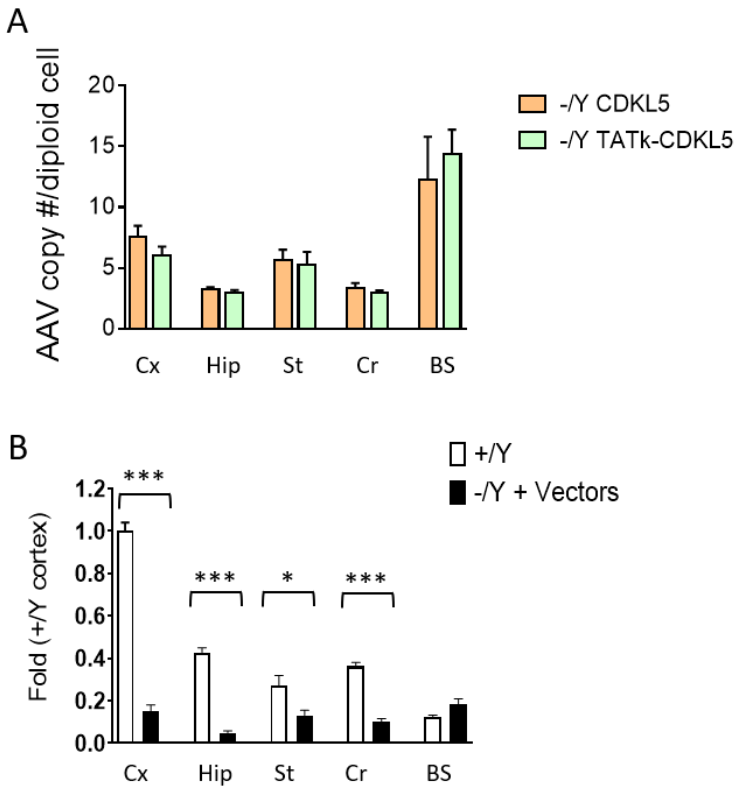

Fig. 28 (A,B): (A) Vector genome copy numbers per diploid genomic equivalent in the cortex (Cx, n = 24), hippocampus (Hip, n = 16), striatum (St, n = 16), cerebellum (Cr, n = 24), and brainstem (Bs, n = 4) of *Cdkl5* -/Y mice treated with AAVPHP.B_CDKL5 or AAVPHP.B_Igk-TATk-CDKL5. (B) Expression of mRNA for *CDKL5* in the cortex (Cx), hippocampus (Hip), striatum (St), cerebellum (Cr), and brainstem (Bs) of vehicle-treated wild-type mice (+/Y, n = 5) and of *Cdkl5* KO mice treated with AAVPHP.B vectors (AAVPHP.B_CDKL5 and AAVPHP.B_Igk-TATk-CDKL5; n = 9). Data are given as the fold change of the +/Y cortex. Data are given as the fold change of the +/Y cortex. Values are represented as means ± SE. *P< 0.05; ***P < 0.001 (ordinary one-way ANOVA).

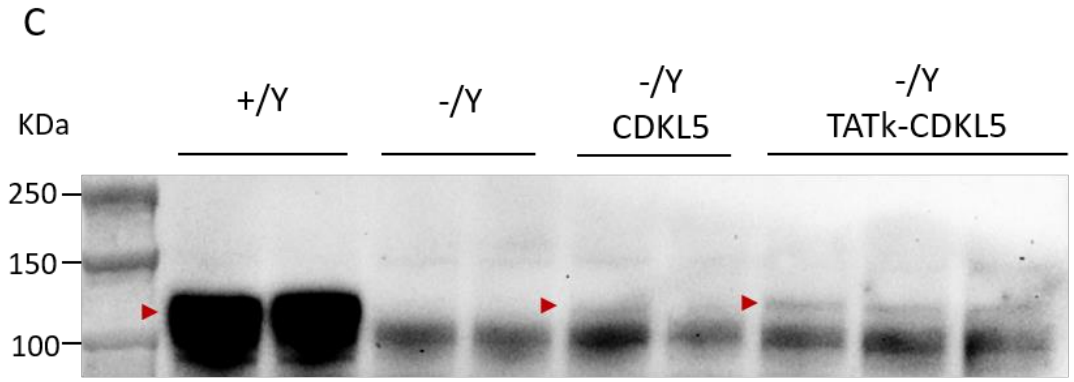

Fig. 28C: Western blot analysis of CDKL5 in brainstem protein extracts from vehicle-treated wild-type (+/Y, n =2) and *Cdkl5* KO (-/Y; n = 2) mice, and those from *Cdkl5* -/Y mice treated with

AAVPHP.B_CDKL5 (n = 2) or AAVPHP.B_Igk-TATk-CDKL5 (n = 3) vectors according to the treatment schedule shown in Fig 17A. Red arrowheads indicate mouse Cdkl5 in *Cdkl5* +/Y extracts, human CDKL5 and TATk-CDKL5 in AAVPHP.B_CDKL5 and AAVPHP.B_Igk-TATk-CDKL5 treated *Cdkl5* -/Y mice.

The low level of CDKL5 expression in the brains of treated *Cdkl5* KO mice was confirmed by the small increase in the phosphorylation levels of the direct CDKL5 target, EB2 (Fig. 29).

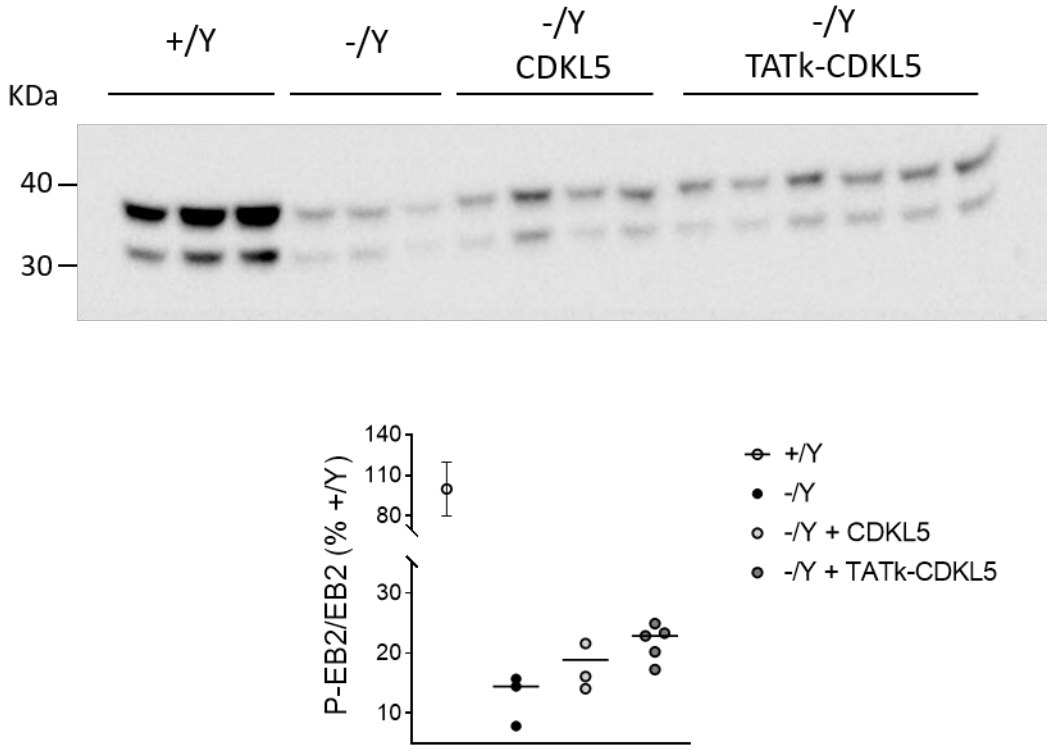

Fig. 29: Western blot analysis of phospho-EB2 in cortical protein extracts from vehicle-treated wild-type (+/Y, n =3) and *Cdkl5* KO (-/Y; n = 3) mice, and those from *Cdkl5* -/Y mice treated with AAVPHP.B_CDKL5 (n = 3) or AAVPHP.B_Igk-TATk-CDKL5 (n = 4) vectors. Data are expressed as a percentage of +/Y and plotted as dots and median.

As previously shown in mice systemically treated (intravenous tail injection) with AAVPHP.B_CDKL5 or AAVPHP.B_Igk-TATk-CDKL5 vectors, (Fig 15), the AAVPHP.B_Igk-TATk-CDKL5 vector showed a similar infection efficiency in comparison with the AAVPHP.B_CDKL5 vector (Fig. 28A), but seems to led to a higher CDKL5-positive immunoreactivity in the brains of intracarotid treated *Cdkl5* KO mice (Fig. 30A,B), suggesting the occurrence of protein replacement not only in AAV vector-infected cells but

also in non-infected neighboring cells by a cross-correction mechanism mediated by the secretable, cell-penetrating TATk-CDKL5 protein (Fig. 30A,B).

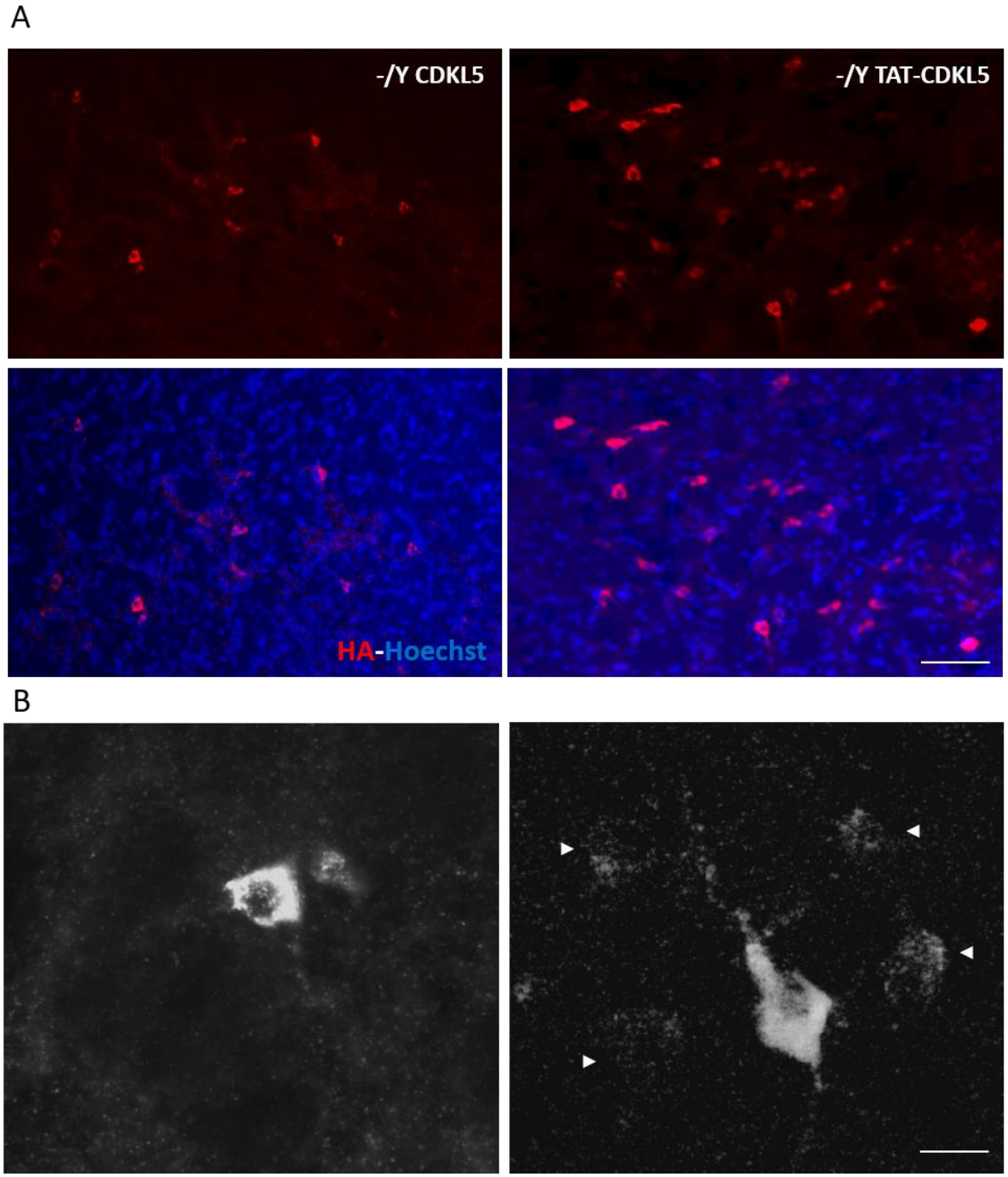

Fig. 30: (A) CDKL5 and TATk-CDKL5 protein distribution in the CNS. Images show TATk-CDKL5 or CDKL5 protein localization in the striatum of treated mice 90 days post-injection. Localization of TATk-CDKL5 or CDKL5 was evaluated through immunohistochemistry using an anti-HA antibody, and nuclei were counterstained with Hoechst. Scale bar = 50 µm. (B) Confocal images show TATk-CDKL5 or CDKL5 protein localization in the striatum of treated mice 90 days post-intracarotid injection with AAVPHP.B_CDKL5, or AAVPHP.B_Igk-TATk-CDKL5. Localization of TATk-CDKL5 or

CDKL5 was evaluated through immunohistochemistry using an anti-HA antibody. Scale bar = 10 μm. The arrows indicate faintly HA-immunopositive cells.

5. DISCUSSION

Many chronic neurological diseases do not respond to small molecule therapeutics, and have no effective therapy. Accordingly, no therapies are presently available for the improvement of the neurological phenotypes associated with CDKL5 deficiency disorder. Gene therapy offers the promise of an effective cure for both genetic and acquired brain disease. However, delivering genetic material efficiently to the CNS still remains a hurdle when developing efficacious gene therapy strategies for CNS disorders characterized by widespread neuropathology in several brain regions. Our study provides novel evidence that a gene therapy approach based on a vector carrying the IgK-TATk-CDKL5 transgene provides an increased protein biodistribution and therapeutic efficacy compared to the same vector carrying only CDKL5. We demonstrated that *Cdkl5* KO mice treated with AAVPHP.B_Igk-TATk-CDKL5 vector underwent a higher neurodevelopmental and behavioral improvement than mice treated with AAVPHP.B_CDKL5 vector. Importantly, no toxic effects, including immunogenicity problems related to the secreted TATk-CDKL5 protein, were observed in AAVPHP.B_Igk-TATk-CDKL5 treated mice, indicating the safety of this approach. These promising results suggest that a gene therapy with the IgK-TATk-CDKL5 transgene may be a successful treatment for CDD.

Following AAVPHP.B_CDKL5 vector delivery, *Cdkl5* KO mice did not exhibit improvement in behavior in comparison with vehicle-treated mice. The poor therapeutic effect of a gene therapy with only CDKL5 has previously been reported (Gao *et al.,* 2020) and was attributed to the necessity of a more robust brain transduction to ameliorate behavioral deficits in this mouse model (Benke & Kind, 2020). Noteworthy, we found that the secretable TATk-CDKL5 protein amplifies the therapeutic effect compared to the CDKL5 alone. With the same infection efficacy as that of the AAVPHP.B_CDKL5 vector, a gene therapy with AAVPHP.B_Igk-TATk-CDKL5 was sufficient to improve various behavioral defects in the *Cdkl5* KO mouse, such as innate behaviors and motor performance. Albeit in a more marginal way, hippocampal-dependent learning and memory were improved. The lesser therapeutic effect may be attributed to the lower number of viral copies reaching the hippocampus compared to other brain regions such as the cortex, striatum and brainstem. The correlation between levels of CDKL5 re-expression and effectiveness of the

gene therapy was confirmed by the finding that in the brainstem, where the CDKL5 endogenous levels are lower than in the rest of the brain (Kilstrup-Nielsen *et al.,* 2012), treatment with either AAVPHP.B_CDKL5 or AAVPHP.B_Igk-TATk-CDKL5 vectors led to a re-expression of CDKL5 to the levels found in the wild-types, and, accordingly, to a restoration of REM sleep apnea occurrence in *Cdkl5* KO mice. On the other hand, the lack of effect on the number of apneas during NREM sleep suggests that a complex behavior such as sleep breathing requires the involvement of other brain regions and, therefore, a broader CDKL5 re-expression.

As an anatomical substrate of the ameliorated behavioral performance, in AAVPHP.B_Igk-TATk-CDKL5-treated *Cdkl5* KO mice we found that their impaired dendritic and synaptic development was restored, as was neuronal survival in the hippocampus. In contrast, the lack of behavioral improvement in *Cdkl5* KO mice treated with AAVPHP.B_CDKL5 may be accounted for by the reduced effect of treatment on neuronal survival and dendritic development. Similarly, microglia over-activation, a recently described alteration in the brains of *Cdkl5* KO mice (Galvani *et al.,* 2021), is inhibited only by treatment with AAVPHP.B_Igk-TATk-CDKL5, further supporting the amplified therapeutic effect of the secretable TATk-CDKL5 protein. Why the restoration of several anatomical defects in the hippocampus of AAVPHP.B_Igk-TATk-CDKL5-treated *Cdkl5* KO mice does not induce the full recovery of hippocampus-dependent cognitive abilities may be attributable to the complex and intricate *in vivo* brain function which goes beyond structural restorations.

Interestingly, we observed unexpected inconsistency between the high viral copy number per cell and the low *CDKL5* mRNA and protein levels. The finding that at the same viral particle dose of 10e12 vg the number of GFP-positive cells is much higher than that of CDKL5-positive cells in the brains of mice injected with the Igk-TATk-CDKL5 or CDKL5 vector suggests a low half-life of the delivered CDKL5, either at the transcript or protein level. The hypothesis of *CDKL5* mRNA instability is in agreement with a recent finding showing that the lack of a long 3'-UTR sequence destabilizes Mecp2 mRNA, significantly reducing its relative half-time (Luoni *et al.,* 2020). In addition, the authors found that viral mRNA, in contrast to endogenous mRNA, was not actively translated by ribosomes, further underlining the importance of complex endogenous regulatory elements for post-transcriptional controls (Luoni *et al.,* 2020). Future studies are needed to characterize

regulatory elements of the *CDKL5* mRNA and to design a CDKL5 transgene cassette that would be useful to obtain higher CDKL5 protein levels. However, it was demonstrated that even a modest 5-10% re-expression of MeCP2 has a promising therapeutic effect on the RTT phenotype in a mouse model of RTT (Carrette *et al.,* 2018). Although the actual quantity of CDKL5 required to achieve therapeutic efficacy is not known, we recently demonstrated, using a protein substitution therapy approach with a TATk-CDKL5 fusion protein (Trazzi *et al.,* 2018) that the amount of CDKL5 protein necessary to rescue neurological phenotypes of a mouse model of CDD is very small. Here we confirmed that the low CDKL5 levels re-expressed in the brains of treated *Cdkl5* KO mice are sufficient to improve CDD phenotypes if supported by an increased biodistribution due to the properties of the IgK-TATk fusion protein.

However, to increase the efficacy of the proposed gene therapy another strategy could be adopted based on hybrid gene delivery technologies, such as the exosome–AAV hybrid. This innovative technique uses extracellular vesicles secreted by cells, like exosomes, that can be used as viral vehicles for gene delivery technology, increasing viral biodistribution across the cell membrane. This strategy shows features including high biocompatibility, low clearance rate, and amenability for cell-targeted delivery (Duan et al., 2021).

We are confident that this study has provided a first proof-of-principle that an innovative gene therapy approach based on the unique advantages of the IgK-TATk-CDKL5 transgene is highly efficient in improving neurodevelopmental and behavioral impairments in a mouse model of CDD. Such exciting results imply that this approach may become a powerful tool for the cure of CDD, and could open avenues to the development of gene therapy for other monogenic diseases based on the unique and compelling properties of the Igk-TATk-fusion protein approach.

6. REFERENCES

Amendola E, Zhan Y, Mattucci C, Castroflorio E, Calcagno E, Fuchs C, Lonetti G, Silingardi D, Vyssotski AL, Farley D, Ciani E, Pizzorusso T, Giustetto M, Gross CT. (2014). Mapping pathological phenotypes in a mouse model of CDKL5 disorder. PLoS One, 9, e91613. doi: 10.1371/journal.pone.0091613.

Amenduni M, De Filippis R, Cheung AY, Disciglio V, Epistolato MC, Ariani F, Mari F, Mencarelli MA, Hayek Y, Renieri A, Ellis J, Meloni I. (2011). iPS cells to model CDKL5-related disorders. Eur J Hum Genet, 19, 1246-55. doi: 10.1038/ejhg.2011.131.

Amir, R. E., Van Den Veyver, I. B., Wan, M., Tran, C. Q., Francke, U., & Zoghbi, H. Y. (1999). Rett syndrome is caused by mutations in X-linked MECP2, encoding methyl- CpG-binding protein 2. Nature Genetics, 23, 185-8, doi: 10.1038/13810.

Angoa-Pérez M, Kane MJ, Briggs DI, Francescutti DM, Kuhn DM. (2013). Marble burying and nestlet shredding as tests of repetitive, compulsive-like behaviors in mice. J Vis Exp., 82, 50978. doi: 10.3791/50978.

Anguela XM, High KA. (2019). Entering the Modern Era of Gene Therapy. Annu Rev., 70, 273-288. doi: 10.1146/annurev-med-012017-043332.

Bahi-Buisson N, Bienvenu T. (2012). CDKL5-Related Disorders: From Clinical Description to Molecular Genetics. Mol Syndromol. 2, 137-152. doi: 10.1159/000331333.

Bahi-Buisson N, Kaminska A, Boddaert N, Rio M, Afenjar A, Gérard M, Giuliano F, Motte J, Héron D, Morel MA, Plouin P, Richelme C, des Portes V, Dulac O, Philippe C, Chiron C, Nabbout R, Bienvenu T. (2008). The three stages of epilepsy in patients with CDKL5 mutations. Epilepsia, 49, 1027-37. doi: 10.1111/j.1528-1167.2007.01520.

Bahi-Buisson N, Nectoux J, Rosas-Vargas H, Milh M, Boddaert N, Girard B, Cances C, Ville D, Afenjar A, Rio M, Héron D, N'guyen Morel MA, Arzimanoglou A, Philippe C, Jonveaux P, Chelly J, Bienvenu T. (2008). Key clinical features to identify girls with CDKL5 mutations. Brain., 131, 2647-61. doi: 10.1093/brain/awn197.

Baltussen LL, Negraes PD, Silvestre M, Claxton S, Moeskops M, Christodoulou E, Flynn HR, Snijders AP, Muotri AR, Ultanir SK. (2018). Chemical genetic identification of CDKL5 substrates reveals its role in neuronal microtubule dynamics. EMBO J., 37(24), e99763. doi: 10.15252/embj.201899763.

Barbiero I, Valente D, Chandola C, Magi F, Bergo A, Monteonofrio L, Tramarin M, Fazzari M, Soddu S, Landsberger N, Rinaldo C, Kilstrup-Nielsen C. (2017). CDKL5 localizes at the centrosome and midbody and is required for faithful cell division. Sci Rep., 7, 6228, doi: 10.1038/s41598-017-05875-z.

Bastianini S, Alvente S, Berteotti C, Lo Martire V, Silvani A, Swoap SJ, Valli A, Zoccoli G, Cohen G. (2017). Accurate discrimination of the wake-sleep states of mice using non-invasive whole-body plethysmography. Sci Rep., 7, 41698. doi: 10.1038/srep41698.

Benke TA, Kind PC. (2020). Proof-of-concept for a gene replacement approach to CDKL5 deficiency disorder. Brain., 143, 716-718. doi: 10.1093/brain/awaa055.

Bertani I, Rusconi L, Bolognese F, Forlani G, Conca B, De Monte L, Badaracco G, Landsberger N, Kilstrup-Nielsen C. (2006). Functional consequences of mutations in CDKL5, an X-linked gene involved in infantile spasms and mental retardation. J Biol Chem., 281, 32048-56. doi: 10.1074/jbc.M606325200.

Bolhassani A, Jafarzade BS, Mardani G. (2016). In vitro and in vivo delivery of therapeutic proteins using cell penetrating peptides. Peptides., 87, 50-63. doi: 10.1016/j.peptides.2016.11.011.

Carrette LLG, Blum R, Ma W, Kelleher RJ 3rd, Lee JT. (2018) Tsix-Mecp2 female mouse model for Rett syndrome reveals that low-level MECP2 expression extends life and improves neuromotor function. Proc Natl Acad Sci U S A., 115, 8185-8190. doi: 10.1073/pnas.1800931115.

Cheadle JP, Gill H, Fleming N, Maynard J, Kerr A, Leonard H, Krawczak M, Cooper DN, Lynch S, Thomas N, Hughes H, Hulten M, Ravine D, Sampson JR, Clarke A. (2000). Long-read sequence analysis of the MECP2 gene in Rett syndrome patients: correlation of disease severity with mutation type and location. Hum Mol Genet., 9, 1119-29. doi: 10.1093/hmg/9.7.1119.

Chen Q, Zhu YC, Yu J, Miao S, Zheng J, Xu L, Zhou Y, Li D, Zhang C, Tao J, Xiong ZQ. (2010). CDKL5, a protein associated with rett syndrome, regulates neuronal morphogenesis via Rac1 signaling. J Neurosci., 30, 12777-86. doi: 10.1523/JNEUROSCI.1102-10.2010.

Chen ZH, Zhu M, Yang J, Liang H, He J, He S, Wang P, Kang X, McNutt MA, Yin Y, Shen WH. (2014). PTEN interacts with histone H1 and controls chromatin condensation. Cell Rep., 8, 2003-2014. doi: 10.1016/j.celrep.2014.08.008.

Coghlan MP, Culbert AA, Cross DA, Corcoran SL, Yates JW, Pearce NJ, Rausch OL, Murphy GJ, Carter PS, Roxbee Cox L, Mills D, Brown MJ, Haigh D, Ward RW, Smith DG, Murray KJ, Reith AD, Holder JC. (2000). Selective small molecule inhibitors of glycogen synthase kinase-3 modulate glycogen metabolism and gene transcription. Chem Biol., 7, 793-803. doi: 10.1016/s1074-5521(00)00025-9.

Cortelazzo A, de Felice C, Leoncini S, Signorini C, Guerranti R, Leoncini R, Armini A, Bini L, Ciccoli L, Hayek J. (2017). Inflammatory protein response in CDKL5-Rett syndrome: evidence of a subclinical smouldering inflammation. Inflamm Res., 66, 269-280. doi: 10.1007/s00011-016-1014.

Crino PB. (2011). mTOR: A pathogenic signaling pathway in developmental brain malformations. Trends Mol Med., 17, 734-42. doi: 10.1016/j.molmed.2011.07.008.

Davidson BL, Stein CS, Heth JA, Martins I, Kotin RM, Derksen TA, Zabner J, Ghodsi A, Chiorini JA. (2000). Recombinant adeno-associated virus type 2, 4, and 5 vectors: transduction of variant cell types and regions in the mammalian central nervous system. Proc Natl Acad Sci U S A.,97, 3428-32. doi: 10.1073/pnas.050581197.

De Simone A, La Pietra V, Betari N, Petragnani N, Conte M, Daniele S, Pietrobono D, Martini C, Petralla S, Casadei R, Davani L, Frabetti F, Russomanno P, Novellino E, Montanari S, Tumiatti V, Ballerini P, Sarno F, Nebbioso A, Altucci L, Monti B, Andrisano V, Milelli A. (2019). Discovery of the First-in-Class GSK-3β/HDAC Dual Inhibitor as Disease-Modifying Agent To Combat Alzheimer's Disease. ACS Med Chem Lett., 10, 469-474. doi: 10.1021/acsmedchemlett.8b00507.

Deacon RM. (2006). Assessing nest building in mice. Nat Protoc., 1, 1117-9. doi: 10.1038/nprot.2006.170.

Della Sala G, Putignano E, Chelini G, Melani R, Calcagno E, Michele Ratto G, Amendola E, Gross CT,

Giustetto M, Pizzorusso T. (2016). Dendritic Spine Instability in a Mouse Model of CDKL5 Disorder Is Rescued by Insulin-like Growth Factor 1. Biol Psychiatry, 80, 302-311. doi: 10.1016/j.biopsych.2015.08.028.

Demarest S, Pestana-Knight EM, Olson HE, Downs J, Marsh ED, Kaufmann WE, Partridge CA, Leonard H, Gwadry-Sridhar F, Frame KE, Cross JH, Chin RFM, Parikh S, Panzer A, Weisenberg J, Utley K, Jaksha A, Amin S, Khwaja O, Devinsky O, Neul JL, Percy AK, Benke TA. (2019). Severity Assessment in CDKL5 Deficiency Disorder. Pediatr Neurol., 97, 38-42. doi: 10.1016/j.pediatrneurol.2019.03.017.

Demarest, S. T., Olson, H. E., Moss, A., Pestana-, E., Zhang, X., Parikh, S., Swanson, L. C., Riley, K. D., Bazin, G. A., Angione, K., Niestroj, M., Lal, D., Juarez-colunga, E., Tim, A., & Colorado, H. (2019). CDKL5 Deficiency Disorder: Relationship between genotype, epilepsy, cortical visual impairment and development. Epilepsia., 60, 1733–1742. doi: 10.1111/epi.16285.CDKL5

Denault JB, Leduc R. (1996). Furin/PACE/SPC1: a convertase involved in exocytic and endocytic processing of precursor proteins. FEBS Lett., 379, 113-6. doi: 10.1016/0014-5793(95)01487-x.

Domínguez JM, Fuertes A, Orozco L, del Monte-Millán M, Delgado E, Medina M. (2012). Evidence for irreversible inhibition of glycogen synthase kinase-3β by tideglusib. J Biol Chem., 287, 893-904. doi: 10.1074/jbc.M111.306472.

Duan L , Xu L , Xu X , Qin Z , Zhou X , Xiao Y , Liang Y , Xia J. (2021). Exosome-mediated delivery of gene vectors for gene therapy. Nanoscale. 13, 1387-1397. doi: 10.1039/d0nr07622h.

Eldar-Finkelman H, Martinez A. GSK-3 Inhibitors: Preclinical and Clinical Focus on CNS. Front Mol Neurosci.;4, 32. doi: 10.3389/fnmol.2011.00032.

Fehr S, Leonard H, Ho G, Williams S, de Klerk N, Forbes D, Christodoulou J, Downs J. (2015). There is variability in the attainment of developmental milestones in the CDKL5 disorder. J Neurodev Disord., 7, 2. doi: 10.1186/1866-1955-7-2.

Fehr, S., Wilson, M., Downs, J., Williams, S., Murgia, A., Sartori, S., Vecchi, M., Ho, G., Polli, R., Psoni, S., Bao, X., De Klerk, N., Leonard, H., & Christodoulou, J. (2013). The CDKL5 disorder is an independent clinical entity associated with early-onset encephalopathy. European Journal of Human Genetics, 21, 266–273. doi: 10.1038/ejhg.2012.156.

Fichou Y, Nectoux J, Bahi-Buisson N, Chelly J, Bienvenu T. (2011). An isoform of the severe encephalopathy-related CDKL5 gene, including a novel exon with extremely high sequence conservation, is specifically expressed in brain. J Hum Genet., 56, 52-7. doi: 10.1038/jhg.2010.143.

Finkel RS, Chiriboga CA, Vajsar J, Day JW, Montes J, De Vivo DC, Yamashita M, Rigo F, Hung G, Schneider E, Norris DA, Xia S, Bennett CF, Bishop KM. (2016). Treatment of infantile-onset spinal muscular atrophy with nusinersen: a phase 2, open-label, dose-escalation study. Lancet, 388, 3017-3026. doi: 10.1016/S0140-6736(16)31408-8.

Flinterman M, Farzaneh F, Habib N, Malik F, Gäken J, Tavassoli M. (2009). Delivery of therapeutic proteins as secretable TAT fusion products. Mol Ther., 17, 334-42. doi: 10.1038/mt.2008.256.

Foust KD, Nurre E, Montgomery CL, Hernandez A, Chan CM, Kaspar BK. (2009). Intravascular AAV9 preferentially targets neonatal neurons and adult astrocytes. Nat Biotechnol., 27, 59-65. doi:

10.1038/nbt.1515.

Frullanti E, Papa FT, Grillo E, Clarke A, Ben-Zeev B, Pineda M, Bahi-Buisson N, Bienvenu T, Armstrong J, Roche Martinez A, Mari F, Nissenkorn A, Lo Rizzo C, Veneselli E, Russo S, Vignoli A, Pini G, Djuric M, Bisgaard AM, Ravn K, Bosnjak VM, Hayek J, Khajuria R, Montomoli B, Cogliati F, Pintaudi M, Hadzsiev K, Craiu D, Voinova V, Djukic A, Villard L, Renieri A. (2019). Analysis of the Phenotypes in the Rett Networked Database. Int J Genomics., 27, 6956934. doi: 10.1155/2019/6956934.

Fuchs C, Gennaccaro L, Trazzi S, Bastianini S, Bettini S, Lo Martire V, Ren E, Medici G, Zoccoli G, Rimondini R, Ciani E. (2018). Heterozygous CDKL5 Knockout Female Mice Are a Valuable Animal Model for CDKL5 Disorder. Neural Plast., 27, 9726950. doi: 10.1155/2018/9726950.

Fuchs C, Medici G, Trazzi S, Gennaccaro L, Galvani G, Berteotti C, Ren E, Loi M, Ciani E. (2019). CDKL5 deficiency predisposes neurons to cell death through the deregulation of SMAD3 signaling. Brain Pathol., 29, 658-674. doi: 10.1111/bpa.12716

Fuchs C, Rimondini R, Viggiano R, Trazzi S, De Franceschi M, Bartesaghi R, Ciani E. (2015). Inhibition of GSK3β rescues hippocampal development and learning in a mouse model of CDKL5 disorder. Neurobiol Dis., 82, 298-310. doi: 10.1016/j.nbd.2015.06.018.

Fuchs C, Trazzi S, Torricella R, Viggiano R, De Franceschi M, Amendola E, Gross C, Calzà L, Bartesaghi R, Ciani E. (2014). Loss of CDKL5 impairs survival and dendritic growth of newborn neurons by altering AKT/GSK-3β signaling. Neurobiol Dis., 70, 53-68. doi: 10.1016/j.nbd.2014.06.006.

Galanello R, Origa R. (2010). Beta-thalassemia. Orphanet J Rare Dis., 5, 11. doi: 10.1186/1750-1172-5-11.

Galvani G, Mottolese N, Gennaccaro L, Loi M, Medici G, Tassinari M, Fuchs C, Ciani E, Trazzi S. (2021). Inhibition of microglia overactivation restores neuronal survival in a mouse model of CDKL5 deficiency disorder. J Neuroinflammation., ;18, 155. doi: 10.1186/s12974-021-02204-0.

Gao G, Vandenberghe LH, Alvira MR, Lu Y, Calcedo R, Zhou X, Wilson JM. (2004). Clades of Adeno-associated viruses are widely disseminated in human tissues. J Virol., 78, 6381-8. doi: 10.1128/JVI.78.12.6381-6388.2004.

Gao Y, Irvine EE, Eleftheriadou I, Naranjo CJ, Hearn-Yeates F, Bosch L, Glegola JA, Murdoch L, Czerniak A, Meloni I, Renieri A, Kinali M, Mazarakis ND. (2020). Gene replacement ameliorates deficits in mouse and human models of cyclin-dependent kinase-like 5 disorder. Brain., 143, 811-832. doi: 10.1093/brain/awaa028.

Gennaccaro L, Fuchs C, Loi M, Pizzo R, Alvente S, Berteotti C, Lupori L, Sagona G, Galvani G, Gurgone A, Raspanti A, Medici G, Tassinari M, Trazzi S, Ren E, Rimondini R, Pizzorusso T, Zoccoli G, Giustetto M, Ciani E. (2021a). Age-Related Cognitive and Motor Decline in a Mouse Model of CDKL5 Deficiency Disorder is Associated with Increased Neuronal Senescence and Death. Aging Dis., 12, 764-785. doi: 10.14336/AD.2020.0827.

Gennaccaro L, Fuchs C, Loi M, Roncacè V, Trazzi S, Ait-Bali Y, Galvani G, Berardi AC, Medici G, Tassinari M, Ren E, Rimondini R, Giustetto M, Aicardi G, Ciani E. (2021b). A $GABA_B$ receptor antagonist rescues functional and structural impairments in the perirhinal cortex of a mouse model of CDKL5 deficiency disorder. Neurobiol Dis., 153, 105304. doi: 10.1016/j.nbd.2021.105304.

Ginhoux F, Lim S, Hoeffel G, Low D, Huber T. (2013). Origin and differentiation of microglia. Front Cell Neurosci.,7, 45. doi: 10.3389/fncel.2013.00045.

Granja A, Frias I, Neves AR, Pinheiro M, Reis S. (2017). Therapeutic Potential of Epigallocatechin Gallate Nanodelivery Systems. Biomed Res Int, 5813793. doi: 10.1155/2017/5813793.

Gray SJ, Foti SB, Schwartz JW, Bachaboina L, Taylor-Blake B, Coleman J, Ehlers MD, Zylka MJ, McCown TJ, Samulski RJ. (2010). Optimizing promoters for recombinant adeno-associated virus-mediated gene expression in the peripheral and central nervous system using self-complementary vectors. Hum Gene Ther., 22, 1143-53. doi: 10.1089/hum.2010.245.

Guerrini R, Parrini E. (2012). Epilepsy in Rett syndrome, and CDKL5- and FOXG1-gene-related encephalopathies. Epilepsia, 53, 2067-78. doi: 10.1111/j.1528-1167.2012.03656.

Guidi S, Stagni F, Bianchi P, Ciani E, Ragazzi E, Trazzi S, Grossi G, Mangano C, Calzà L, Bartesaghi R. (2013). Early pharmacotherapy with fluoxetine rescues dendritic pathology in the Ts65Dn mouse model of down syndrome. Brain Pathol., 23, 129-43. doi: 10.1111/j.1750-3639.2012.00624.

Hagberg B, Aicardi J, Dias K, Ramos O. (1983). A progressive syndrome of autism, dementia, ataxia, and loss of purposeful hand use in girls: Rett's syndrome: report of 35 cases. Ann Neurol., 14, 471-9. doi: 10.1002/ana.410140412.

Hagebeuk EE, Marcelis CL, Alders M, Kaspers A, de Weerd AW. (2015). Two Siblings With a CDKL5 Mutation: Genotype and Phenotype Evaluation. J Child Neurol., 30, 1515-9. doi: 10.1177/0883073815573317.

Hagebeuk EE, van den Bossche RA, de Weerd AW. (2013). Respiratory and sleep disorders in female children with atypical Rett syndrome caused by mutations in the CDKL5 gene. Dev Med Child Neurol., 55, 480-4. doi: 10.1111/j.1469-8749.2012.04432.

Hanefeld, F. (1985). The clinical pattern of the rett syndrome. Brain and Development, *7*, 320–325. doi: 10.1016/S0387-7604(85)80037-1.

Hector RD, Dando O, Landsberger N, Kilstrup-Nielsen C, Kind PC, Bailey ME, Cobb SR. (2016). Characterisation of CDKL5 Transcript Isoforms in Human and Mouse. PLoS One.,17, e0157758. doi: 10.1371/journal.pone.0157758.

Hector RD, Kalscheuer VM, Hennig F, Leonard H, Downs J, Clarke A, Benke TA, Armstrong J, Pineda M, Bailey MES, Cobb SR. (2017). "*CDKL5*"variants: Improving our understanding of a rare neurologic disorder. Neurol Genet., 3, e200. doi: 10.1212/NXG.0000000000000200.

High KA, Roncarolo MG. (2019). Gene Therapy. N Engl J Med., 381, 455-464. doi: 10.1056/NEJMra1706910.

Hsieh J, Nakashima K, Kuwabara T, Mejia E, Gage FH. (2004). Histone deacetylase inhibition-mediated neuronal differentiation of multipotent adult neural progenitor cells. Proc Natl Acad Sci U S A.,101, 16659-64. doi: 10.1073/pnas.0407643101.

Jacobs JD, Hopper-Borge EA. (2014). Carotid artery infusions for pharmacokinetic and pharmacodynamic analysis of taxanes in mice. J Vis Exp., 27, e51917. doi: 10.3791/51917.

Jakimiec M, Paprocka J, Śmigiel R. (2020). CDKL5 Deficiency Disorder-A Complex Epileptic Encephalopathy. Brain Sci.,10, 107. doi: 10.3390/brainsci10020107.

Jhang CL, Huang TN, Hsueh YP, Liao W. (2017). Mice lacking cyclin-dependent kinase-like 5 manifest autistic and ADHD-like behaviors. Hum Mol Genet., 26, 3922-3934. doi: 10.1093/hmg/ddx279.

Kadam SD, Sullivan BJ, Goyal A, Blue ME, Smith-Hicks C. (2019). Rett Syndrome and CDKL5 Deficiency Disorder: From Bench to Clinic. Int J Mol Sci., 20, 5098. doi: 10.3390/ijms20205098.

Kalscheuer VM, Tao J, Donnelly A, Hollway G, Schwinger E, Kübart S, Menzel C, Hoeltzenbein M, Tommerup N, Eyre H, Harbord M, Haan E, Sutherland GR, Ropers HH, Gécz J. (2003). Disruption of the serine/threonine kinase 9 gene causes severe X-linked infantile spasms and mental retardation. Am J Hum Genet., 72, 1401-11. doi: 10.1086/375538.

Kameshita I, Sekiguchi M, Hamasaki D, Sugiyama Y, Hatano N, Suetake I, Tajima S, Sueyoshi N. (2008). Cyclin-dependent kinase-like 5 binds and phosphorylates DNA methyltransferase 1. Biochem Biophys Res Commun.,377, 1162-7. doi: 10.1016/j.bbrc.2008.10.113.

Kaplitt MG, Feigin A, Tang C, Fitzsimons HL, Mattis P, Lawlor PA, Bland RJ, Young D, Strybing K, Eidelberg D, During MJ. (2007). Safety and tolerability of gene therapy with an adeno-associated virus (AAV) borne GAD gene for Parkinson's disease: an open label, phase I trial. Lancet., 369, 2097-105. doi: 10.1016/S0140-6736(07)60982-9.

Katayama S, Senga Y, Oi A, Miki Y, Sugiyama Y, Sueyoshi N, Kameshita I. (2016). Expression analyses of splice variants of zebrafish cyclin-dependent kinase-like 5 and its substrate, amphiphysin 1. Gene., 583, . doi: 10.1016/j.gene.2016.02.036.

Katayama S, Sueyoshi N, Inazu T, Kameshita I. (2020). Cyclin-Dependent Kinase-Like 5 (CDKL5): Possible Cellular Signalling Targets and Involvement in CDKL5 Deficiency Disorder. Neural Plast., 6970190. doi: 10.1155/2020/6970190.

Katayama S, Sueyoshi N, Kameshita I. (2015). Critical Determinants of Substrate Recognition by Cyclin-Dependent Kinase-like 5 (CDKL5). Biochemistry., 54, 2975-87 . doi: 10.1021/bi501308k.

Kilstrup-Nielsen C, Rusconi L, La Montanara P, Ciceri D, Bergo A, Bedogni F, Landsberger N. (2012). What we know and would like to know about CDKL5 and its involvement in epileptic encephalopathy. Neural Plast., 728267. doi: 10.1155/2012/728267.

Korcsmáros T, Szalay MS, Böde C, Kovács IA, Csermely P. (2007). How to design multi-target drugs. Expert Opin Drug Discov., 2, 799-808. doi: 10.1517/17460441.2.6.799.

La Montanara P, Hervera A, Baltussen LL, Hutson TH, Palmisano I, De Virgiliis F, Kong G, Chadwick J, Gao Y, Bartus K, Majid QA, Gorgoraptis N, Wong K, Downs J, Pizzorusso T, Ultanir SK, Leonard H, Yu H, Millar DS, Istvan N, Mazarakis ND, Di Giovanni S. (2020). Cyclin-dependent-like kinase 5 is required for pain signaling in human sensory neurons and mouse models. Sci Transl Med., 12, eaax4846. doi: 10.1126/scitranslmed.aax4846.

La Montanara P, Rusconi L, Locarno A, Forti L, Barbiero I, Tramarin M, Chandola C, Kilstrup-Nielsen C, Landsberger N. (2015). Synaptic synthesis, dephosphorylation, and degradation: a novel paradigm for an activity-dependent neuronal control of CDKL5. J Biol Chem., 290, 4512-27. doi: 10.1074/jbc.M114.589762.

Lalonde R, Strazielle C. (2011). Brain regions and genes affecting limb-clasping responses. Brain Res

Rev., 67, 252-9. doi: 10.1016/j.brainresrev.2011.02.005.

Leoncini S, De Felice C, Signorini C, Zollo G, Cortelazzo A, Durand T, Galano JM, Guerranti R, Rossi M, Ciccoli L, Hayek J. (2015). Cytokine Dysregulation in MECP2- and CDKL5-Related Rett Syndrome: Relationships with Aberrant Redox Homeostasis, Inflammation, and ω-3 PUFAs. Oxid Med Cell Longev., 421624. doi: 10.1155/2015/421624.

Lin C, Franco B, Rosner MR. (2005). CDKL5/Stk9 kinase inactivation is associated with neuronal developmental disorders. Hum Mol Genet., 14, 3775-86. doi: 10.1093/hmg/ddi391.

Lin JC, Ho WH, Gurney A, Rosenthal A. (2003). The netrin-G1 ligand NGL-1 promotes the outgrowth of thalamocortical axons. Nat Neurosci., 6, 1270-6. doi: 10.1038/nn1148.

Livide G, Patriarchi T, Amenduni M, Amabile S, Yasui D, Calcagno E, Lo Rizzo C, De Falco G, Ulivieri C, Ariani F, Mari F, Mencarelli MA, Hell JW, Renieri A, Meloni I. (2014). GluD1 is a common altered player in neuronal differentiation from both MECP2-mutated and CDKL5-mutated iPS cells. Eur J Hum Genet., 23, 195-201. doi: 10.1038/ejhg.2014.81.

Lo Martire V, Alvente S, Bastianini S, Berteotti C, Silvani A, Valli A, Viggiano R, Ciani E, Zoccoli G. 8 2017). CDKL5 deficiency entails sleep apneas in mice. J Sleep Res., 26, 495-497. doi: 10.1111/jsr.12512.

Loi M, Gennaccaro L, Fuchs C, Trazzi S, Medici G, Galvani G, Mottolese N, Tassinari M, Giorgini RR, Milelli A, Ciani E. (2021). Treatment with a GSK-3β/HDAC Dual Inhibitor Restores Neuronal Survival and Maturation in an In Vitro and In Vivo Model of *CDKL5* Deficiency Disorder. Int J Mol Sci., 22, 5950. doi: 10.3390/ijms22115950.

Loi M, Trazzi S, Fuchs C, Galvani G, Medici G, Gennaccaro L, Tassinari M, Ciani E. (2020). Increased DNA Damage and Apoptosis in CDKL5-Deficient Neurons. Mol Neurobiol., 57, 2244-2262. doi: 10.1007/s12035-020-01884-8.

Lowry OH, Rosebrough NJ, Farr AL, Randall RJ. (1951). Protein measurement with the Folin phenol reagent. J Biol Chem.,193, 265-75.

Luoni M, Giannelli S, Indrigo MT, Niro A, Massimino L, Iannielli A, Passeri L, Russo F, Morabito G, Calamita P, Gregori S, Deverman B, Broccoli V. (2020). Whole brain delivery of an instability-prone *Mecp2* transgene improves behavioral and molecular pathological defects in mouse models of Rett syndrome. Elife.,9, e52629. doi: 10.7554/eLife.52629.

Lupori L, Sagona G, Fuchs C, Mazziotti R, Stefanov A, Putignano E, Napoli D, Strettoi E, Ciani E, Pizzorusso T. (2019). Site-specific abnormalities in the visual system of a mouse model of CDKL5 deficiency disorder. Hum Mol Genet., 28, 2851-2861. doi: 10.1093/hmg/ddz102.

MacKay CI, Wong K, Demarest ST, Benke TA, Downs J, Leonard H. (2021). Exploring genotype-phenotype relationships in the CDKL5 deficiency disorder using an international dataset. Clin Genet., 99, 157-165. doi: 10.1111/cge.13862.

Mangatt M, Wong K, Anderson B, Epstein A, Hodgetts S, Leonard H, Downs J. (2016). Prevalence and onset of comorbidities in the CDKL5 disorder differ from Rett syndrome. Orphanet J Rare Dis., 11, 39. doi: 10.1186/s13023-016-0418-y.

Marek L, Hamacher A, Hansen FK, Kuna K, Gohlke H, Kassack MU, Kurz T. (2013). Histone

deacetylase (HDAC) inhibitors with a novel connecting unit linker region reveal a selectivity profile for HDAC4 and HDAC5 with improved activity against chemoresistant cancer cells. J Med Chem., 56, 427-36. doi: 10.1021/jm301254q.

Mari F, Azimonti S, Bertani I, Bolognese F, Colombo E, Caselli R, Scala E, Longo I, Grosso S, Pescucci C, Ariani F, Hayek G, Balestri P, Bergo A, Badaracco G, Zappella M, Broccoli V, Renieri A, Kilstrup-Nielsen C, Landsberger N. (2005). CDKL5 belongs to the same molecular pathway of MeCP2 and it is responsible for the early-onset seizure variant of Rett syndrome. Hum Mol Genet., 14, 1935-46. doi: 10.1093/hmg/ddi198.

Mazziotti R, Lupori L, Sagona G, Gennaro M, Della Sala G, Putignano E, Pizzorusso T. (2017). Searching for biomarkers of CDKL5 disorder: early-onset visual impairment in CDKL5 mutant mice. Hum Mol Genet., 26, 2290-2298. doi: 10.1093/hmg/ddx119.

McPhee SW, Janson CG, Li C, Samulski RJ, Camp AS, Francis J, Shera D, Lioutermann L, Feely M, Freese A, Leone P. (2006). Immune responses to AAV in a phase I study for Canavan disease. J Gene Med., 8, 577-88. doi: 10.1002/jgm.885.

Melani F, Mei D, Pisano T, Savasta S, Franzoni E, Ferrari AR, Marini C, Guerrini R. (2011). CDKL5 gene-related epileptic encephalopathy: electroclinical findings in the first year of life. Dev Med Child Neurol., 53, 354-60. doi: 10.1111/j.1469-8749.2010.03889.

Mendell JR, Al-Zaidy S, Shell R, Arnold WD, Rodino-Klapac LR, Prior TW, Lowes L, Alfano L, Berry K, Church K, Kissel JT, Nagendran S, L'Italien J, Sproule DM, Wells C, Cardenas JA, Heitzer MD, Kaspar A, Corcoran S, Braun L, Likhite S, Miranda C, Meyer K, Foust KD, Burghes AHM, Kaspar BK. (2017). Single-Dose Gene-Replacement Therapy for Spinal Muscular Atrophy. N Engl J Med., 377, 1713-1722. doi: 10.1056/NEJMoa1706198.

Mingozzi F, High KA. (2011). Therapeutic in vivo gene transfer for genetic disease using AAV: progress and challenges. Nat Rev Genet., 12, 341-55. doi: 10.1038/nrg2988.

Montini E, Andolfi G, Caruso A, Buchner G, Walpole SM, Mariani M, Consalez G, Trump D, Ballabio A, Franco B. (1998). Identification and characterization of a novel serine-threonine kinase gene from the Xp22 region. Genomics,51, 427-33. doi: 10.1006/geno.1998.5391.

Morales-Garcia JA, Luna-Medina R, Alonso-Gil S, Sanz-Sancristobal M, Palomo V, Gil C, Santos A, Martinez A, Perez-Castillo A. (2012). Glycogen synthase kinase 3 inhibition promotes adult hippocampal neurogenesis in vitro and in vivo. ACS Chem Neurosci., 3, 963-71. doi: 10.1021/cn300110c.

Morrison-Levy N, Borlot F, Jain P, Whitney R. (2021). Early-Onset Developmental and Epileptic Encephalopathies of Infancy: An Overview of the Genetic Basis and Clinical Features. Pediatr Neurol., 16, 85-94. doi: 10.1016/j.pediatrneurol.2020.12.001.

Muñoz IM, Morgan ME, Peltier J, Weiland F, Gregorczyk M, Brown FC, Macartney T, Toth R, Trost M, Rouse J. (2018). Phosphoproteomic screening identifies physiological substrates of the CDKL5 kinase. EMBO J., 37, e99559. doi: 10.15252/embj.201899559.

Nagahara H, Vocero-Akbani AM, Snyder EL, Ho A, Latham DG, Lissy NA, Becker-Hapak M, Ezhevsky SA, Dowdy SF. (1998). Transduction of full-length TAT fusion proteins into mammalian cells: TAT-p27Kip1 induces cell migration. Nat Med., 4, 1449-52. doi: 10.1038/4042.

Nakano-Kobayashi A, Awaya T, Kii I, Sumida Y, Okuno Y, Yoshida S, Sumida T, Inoue H, Hosoya T, Hagiwara M. (2017). Prenatal neurogenesis induction therapy normalizes brain structure and function in Down syndrome mice. Proc Natl Acad Sci U S A., 114, 10268-10273. doi: 10.1073/pnas.1704143114.

Naldini L. (2011). Ex vivo gene transfer and correction for cell-based therapies. Nat Rev Genet., 12, 301-15. doi: 10.1038/nrg2985.

Negraes PD, Trujillo CA, Yu NK, Wu W, Yao H, Liang N, Lautz JD, Kwok E, McClatchy D, Diedrich J, de Bartolome SM, Truong J, Szeto R, Tran T, Herai RH, Smith SEP, Haddad GG, Yates JR 3rd, Muotri AR. (2021). Altered network and rescue of human neurons derived from individuals with early-onset genetic epilepsy. Mol Psychiatry, Epub ahead of print. doi: 10.1038/s41380-021-01104-2.

Oi A, Katayama S, Hatano N, Sugiyama Y, Kameshita I, Sueyoshi N. (2017). Subcellular distribution of cyclin-dependent kinase-like 5 (CDKL5) is regulated through phosphorylation by dual specificity tyrosine-phosphorylation-regulated kinase 1A (DYRK1A). Biochem Biophys Res Commun., 482, 239-245. doi: 10.1016/j.bbrc.2016.11.048.

Okuda K, Kobayashi S, Fukaya M, Watanabe A, Murakami T, Hagiwara M, Sato T, Ueno H, Ogonuki N, Komano-Inoue S, Manabe H, Yamaguchi M, Ogura A, Asahara H, Sakagami H, Mizuguchi M, Manabe T, Tanaka T. (2017). CDKL5 controls postsynaptic localization of GluN2B-containing NMDA receptors in the hippocampus and regulates seizure susceptibility. Neurobiol Dis., 106, 158-170. doi: 10.1016/j.nbd.2017.07.002.

Okuda K, Takao K, Watanabe A, Miyakawa T, Mizuguchi M, Tanaka T. (2018). Comprehensive behavioral analysis of the Cdkl5 knockout mice revealed significant enhancement in anxiety- and fear-related behaviors and impairment in both acquisition and long-term retention of spatial reference memory. PLoS One.,13, e0196587. doi: 10.1371/journal.pone.0196587.

Olson, H. E., Demarest, S. T., Pestana-Knight, E. M., Swanson, L. C., Iqbal, S., Lal, D., Leonard, H., Cross, J. H., Devinsky, O., & Benke, T. A. (2019). Cyclin-Dependent Kinase-Like 5 Deficiency Disorder: Clinical Review. In Pediatric Neurology, 97, 18–25 . doi: 10.1016/j.pediatrneurol.2019.02.015

Pizzo R, Gurgone A, Castroflorio E, Amendola E, Gross C, Sassoè-Pognetto M, Giustetto M. (2016). Lack of Cdkl5 Disrupts the Organization of Excitatory and Inhibitory Synapses and Parvalbumin Interneurons in the Primary Visual Cortex. Front Cell Neurosci., 10, 261. doi: 10.3389/fncel.2016.00261.

Pizzo R, Lamarca A, Sassoè-Pognetto M, Giustetto M. (2020). Structural Bases of Atypical Whisker Responses in a Mouse Model of CDKL5 Deficiency Disorder. Neuroscience, 445, 130-143. doi: 10.1016/j.neuroscience.2019.08.033.

Rademacher N, Hambrock M, Fischer U, Moser B, Ceulemans B, Lieb W, Boor R, Stefanova I, Gillessen-Kaesbach G, Runge C, Korenke GC, Spranger S, Laccone F, Tzschach A, Kalscheuer VM. (2011). Identification of a novel CDKL5 exon and pathogenic mutations in patients with severe mental retardation, early-onset seizures and Rett-like features. Neurogenetics, 12, 165-7. doi: 10.1007/s10048-011-0277-6.

Ren E, Roncacé V, Trazzi S, Fuchs C, Medici G, Gennaccaro L, Loi M, Galvani G, Ye K, Rimondini R,

Aicardi G, Ciani E. (2019). Functional and Structural Impairments in the Perirhinal Cortex of a Mouse Model of CDKL5 Deficiency Disorder Are Rescued by a TrkB Agonist. Front Cell Neurosci., 30, 169. doi: 10.3389/fncel.2019.00169.

Ricciardi S, Ungaro F, Hambrock M, Rademacher N, Stefanelli G, Brambilla D, Sessa A, Magagnotti C, Bachi A, Giarda E, Verpelli C, Kilstrup-Nielsen C, Sala C, Kalscheuer VM, Broccoli V. (2012). CDKL5 ensures excitatory synapse stability by reinforcing NGL-1-PSD95 interaction in the postsynaptic compartment and is impaired in patient iPSC-derived neurons. Nat Cell Biol., 14, 911-23. doi: 10.1038/ncb2566.

Ring DB, Johnson KW, Henriksen EJ, Nuss JM, Goff D, Kinnick TR, Ma ST, Reeder JW, Samuels I, Slabiak T, Wagman AS, Hammond ME, Harrison SD. (2003). Selective glycogen synthase kinase 3 inhibitors potentiate insulin activation of glucose transport and utilization in vitro and in vivo. Diabetes., 52, 588-95. doi: 10.2337/diabetes.52.3.588.

Rosas-Vargas H, Bahi-Buisson N, Philippe C, Nectoux J, Girard B, N'Guyen Morel MA, Gitiaux C, Lazaro L, Odent S, Jonveaux P, Chelly J, Bienvenu T. (2008). Impairment of CDKL5 nuclear localisation as a cause for severe infantile encephalopathy. J Med Genet., 45, 172-8. doi: 10.1136/jmg.2007.053504.

Rosenberg SA, Aebersold P, Cornetta K, Kasid A, Morgan RA, Moen R, Karson EM, Lotze MT, Yang JC, Topalian SL. (1990). Gene transfer into humans--immunotherapy of patients with advanced melanoma, using tumor-infiltrating lymphocytes modified by retroviral gene transduction. N Engl J Med., 323, 570-8. doi: 10.1056/NEJM199008303230904.

Rosenthal N, Brown S. (2007). The mouse ascending: perspectives for human-disease models. Nat Cell Biol., 9, 993-9. doi: 10.1038/ncb437.

Rusconi L, Kilstrup-Nielsen C, Landsberger N. Extrasynaptic. (2011). N-methyl-D-aspartate (NMDA) receptor stimulation induces cytoplasmic translocation of the CDKL5 kinase and its proteasomal degradation. J Biol Chem.,286, 36550-8. doi: 10.1074/jbc.M111.235630.

Rusconi L, Salvatoni L, Giudici L, Bertani I, Kilstrup-Nielsen C, Broccoli V, Landsberger N. (2008). CDKL5 expression is modulated during neuronal development and its subcellular distribution is tightly regulated by the C-terminal tail. J Biol Chem., 283, 30101-11. doi: 10.1074/jbc.M804613200.

Schwarze SR, Ho A, Vocero-Akbani A, Dowdy SF. (1999). In vivo protein transduction: delivery of a biologically active protein into the mouse. Science., 285, 1569-72. doi: 10.1126/science.285.5433.1569.

Sekiguchi M, Katayama S, Hatano N, Shigeri Y, Sueyoshi N, Kameshita I. (2013). Identification of amphiphysin 1 as an endogenous substrate for CDKL5, a protein kinase associated with X-linked neurodevelopmental disorder. Arch Biochem Biophys., 535, 257-67. doi: 10.1016/j.abb.2013.04.012.

Serenó L, Coma M, Rodríguez M, Sánchez-Ferrer P, Sánchez MB, Gich I, Agulló JM, Pérez M, Avila J, Guardia-Laguarta C, Clarimón J, Lleó A, Gómez-Isla T. (2009). A novel GSK-3beta inhibitor reduces Alzheimer's pathology and rescues neuronal loss in vivo. Neurobiol Dis., 5, 359-67. doi: 10.1016/j.nbd.2009.05.025.

Shankar S, Suthakar G, Srivastava RK. (2007). Epigallocatechin-3-gallate inhibits cell cycle and

induces apoptosis in pancreatic cancer. Front Biosci., 12, 5039-51. doi: 10.2741/2446.

Sharma S, Taliyan R. (2015). Synergistic effects of GSK-3β and HDAC inhibitors in intracerebroventricular streptozotocin-induced cognitive deficits in rats. Naunyn Schmiedebergs Arch Pharmacol., 388, 337-49. doi: 10.1007/s00210-014-1081-2.

Sivilia S, Mangano C, Beggiato S, Giuliani A, Torricella R, Baldassarro VA, Fernandez M, Lorenzini L, Giardino L, Borelli AC, Ferraro L, Calzà L. (2016). CDKL5 knockout leads to altered inhibitory transmission in the cerebellum of adult mice. Genes Brain Behav., 15, 491-502. doi: 10.1111/gbb.12292.

Steffin DHM, Hsieh EM, Rouce RH. (2019). Gene Therapy: Current Applications and Future Possibilities. Adv Pediatr., 66, 37-54. doi: 10.1016/j.yapd.2019.04.001.

Symonds, J. D., Zuberi, S. M., Stewart, K., McLellan, A., O'Regan, M., MacLeod, S., Jollands, A., Joss, S., Kirkpatrick, M., Brunklaus, A., Pilz, D. T., Shetty, J., Dorris, L., Abu-Arafeh, I., Andrew, J., Brink, P., Callaghan, M., Cruden, J., Diver, L. A., Wilson, M. (2019). Incidence and phenotypes of childhood-onset genetic epilepsies: A prospective population-based national cohort. Brain, 142, 2303–2318. doi: 10.1093/brain/awz195.

Takahashi K, Tanabe K, Ohnuki M, Narita M, Ichisaka T, Tomoda K, Yamanaka S. (2007). Induction of pluripotent stem cells from adult human fibroblasts by defined factors. Cell., 131, 861-72. doi: 10.1016/j.cell.2007.11.019.

Tang S, Terzic B, Wang IJ, Sarmiento N, Sizov K, Cui Y, Takano H, Marsh ED, Zhou Z, Coulter DA. (2019). Altered NMDAR signaling underlies autistic-like features in mouse models of CDKL5 deficiency disorder. Nat Commun., 10, 2655. doi: 10.1038/s41467-019-10689-w.

Tang S, Wang IJ, Yue C, Takano H, Terzic B, Pance K, Lee JY, Cui Y, Coulter DA, Zhou Z. (2017). Loss of CDKL5 in Glutamatergic Neurons Disrupts Hippocampal Microcircuitry and Leads to Memory Impairment in Mice. J Neurosci., 37, 7420-7437. doi: 10.1523/JNEUROSCI.0539-17.2017

Tanudji M, Hevi S, Chuck SL. (2002). Improperly folded green fluorescent protein is secreted via a non-classical pathway. J Cell Sci., 115, 3849-57. doi: 10.1242/jcs.00047.

Terzic B, Cui Y, Edmondson AC, Tang S, Sarmiento N, Zaitseva D, Marsh ED, Coulter DA, Zhou Z. (2021). X-linked cellular mosaicism underlies age-dependent occurrence of seizure-like events in mouse models of CDKL5 deficiency disorder. Neurobiol Dis., 148, 105176. doi: 10.1016/j.nbd.2020.105176.

Thomas A, Burant A, Bui N, Graham D, Yuva-Paylor LA, Paylor R. (2009). Marble burying reflects a repetitive and perseverative behavior more than novelty-induced anxiety. Psychopharmacology (Berl), 204, 361-73. doi: 10.1007/s00213-009-1466-y.

Thurn KT, Thomas S, Moore A, Munster PN. (2011). Rational therapeutic combinations with histone deacetylase inhibitors for the treatment of cancer. Future Oncol., 7, 263-83. doi: 10.2217/fon.11.2.

Tramarin M, Rusconi L, Pizzamiglio L, Barbiero I, Peroni D, Scaramuzza L, Guilliams T, Cavalla D, Antonucci F, Kilstrup-Nielsen C. (2018). The antidepressant tianeptine reverts synaptic AMPA receptor defects caused by deficiency of CDKL5. Hum Mol Genet.,27, 2052-2063. doi: 10.1093/hmg/ddy108.

Trazzi S, De Franceschi M, Fuchs C, Bastianini S, Viggiano R, Lupori L, Mazziotti R, Medici G, Lo Martire V, Ren E, Rimondini R, Zoccoli G, Bartesaghi R, Pizzorusso T, Ciani E. (2018). CDKL5 protein substitution therapy rescues neurological phenotypes of a mouse model of CDKL5 disorder. Hum Mol Genet., 27, 1572-1592. doi: 10.1093/hmg/ddy064.

Trazzi S, Fuchs C, Viggiano R, De Franceschi M, Valli E, Jedynak P, Hansen FK, Perini G, Rimondini R, Kurz T, Bartesaghi R, Ciani E. (2016). HDAC4: a key factor underlying brain developmental alterations in CDKL5 disorder. Hum Mol Genet., 25, 3887-3907. doi: 10.1093/hmg/ddw231.

Trovò L, Fuchs C, De Rosa R, Barbiero I, Tramarin M, Ciani E, Rusconi L, Kilstrup-Nielsen C. (2020). The green tea polyphenol epigallocatechin-3-gallate (EGCG) restores CDKL5-dependent synaptic defects in vitro and in vivo. Neurobiol Dis., 138, 104791. doi: 10.1016/j.nbd.2020.104791.

Valli E, Trazzi S, Fuchs C, Erriquez D, Bartesaghi R, Perini G, Ciani E. (2012). CDKL5, a novel MYCN-repressed gene, blocks cell cycle and promotes differentiation of neuronal cells. Biochim Biophys Acta.,1819, 1173-85. doi: 10.1016/j.bbagrm.2012.08.001.

Wang D, Tai PWL, Gao G. (2019). Adeno-associated virus vector as a platform for gene therapy delivery. Nat Rev Drug Discov., 18, 358-378. doi: 10.1038/s41573-019-0012-9.

Wang HT, Zhu ZA, Li YY, Lou SS, Yang G, Feng X, Xu W, Huang ZL, Cheng X, Xiong ZQ. (2021). CDKL5 deficiency in forebrain glutamatergic neurons results in recurrent spontaneous seizures. Epilepsia., 62, 517-528. doi: 10.1111/epi.16805.

Wang IT, Allen M, Goffin D, Zhu X, Fairless AH, Brodkin ES, Siegel SJ, Marsh ED, Blendy JA, Zhou Z. (2012). Loss of CDKL5 disrupts kinome profile and event-related potentials leading to autistic-like phenotypes in mice. Proc Natl Acad Sci U S A., 109, 21516-21. doi: 10.1073/pnas.1216988110.

Weaving LS, Christodoulou J, Williamson SL, Friend KL, McKenzie OL, Archer H, Evans J, Clarke A, Pelka GJ, Tam PP, Watson C, Lahooti H, Ellaway CJ, Bennetts B, Leonard H, Gécz J. (2004). Mutations of CDKL5 cause a severe neurodevelopmental disorder with infantile spasms and mental retardation. Am J Hum Genet., 75, 1079-93. doi: 10.1086/426462.

Williamson SL, Giudici L, Kilstrup-Nielsen C, Gold W, Pelka GJ, Tam PP, Grimm A, Prodi D, Landsberger N, Christodoulou J. (2012). A novel transcript of cyclin-dependent kinase-like 5 (CDKL5) has an alternative C-terminus and is the predominant transcript in brain. Hum Genet., 131, 187-200. doi: 10.1007/s00439-011-1058-x.

Worgall S, Sondhi D, Hackett NR, Kosofsky B, Kekatpure MV, Neyzi N, Dyke JP, Ballon D, Heier L, Greenwald BM, Christos P, Mazumdar M, Souweidane MM, Kaplitt MG, Crystal RG. (2008). Treatment of late infantile neuronal ceroid lipofuscinosis by CNS administration of a serotype 2 adeno-associated virus expressing CLN2 cDNA. Hum Gene Ther., 19, 463-74. doi: 10.1089/hum.2008.022.

Xia H, Mao Q, Davidson BL. (2001). The HIV Tat protein transduction domain improves the biodistribution of beta-glucuronidase expressed from recombinant viral vectors. Nat Biotechnol., 19, 640-4. doi: 10.1038/90242.

Yoder JA, Soman NS, Verdine GL, Bestor TH. (1997). DNA (cytosine-5)-methyltransferases in mouse cells and tissues. Studies with a mechanism-based probe. J Mol Biol., 270, 385-95. doi: 10.1006/jmbi.1997.1125.

Zhang H, Yang B, Mu X, Ahmed SS, Su Q, He R, Wang H, Mueller C, Sena-Esteves M, Brown R, Xu Z, Gao G. (2011). Several rAAV vectors efficiently cross the blood-brain barrier and transduce neurons and astrocytes in the neonatal mouse central nervous system. Mol Ther., 19, 1440-8. doi: 10.1038/mt.2011.98.

Zhang Y, Matt L, Patriarchi T, Malik ZA, Chowdhury D, Park DK, Renieri A, Ames JB, Hell JW. (2014). Capping of the N-terminus of PSD-95 by calmodulin triggers its postsynaptic release. EMBO J., 33, 1341-53. doi: 10.1002/embj.201488126.

Zhu JW, Li YF, Wang ZT, Jia WQ, Xu RX. (2016). Toll-Like Receptor 4 Deficiency Impairs Motor Coordination. Front Neurosci., 16, 10:33. doi: 10.3389/fnins.2016.00033.

Zhu YC, Li D, Wang L, Lu B, Zheng J, Zhao SL, Zeng R, Xiong ZQ. (2013). Palmitoylation-dependent CDKL5-PSD-95 interaction regulates synaptic targeting of CDKL5 and dendritic spine development. Proc Natl Acad Sci U S A., 110, 9118-23. doi: 10.1073/pnas.1300003110.

Zhu YC, Xiong ZQ. (2019). Molecular and Synaptic Bases of CDKL5 Disorder. Dev Neurobiol., 79, 8-19. doi: 10.1002/dneu.22639.